ON THE APPLICATION OF MASTIC MATERIALS AS PANEL VIBRATION DAMPERS TO FAN HOUSINGS AND VENTILATION DUCTS

by

M.A. Hamid, B.Eng.

A thesis submitted to the Faculty of Graduate Studies and Research in partial fulfilment of the requirements for the degree of Master of Engineering.

Department of Electrical Engineering
McGill University
Montreal.

November, 1961

ACKNOWLEDGEMENTS

I wish to extend my thanks to Dr. F. S. Howes, who proposed this project and supervised it with extreme patience and co-operation.

I also wish to thank Messrs. J. Turley, P. Conroy, M. Zegel, R. F. Flegg for making the measuring equipment available to me.

This project was supported in part by a grant from The National Research Council, Ottawa.

I also would like to record my indebtedness to Mrs. J. R. Horner and Messrs. E. Adler, P. Silvester, A. Malowany for reading the entire manuscript and offering helpful suggestions. Mrs. Horner also carried out, with excellent capability, the difficult task of typing this manuscript.

Thanks are also due to Mr. B. Ogilvy, Chief Engineer, Aluminum Company of Canada, Limited, for arranging to re-produce, at a minimum cost, all the diagrams and photographs in this thesis.

TABLE OF CONTENTS

LIST OF FIGURES

LIST OF PHOTOGRAPHS

LIST OF TABLES

ABSTRACT

The Geiger and Complex Modulus standard methods used to obtain the damping properties of viscoelastic materials were compared. The tests, using both methods, are described for a number of available materials. The results are in good agreement. It was found that a uniform coating of the entire vibrating surface did not correspond to the highest damping efficiency.

An equivalent circuit, based on electro-mechanical analogies, was derived. This circuit proved to be a powerful technique in the study of vibration damping, and some of its parameters were combined in a universal curve.

One viscoelastic material was chosen for most efficient application to a ventilation-duct model. At one anti-node the velocity-amplitude was reduced by 78.9%.

CHAPTER I

INTRODUCTION

1.1 General

The study of vibrations is the study of the behaviour of the bodies and systems as they undergo motion due to varying internal or external forces. While such forces can be periodic or random in character, the behaviour is often complex when we try to explain or investigate the mechanisms which cause machine parts to fail or generate noise etc.

The seriousness of the problems arising from vibrations has been fully recognized in recent years. It has led to the introduction of some means of damping into the design of machinery, building partitions, ventilation ducts etc.

The study of damping requires the knowledge of the properties of the materials involved and their mechanical or structural assembly as they appear in the vibrating system. The aim of damping is to convert the mechanical vibrational energy into heat. The methods of damping are to increase the internal inherent mechanical friction of these materials, or to operate externally on the various system components with other materials or artificial means which will increase the system losses. Finally, the amount of damping can be evaluated by essentially comparing the losses introduced to those inherent in the system. For this purpose, practical testing techniques and instruments have been developed to fit even the most complicated structures.

1.2 Nature of the Problem

The problem being investigated here involves the possibilities and advantages of using mastic vibration-damping materials on ventilation ducts and fan housings to reduce vibrations set up by air turbulence.

While the application of such materials is common in many industrial situations, it is believed that there may also be an application in connection with ventilation systems. At present, the lining of ducts with sound-absorbing materials, while common, is not an entirely satisfactory solution because these materials do not attenuate noise in the low frequency range.

Figure (1) is a simplified representation of the problem. The turbulent air incident on a thin metal plate, of thickness "h" causes this plate to deflect and move the adjacent air in the same manner. Since vibrations of air create sound waves, the adjacent air will generate sound waves to be propagated to the external medium.

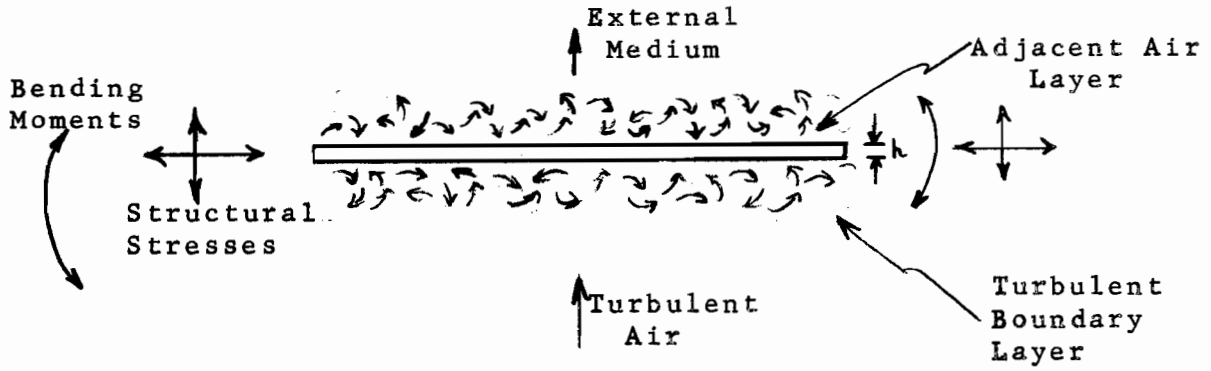

Fig. (1): Transmission and Distribution of Air-borne Sound and Bending Energy in an Infinitesimal area of a Turbulent Duct.

In this thesis an analysis of the damping of steel plates and bars under harmonic excitation is presented. This simplifies the picture since any random excitation due to turbulent air can be thought of as composed of a number of superimposed Fourier components or harmonics. Also since the plate shown in Figure (1) may be considered to be part of an air duct or fan housing, only lateral flexural waves due to shear stresses are considered here. This further simplification makes the comparison between mastic materials, coated on simply supported plates, far more accurate and equally useful.

1.3 Historical Review of the Problem

The first major effort to make practical use of the damping properties of mastic materials coated on vibrating plate was made in 1933 when P.H.Geiger[1] introduced a satisfactory damping treatment to door panels used in the automobile industry. He developed a simple technique to measure the effectiveness of the few damping materials available to him at that time. Figure (2) is a schematic of his thick-plate test. In principle, the experiment requires no more than the accurate measurement of the time in seconds required for the vibration amplitude of the treated

---

[1] P.H.Geiger, Noise-Reduction Manual (Engineering Research Institute, University of Michigan, 1956)Chap.4, pp. 60-100.

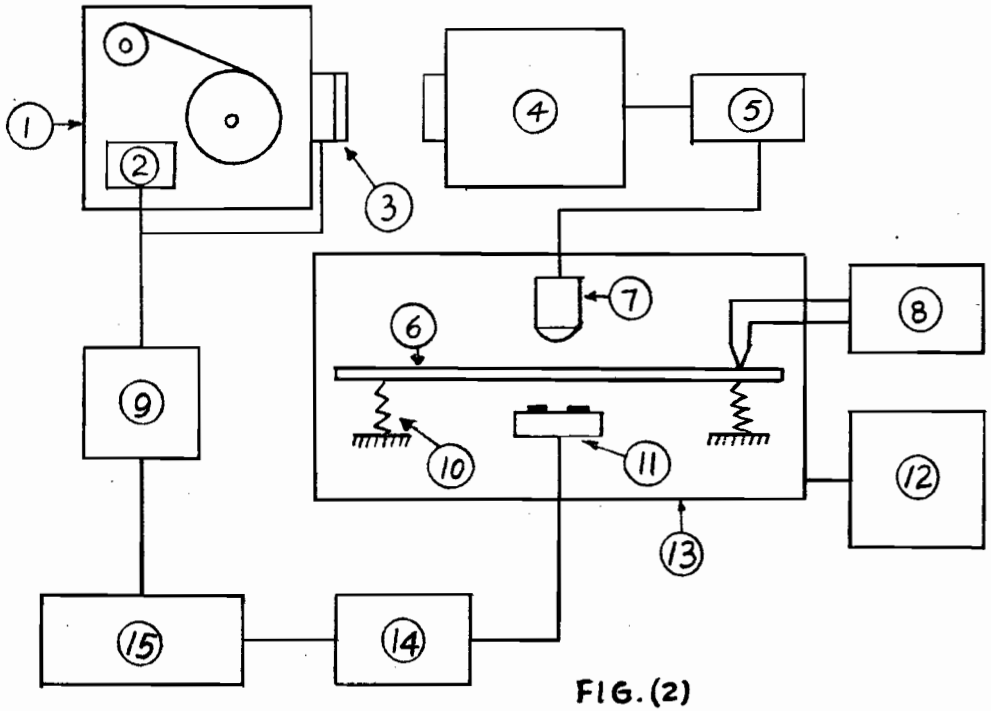

FIG. (2)

Schematic Block Diagram Of Vibration-Damping Thick Plate Test Apparatus (After P.H.Geiger)

1. Moving-Film Camera
2. Motor
3. Shutter
4. Cathode-Ray Oscilloscope
5. Amplifier
6. Test Panel
7. Microphone
8. Thermocouple Galvan.
9. Actuator
10. Modal Suspension
11. Magnetic Exciter
12. Temperature Control Apparatus
13. Insulating Jacket
14. Power Amplifier
15. Audio Oscillator

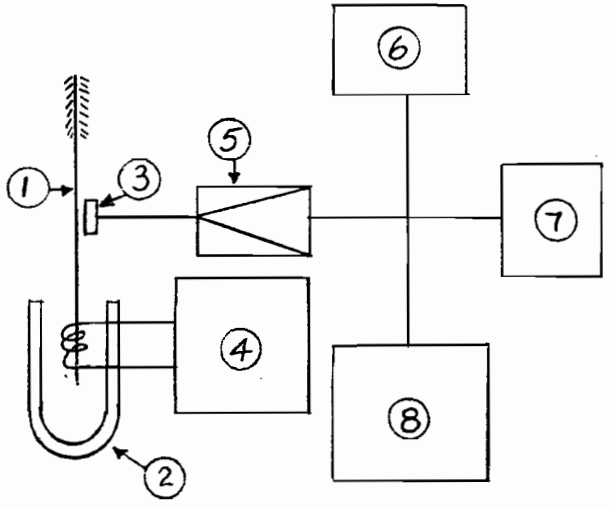

FIG.(3)

Block Diagram For the Measurement Of The Elastic Modulus E_2^* and the Loss Coefficient η Of A Uniform Rod(After Naumkina,Tartakovskii And Efrussi-Academy Of Sciences, Moscow,USSR).

1. Measured Sample
2. Electromagnetic Exciter
3. Electromagnetic Pickup
4. Audio Oscillator
5. Amplifier 6. Electron Oscillograph
7. Vacuum Tube Voltmeter 8. Level Recorder.

panel to decay a specified number of decibels. The panel is ordinarily excited by a polarized electromagnet driven by an audio oscillator which is tuned to the natural resonant frequency of the panel. Under these conditions only the fundamental mode of vibration is excited and the decay is logarithmic once the driving force is removed. The vibration level of the panel is detected as sound by a pressure-sensitive microphone suspended a few inches above the centre of the vibrating panel. The decaying signal is amplified and displayed on a cathode-ray tube. A moving-film camera is used to record the decaying trace on the cathode-ray oscilloscope as a function of time. The "Geiger Rating", which is the decay rate in decibels per second, is still being used as the criterion for damping effectiveness of surface treatments for automotive panels.

Oberst and Frankenfeld[2] introduced the Complex Modulus Method in 1952. This method employs sample bars with suitable mechanical mounting. The bar is axially excited at the lower end by an electromagnetic transducer fed from the load terminals of a beat frequency oscillator. The deflection at any point along the free length of the bar induces a signal in an electromagnetic transducer. The pick-up signal is fed

---

[2]H.Oberst and K.Frankenfeld, "The Damping of Flexural Vibrations of Thin Sheet Metal by Strongly Adhesive Coatings", Acoustica, Vol.IV, (1952) Parts I and 2.

into a microphone amplifier. The amplified signal is then automatically recorded on paper using a level recorder. If the oscillator sweep is adjusted to be in synchronism with the recorder paper speed, resonance curves of coated and uncoated bars can be obtained and compared. These curves are traced as amplitude in db. vs. frequency in cycles per second. This method is known as the Frequency Response Method. However, if the oscillator is tuned manually to the resonant modes of the sample bar, the method is then called the Reverberation-time Method and resembles the Geiger Method. This is so because once the bar is forced to vibrate with a steady amplitude at any of its resonant modes, the amplitude will decay exponentially when the driving force is removed. Thus, the first method is used to measure the damping of bars under forced vibrations, while the second is under free vibrations.

The authors also developed two non-resonant methods for special cases. These are the Progressive Wave and the Standing Wave Methods. For details of these two methods the reader is referred to two excellent articles[3].

The above discoveries of Oberst and Frankenfeld were the basis for many research experiments and commercial applications. One of these experiments was conducted by

---

[3] A.Schlägel, Brüel and Kjaer Technical Review, No.4 (November,1957), and No.1 (January, 1958).

Naumkina, Tartakovskii and Efrussi[4] and a schematic diagram is shown in Figure (3). The authors investigated a group of synthetic materials, made from a bituminous base, in the frequency range of 10-100 cps.

The best material was found to be bitumen-impregnated felt having a Young's modulus of 10^9 dynes/cm^2 and a loss coefficient of 2.5.

A rig for mounting the sample bars has been built by Brüel and Kjaer Company and is known as the Bending Wave Apparatus. This apparatus is shown in Photograph (1). It has provisions for clamping the sample bars at one or both ends. The transducers can be placed practically at any point along the free length of the bar using screw and clamp arrangements as shown.

The work of Oberst and Frankenfeld led to the experiments carried out by Kerwin, Kuntze and Mead. Kerwin[5] extended the analysis of a thin bar coated by one damping layer to one coated by a constrained damping layer. His aim was primarily the investigation of the damping tape currently used in aircraft. His results were fairly accurate within the frequency range 100-4000 cycles per second and for various

---

[4] Naumkina, Tartakovskii and Efrussi, "Experimental Study of Some Vibration Damping Materials", Soviet Physics, Acoustics, Vol.5, No.2 (1959) pp.196-201.

[5] E.M.Kerwin, "Damping of Flexural Waves by a Constrained Viscoelastic Layer", JASA, Vol.3, No.7, (July,1959) pp.952-962.

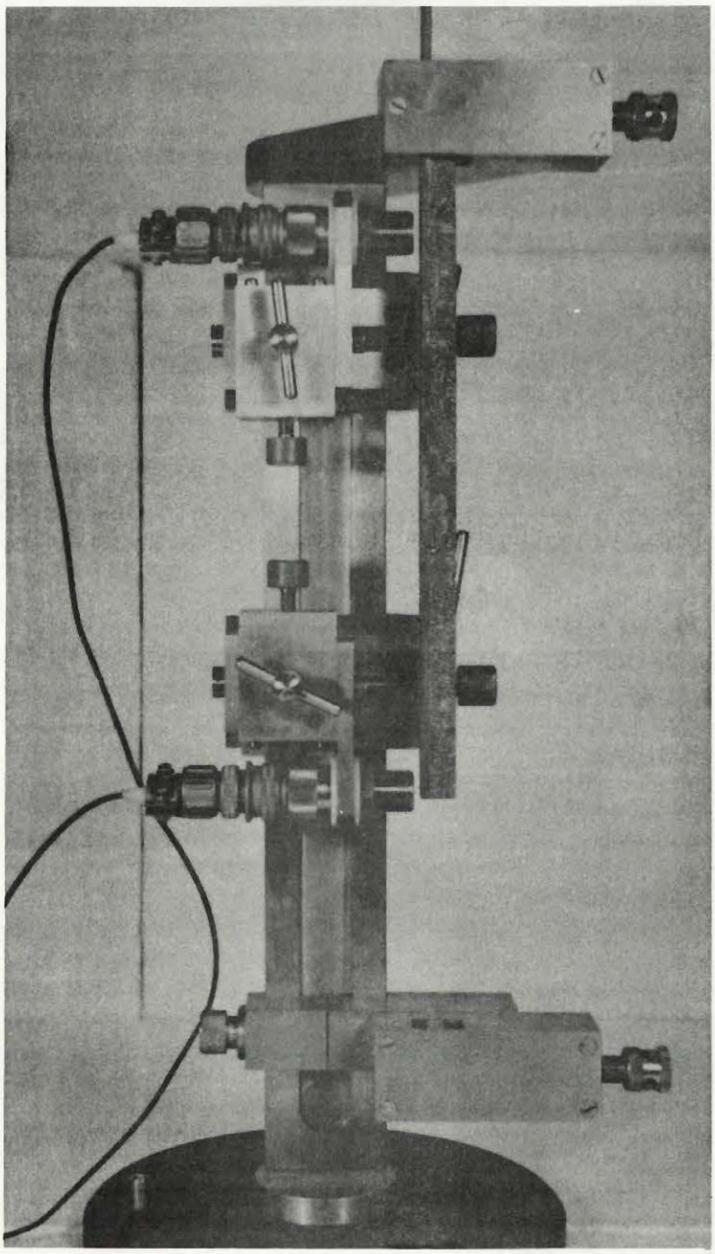

Photograph (1) Bending Wave Apparatus

operating temperatures and geometrical configurations of the damped bar.

Kuntze[6] in 1959, extended the works of his predecessors. He investigated the properties of two types of multilayer damping treatments. One type contained a constrained viscous liquid and the other a constrained air-filled porous material. He analyzed both cases using an electrical circuit analog. Namkina, Tartakovskii and Efrussi[7] extended their previously mentioned work to the multilayer case also.

Mead[8,9] has analyzed the damping due to viscoelastic materials coated on structures in general, with special emphasis on aircraft structures.

Finally, Bertzhold[10] in 1961, presented his results regarding the acoustic and vibration treatments for vehicles. He analyzed single and multilayer cases from the point of view of maximum driving comfort and safety.

---

[6] G.Kuntze, "Bending Wave Propagation in Multilayer Plates", JASA, Vol.31, No.9, (September, 1959) pp.1183-1201.

[7] N.I.Naumkina, B.D.Tartakovskii and M.M.Efrussi, "A Two-layer Vibration-Absorbing Structure", Soviet Physics, Acoustics, Vol.5, No.4, (April,1960), pp.514-517.

[8] D.J.Mead, "The Effect of a Damping Compound on Jet-Efflux Excited Vibrations", Aircraft Engineering, Part I, (March,1960).

[9] D.J.Mead, "Criteria for Comparing the Effectiveness of Damping Treatments", Noise Control, Vol.7, No.3, (May, 1961), pp.27-38.

[10] Bertzhold, "On the Problem of Air Sound Damping", A lecture delivered at the Vibrations Conference, Philadelphia, 1961.

Chapter 2

BASIC THEORY

2.1 General

Damping compounds are designed to reduce drumming in metal panels and casings. Analysis of experimental data shows that in many cases where moving machinery or fluids are enclosed, panel vibration contributes more to the general or diffused sound field level than the machinery itself. Furthermore, since these vibrations may occur at frequencies within the audible range, their reduction or elimination is important. As will be shown later, metallic plates have relatively low internal damping at their fundamental resonant frequencies and, hence without damping, vibration amplitudes may become quite large.

The primary function of mastic materials used for damping is therefore to reduce the amplitude of flexural vibrations in metal panels. The panels when treated with these materials efficiently, will have a higher stiffness modulus under incident bending forces . The life of the metal will thus be increased while the generated noise level will decrease.

In the case of ventilation ducts, air turbulence creates random vibrations. However, the duct shell will have certain natural resonant frequencies or free modes depending on its mechanical dimensions and supports. The radiated sound field could include many discrete frequencies within the audible range thus approximating white noise. If the duct is treated with a mastic vibration damper both its mass and stiffness increase. The increase in mass lowers the natural resonant frequencies while the increase in stiffness raises them. It appears, therefore, that there are three quantities of major interest in this problem. The first is the shift in the natural resonant frequencies for a given

damping treatment. The second is the effective damping obtainable with a certain treatment. The third is the damping vs. frequency characteristic. These quantities can be more readily obtained by varying the coverage area and thickness of the damping layers coated on plate and bar specimens. The testing procedure is described in Chapter 4.

2.2 Some Physical Properties of Mastic Damping Materials

2.2.1 Types Commercially Available

Mastic damping materials are commercially available in the pad, tape and liquid forms. Mastic pads have the advantage of ease of manufacture and application. Their thickness and weights can be determined with fair accuracy. They must, however, be glued firmly to the vibrating panel before they can have any appreciable effect.

Mastic tapes are extremely easy to apply and remove. Their light weights make them suitable for aircraft applications.

Liquid mastics are the most common ones and are used in the automotive industry, building partitions and industrial plants in general. They are normally sprayed under air pressure. Some of these materials have the disadvantage of long drying times.

2.2.2 Mechanisms of Hysteretic Damping

There are four main types of damping associated with free vibrations of single-degree of freedom systems.[12]

---

[12] W.T.Thomson, Mechanical Vibrations, (2nd Ed.Prentice-Hall July, 1959) pp.44-45.

(a) Viscous: This is encountered by bodies moving at moderate speeds through a fluid (e.g. hydraulic dashpots). Here the resisting or damping force is directly proportional to the velocity of motion.

(b) Coulomb: This arises from the sliding of dry surfaces in contact. It is approximately constant and depends on the nature of the sliding surfaces and the normal pressure between them. It generally predominates in damped free oscillations during the final stages of the motion when other types of damping become negligible.

(c) Solid or structural: This is due to the internal friction of the material itself. It is independent of frequency and proportional to the maximum stress of the vibration cycle. Since in the elastic range the stress and the strain can be considered linearly proportional, solid damping may alternatively be considered as proportional to the displacement.

(d) Hysteretic: This is due to the inherent properties of mastic materials and their method of application. By hysteretic damping we usually mean a process where the applied mechanical bending energy is being partially dissipated and converted into the following:

(i) Heat energy: This is contained in the randomly-excited molecules of the mastic material and part of it can be radiated.

(ii) Surface energy: This manifests itself by a progressive damage of the cohesive bonds of the damping material by means of a disruption process.

The mechanism of energy dissipation into heat is complex. For a given material it is a function of the deformation amplitude and frequency.

The classical heat-dissipation theory is not, however, sufficient to interpret all the peculiarities of damping observations. The reason for this is the interaction between the internal (mentioned above) and the external means of energy dissipation. Thus, in order to justify these observations, we can only seperate the losses experimentally and attempt to correlate them, (individually or as groups) with the physical behaviour. Ferry[13] investigated these losses in detail. His results can be summarized as follows.

(a) External Damping: This is mainly caused by friction with the surrounding medium and other structures.

(b) Internal Damping: This is due to:

(i) The random displacement of the particles in an essentially amorphous material, where momentum or energy can be lost in collisions.

(ii) The energy absorbed by some crystals, or their aggregates, tending to harden their structure.

(iii) The thermal energy absorbed by crystals which are continuously being broken and re-formed.

(iv) Dissipation of energy on the surface of the material.

Finally, since the damping properties of a known specimen can be rapidly and accurately determined, some damping compounds have been used to investigate the fatigue performance and impact strength of some important metals used in industry. The compound is coated on the metal sample and the properties of the metal are then seperated after knowing properties of one coated

---

[13] J.D.Ferry, Viscoelastic Properties of Polymers, (Wiley, N.Y. 1961)

sample and the compound alone.

2.3 Mechanical Impedance Approach

In a vibrating panel, the dissipation of energy is due to the internal as well as the external losses. Only the internal ones will be considered here, since the external ones are difficult to determine, air damping being an example. In practice and under normal pressure and temperature the losses are small compared to the internal ones, and thus can be neglected. The simplified analysis, presented below, is based on the electromechanical analogy[14] for one-degree-of-freedom systems and the subsequent application of linear circuit theory.

In general, ideal elastic materials, which obey Hooke's law, can be visualized by considering that during a complete vibration cycle, the acting force and the resulting displacement are in phase. If these two quantities are plotted as vectors, then the phase angle between them is zero. Also, when these materials are cyclicly deformed, the stored potential energy is restored as kinetic energy every half-cycle and the net work or energy dissipation is zero.

Ideal viscous materials, on the other hand, dissipate maximum energy. This is due to the fact that the force and displacement vectors are 90^{o} out of phase. If these two vectors are plotted, (force vs, displacement), for a complete vibration cycle a full circle will be obtained. The area of this circle is a measure of the dissipated mechanical energy. It can be shown[15] that for energy to be dissipated during harmonic motion, a component of the force must lag the displacement by 90^{o}. In forced vibrations, the displacement lags the

---

[14] Thomson, op cit. p.225.

[15] Thomson, op cit. pp.44-45

external exciting force, and the component of the force leading the displacement vector by 90° will tend to overcome the energy dissipated by damping.

A chemical combination of elastic and viscous materials gives visco-elastic compounds. The energy loss will then lie between the two ideal cases, and the phase angle, mentioned above, will be between zero and 90°. Unfortunately, this phase angle has to be small for practical reasons. Extra amounts of the elastic ingredients, which do not contribute to the phase angle have to be added in order to give the overall coating more mechanical flexibility and avoid its cracking. On the other hand, the proportion of viscous ingredients, which contribute to the phase angle, have to be kept low since that is essential for ease in spraying the compound. For these reasons, the damping efficiency of visco-elastics is decreased.

For small values of one phase angle, the instantaneous values of the applied force and the resulting deformation are located on a hysteresis loop. This loop is analogous to the B-H curves for ferrous materials and its area (which can be approximated by an ellipse) is a measure of the dissipated energy.

The above qualitative introduction helps to introduce the mechanical impedance concept. For this, let us choose a convenient electro-mechanical analogy. If we choose the force-voltage analogy, the analogous electrical and mechanical quantities can be listed as follows:

Mechanical Quantity	Electrical Quantity
Force (pound) - f	Voltage (volt) - e
Velocity (inch/sec) - v	Current (ampere) - i
Displacement (inch) - $x = \int_0^t v\,dt$	Charge (coulomb) - $q = \int_0^t i\,dt$
Mass (lb.sec^2/inch) - m	Inductance (henry) - L
Compliance (inch/lb.) - 1/K	Capacitance (farad) - C
Resistance (lb.sec/in.) -c	Resistance (ohm) - R

The differential equations can now be written for an R-L-C series electrical circuit simulating a single degree-of-freedom vibrating mass coated with a visco-elastic layer:-

$$Ri + L\, di/dt + (1/C) \int_o^t i\, dt = e(t) \qquad .....2.3.1$$

$$cv + m\, dv/dt + k \int_o^t v\, dt = f(t) \qquad .....2.3.2$$

We can now define the mechanical impedance as the force divided by the displacement. Hence, solving equation 2.3.2 we get:

$$Z = f(t)/x(t) = Zo\ (A \sin \omega t + B \cos \omega t) \qquad .....2.3.3$$

where

$$x(t) = \int_o^t v\, dt,$$

Zo, A, B are values fixed for each numerical case.

Hence, the mechanical impedance function, Z, can be obtained by drawing the force vector along the ordinate (imaginary axis) and the displacement vector along the abscissa (real axis) and then taking the complex ratio in the impedance plane.

The mechanical impedance function is analogous to the steady-state response of a linear electrical circuit. Since linear circuit theory applies to this analog as well, the introduction of the mechanical impedance concept to represent the steady-state response of oscillating mechanical systems can be most useful.

The mechanical impedance, Z, represents a generalized or complex spring constant in purely elastic systems. This is due

to the fact that in such systems, the force is equal to the product of the displacement and the spring constant. In viscous systems, Z is the ratio of the force and velocity vectors and hence can be considered as a generalized viscosity coefficient.

The real component related to the complex spring constant defines the amplitude of the displacement in phase with the force. Hence, it is a measure of the elastic response of the vibrating system. The imaginary component, related to the amplitude of the displacement 90° out of phase with the force, represents the inelastic effect of the impedance.

2.4 Equivalent Circuit for the Coated Plate

From the previous section we can now pursue the idea of an equivalent electrical circuit and apply it to the case of a coated plate (as the Geiger plate for example). The analysis applies equally well to coated bars.

Let:

NOTE: Subscript "p" refers to steel plate alone; "g" to coating layer alone. No subscript refers to coated plate.

P	=	induced sound pressure in microbars at time t.
$t < 0$	=	time during which the plate vibrates at a steady-state sound pressure, P_1.
$t = 0$	=	instance of removing the driving force on the plate.
$t > 0$	=	time during which the plate oscillations decay exponentially.
P_1	=	steady-state sound pressure in microbars at $t = 0$.
P'	=	reference sound pressure (0.0002 microbars).
α	=	damping constant (known as the attenuation constant in transmission-line theory) in nepers.
Q	=	Quality-factor.

δ = decay-rate in decibels/sec.

ω = radian frequency.

ω_o = radian frequency at plate resonance.

R,L,C = resistance, inductance and capacitance parameters of the equivalent circuit in ohms, henrys and farads.

s = symbol representing the frequency domain

= $\alpha \pm j\omega$

δ_c = decay rate in decibels/sec. of the coated plate corrected for a lossless steel plate.

T = decay time in seconds.

τ = thickness of the coating layer in inches.

e = base for natural logarithms.

For a Geiger plate, coated with any damping material and generating a sound pressure detectable by the measuring equipment we can write:

$$P = P_1 e^{-\alpha t} \qquad .....2.4.1$$

normalizing with respect to P' and taking the common logarithm of both sides of equation 2.4.1 and then multiplying through by 20 we get:

$$20 \log \frac{P}{P'} = 20 \log \left(\frac{P_1}{P'} e^{-\alpha t} \right) \qquad .....2.4.2$$

or

$$\left[20 \log(P/P') - 20 \log (P_1/P') \right] = - 20 \alpha \log e = -8.686 \alpha \qquad .....2.4.3$$

The left-hand side of equation 2.4.3 can be determined experimentally from the recorded decay curves, and is equal to the decay rate for appropriate potentiometer and paper speed settings of the level recorder. Thus:

$$\delta = -8.686 \alpha \qquad .....2.4.4$$

Now, "α" can be determined from the R-L-C equivalent circuit as follows:

$$Z = R + L\,s + 1/Cs = (1 + RCs + LCs^2)/Cs \qquad .....2.4.5$$

At resonance "s" has the value:

$$s = \left[- RC \pm (R^2C^2 - 4LC)^{1/2} \right] /2LC \qquad .....2.4.6$$

but, by definition

$$s = \alpha \pm j\omega$$

hence,

$$\alpha = -R/2L \qquad .....2.4.7$$

or

$$Q\alpha = - (\omega_o L/R)(R/2L) = - \pi f_o \qquad .....2.4.8$$

Combining equations 2.4.4 and 2.4.8 we get:

$$\delta = - 27.29\ f_o/Q = - 4.343\ R/L \text{ db/sec.} \qquad .....2.4.9$$

By examining Figure (4) we can now determine easily two useful quantities:

$$\delta_p = -4.343\ R_p/L_p \text{ db/sec.} \qquad .....2.4.10$$

$$\delta_g = -4.343\ R_g/L_g \text{ db/sec.} \qquad .....2.4.11$$

The quantity δ_g can be determined following the steps listed below in sequence:

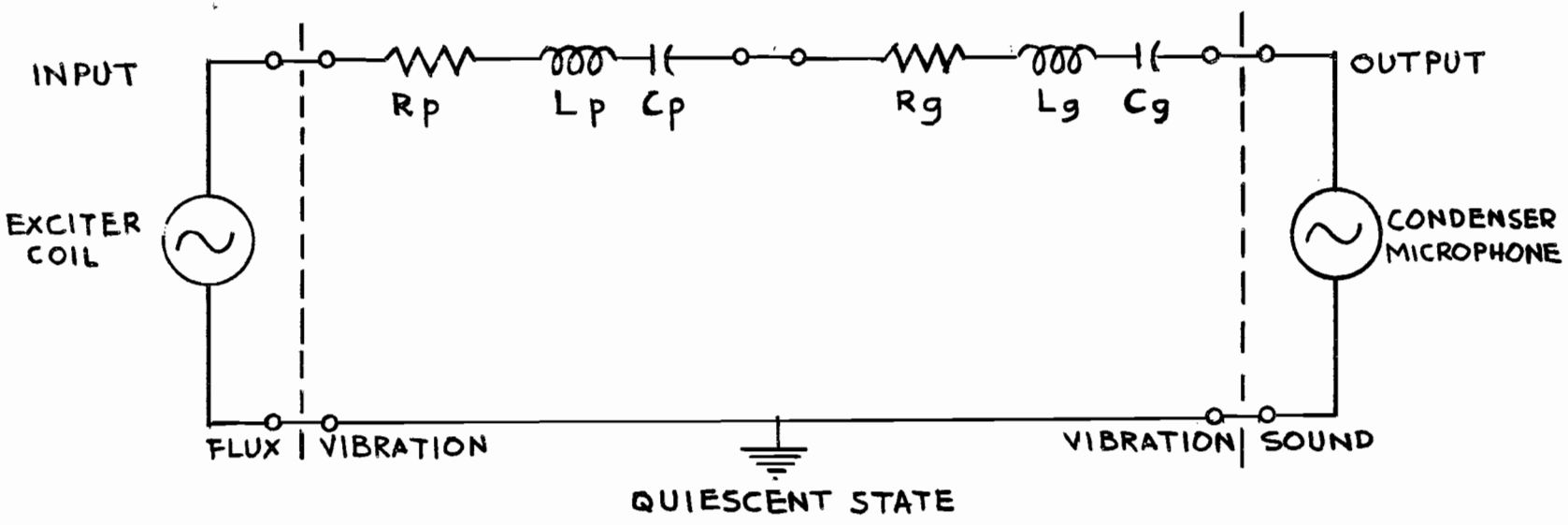

$$R = R_p + R_g$$

$$L = L_p + L_g$$

$$C = \frac{C_p C_g}{C_p + C_g}$$

Fig. (4) - ELECTRICAL EQUIVALENT CIRCUIT OF THE COATED GEIGER PLATE

1. From the recorded decay curves and using the reverberation-time protractor (see Chapter 3), we calculate the Decay rate of the bare plate as follows:

$$\delta_p = 60/T_p \text{ db/sec.} \qquad \text{.....2.4.12}$$

2. Knowing the resonant frequency of the bare plate we can calculate the quality-factor Q_p:

$$Q_p = 27.29\ (f_{op})/T_p \qquad \text{.....2.4.13}$$

3. Knowing the mass of the bare plate, and equating one henry for each pound mass (this is only to simplify the units), we can calculate R_p:

$$R_p = 2\pi(f_{op})(L_p)/Q_p \text{ ohms} \qquad \text{.....2.4.14}$$

4. Knowing the resonant frequency f_{op} and the inductance L_p of the bare plate, we can calculate the equivalent capacitance C_p:

$$C_p = 1/(\omega_o^2\ L_p) \text{ farads} \qquad \text{.....2.4.15}$$

5. The above four steps can then be repeated for the case of the coated plate to obtain the values of Q, R, L, C in the equivalent circuit.
6. The values of R_g, L_g and C_g for the coating layer can now be determined easily thus:

$$R_g = R - R_p \text{ ohms} \qquad .....2.4.16$$

$$L_g = L - L_p \text{ henrys} \qquad .....2.4.17$$

$$C_g = (C_p)(C)/(C_p - C) \text{ farads} \qquad .....2.4.18$$

7. The quality factor, resonant frequency and decay rate of one coating layer alone can be obtained by using the calculated values of R_g, L_g and C_g from step 6. Thus:

$$f_{og} = \frac{1}{2\pi (L_g C_g)^{1/2}} \text{ cycles/sec.} \qquad .....2.4.19$$

$$Q = \frac{2\pi f_{og} L_g}{R_g} \qquad .....2.4.20$$

$$\delta_g = -4.343 \frac{R_g}{L_g} \text{ db/sec} \qquad .....2.4.21$$

Since the above computations are repetitive, a Fortran program was prepared on the 650 I.B.M. Digital Computer, and once optimized, gave answers at the rate of 200 per minute.

The previous calculations are necessary to find the Geiger rating of the material. As will be shown in Chapter 5, the quantities δ_p, Q_p, f_{op} of a steel plate or bar are not necessarily equal to those for another plate of identical dimensions and weight. Moreover Geiger used a standard cold-rolled steel plate for which he neglected R_p and considered $R \neq R_g$. However, since the four plates used in this project were found to have appreciable values of R_p, a correction was

necessary before they could be considered lossless. This was done simply by eliminating the effect of R_p in the final result in the following manner:

$$\delta_c = \delta\left[R_g/(R_g + R_p)\right] \text{ db/sec.} \qquad .....2.4.22$$

The quantity δ_c always turns out to be slightly less than δ as seen from equation 2.4.22. It is a true value of the Geiger rating of the damping material and can be obtained using the equivalent circuit.

An accurate comparison between the ten different materials tested here was possible only after corrections were made to obtain δ_c for each thickness τ.

The concept of a hypothetical damping layer will be extended further in Chapter 7 where the specific decay rate and the universal damping curve are derived.

2.5 The Concept of the Complex Modulus of Elasticity

Usually we define the static modulus of elasticity as the ratio of the stress to the resulting strain. The value of this modulus is constant in the linear region of the stress-strain diagram, shown in Figure (5). This diagram represents the response of steel to static loadings and is composed of:

1. The elastic, or proportional, region where the material obeys Hooke's law.
2. The plastic, or non-linear, region where the material yields slowly until the critical strain when it reaches the breakdown point.

Obviously, any non-destructive test on steel plates or bars must be such that the metal remains in its elastic region. This is achieved simply by keeping the vibration amplitudes as low as possible. It is important to note that if a bare steel sample gives any appreciable damping in the low frequency range, then it must be undergoing destruction.

The concept of the static modulus is not too important in the study of vibrations. It is the dynamic modulus in which we are usually interested, since vibrations are manifestations of dynamic forces or loadings in the material. This dynamic modulus is usually represented by E* and defined as:

$$E^* = d\delta / d\epsilon \qquad \text{.....2.5.1}$$

where δ = stress in pounds/square inch.

ϵ = strain in inches of elongation per inch of original length.

The derivative sign is due to the fact that both the stress and the strain vary under dynamic loading in a cyclic manner.

As mentioned in Section 2.3, there is a phase shift between the applied force and the resulting strain in the case of damped vibrations. This is due to the internal friction and random motion of the damping material particles dissipating some energy. This leaves E* complex, as shown in Figure (6). E* can then be represented as a vector having a component along the real axis and another along the imaginary axis. It can thus be written as follows:

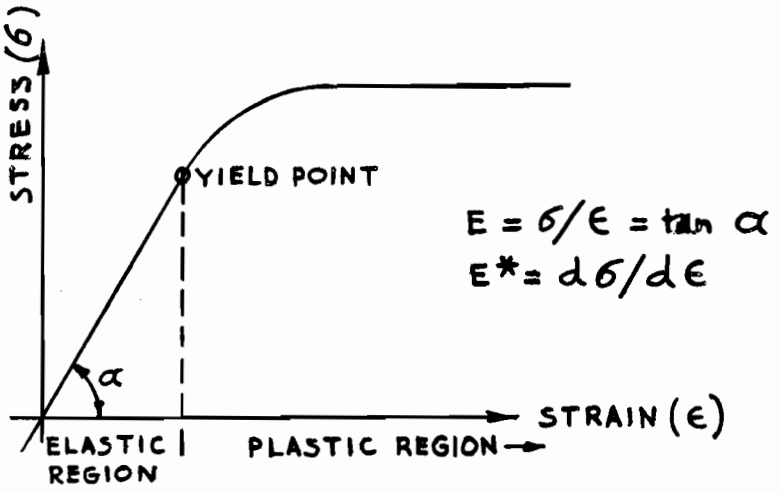

Fig. (5)- STRESS-STRAIN SCHEMATIC DIAGRAM FOR STEEL

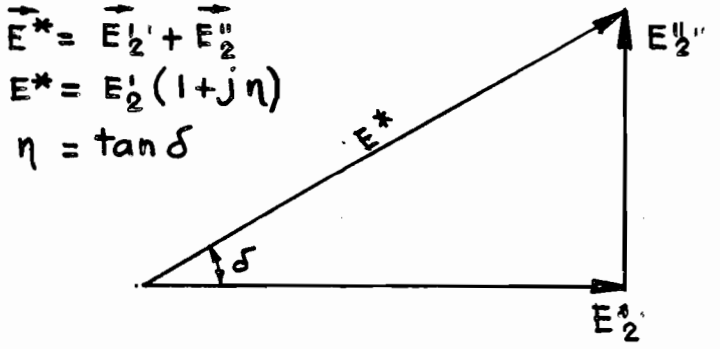

Fig. (6)- VECTOR DIAGRAM OF E^*

$$E^* = E_2' + E_2'' = E_2' (1 + j\eta) \qquad .....2.5.2$$

where E_2' and E_2'' are the real and imaginary components of the dynamic modulus of elasticity of the damping material respectively - pounds/square foot.

η = loss factor = E_2''/E_2'.

E_1' = Dynamic modulus of elasticity of steel sample.

Similarly, the flexural rigidity of the damped steel bar becomes also complex.

The complex modulus method is basically the measurement of E^*. Usually this is done by measuring the real part of the dynamic modulus E_2' and the loss factor η.

CHAPTER 3

APPARATUS

3.1 General

The laboratory equipment described in this chapter was set up to perform the Geiger and the Complex Modulus tests. The first test is described by P.H.Geiger [16], while the second test is described by H.Oberst[17] in two articles published in the "Acoustica".

Every effort was made to keep the measuring techniques as close as possible to those specified by these authors. Any major deviations from the original methods will be mentioned in this chapter.

3.2 Laboratory Equipment

The laboratory equipment necessary to obtain the desired physical quantities of both tests can be classified and listed as follows:

A. Electronic Equipment

ITEM	QUANTITY	DESCRIPTION
(1)	1	Beat Frequency Oscillator, Bruel & Kjaer, Type 1014, Serial 20491.
(2)	1	Microphone Amplifier, Bruel & Kjaer, Type 2603, Serial 40914.
(3)	1	Level Recorder, Bruel & Kjaer, Type 2304, Serial 21743.

---

[16] P.H.Geiger, op.cit.

[17] H.Oberst, op.cit.

ITEM	QUANTITY	DESCRIPTION
(4)	1	One-third Octave set Filter, Bruel & Kjaer, Type 1609, Serial 22230.
(5)	1	Condenser Microphone, Bruel & Kjaer, Type 4131, Serial 40716, with a built-in cathode follower, Bruel & Kjaer type 2612.
(6)	1	Vacuum Tube Voltmeter, Bruel & Kjaer, Type 2409, Serial 41049.
(7)	1	Cathode-ray Oscilloscope, Hewlett-Packard, Model 120A, Serial 2566.
(8)	1	Precision Phase Meter, Ad-Yu Type 405H, Serial 1146.
(9)	1	Frequency Analyzer, Bruel & Kjaer, Type 2105, Serial 38272.
(10)	1	Frequency Counter, Beckman Model 5230 Bp, Serial 356.
(11)	1	Power Amplifier, Heathkit Model W-5M.
(12)	1	Audio Signal Generator, Hewlett-Packard Model 205 AG, Serial ASGA21.
(13)	1	Sound-level meter, General Radio Type 1551-A, Serial 244, with attached power supply, General Radio Type 1262-A, Serial 266.
(14)	1	Accelerometer Set, Bruel & Kjaer Type 4308, Serial 41322.
(15)	1	Vibration Pick-up Preamplifier, Bruel & Kjaer, Type 1606, Serial 39810.

B. Mechanical Equipment

ITEM	QUANTITY	DESCRIPTION
(1)	1	Bending Wave Apparatus, Bruel & Kjaer, Type 3930, Serial 56844.
(2)	1	Flynn-Weichsel, Self-excited Synchronous motor, Wagner Electric Corp., type 113, 3-phase, 5 h.p. 1800 r.p.m. 220 volts, 11.1 amps, 60 c.p.s. Serial 339218
(3)	1	"Sirocco" fan. Canadian Sirocco Co., Size 135.

ITEM	QUANTITY	DESCRIPTION
(4)	1	14 inch diameter Air Duct, 18 gauge, terminated with acoustical horn, as shown in Photograph (4).

C. Auxiliary Equipment

ITEM	QUANTITY	DESCRIPTION
(1)	1	0-100 grams scale, Henry Troemner Co.
(2)	1	Junction Box, Bruel & Kjaer, Type JJ 0004.
(3)	1	Ohmmeter, Heathkit Model MM1.
(4)	1	Recording Paper, Bruel & Kjaer Type 3612.
(5)	1	Variac, Type 200-CM
(6)	1	Lens, Stanley Type 701, Serial R.E.L. os 939
(7)	1	Microscope Stand, Spencer Lens Serial No. os 950.
(8)	1	0-25 mm Micrometer Caliper Head, Brown & Sharpe, Mfg.Co.
(9)	1	o-25 mm Outside Micrometer Caliper, Central Scientific, Model 72655.
(10)	1	Bars, and four plates with suitable cross-sections and finished surfaces for proper clamping and coating. The dimensions were as follows:
	25	bars cold-rolled, 1 foot length, 5/16 in. width, 1/8 inch thickness.
	11	bars, cold-rolled, 1 foot long, 5/16 in. wide, 1/4 in. thick.
	4	plates, hot-rolled, 20 in. long, 20 in. wide, 1/4 inch thick.
(11)	1	Electromagnetic Exciter (See Figure (7)).
(12)	1	0-300 pounds lever-arm balance. Fairbanks-Morse.
(13)	1	Reverberation-time Protractor, Bruel & Kjaer, Type SC. 3361.

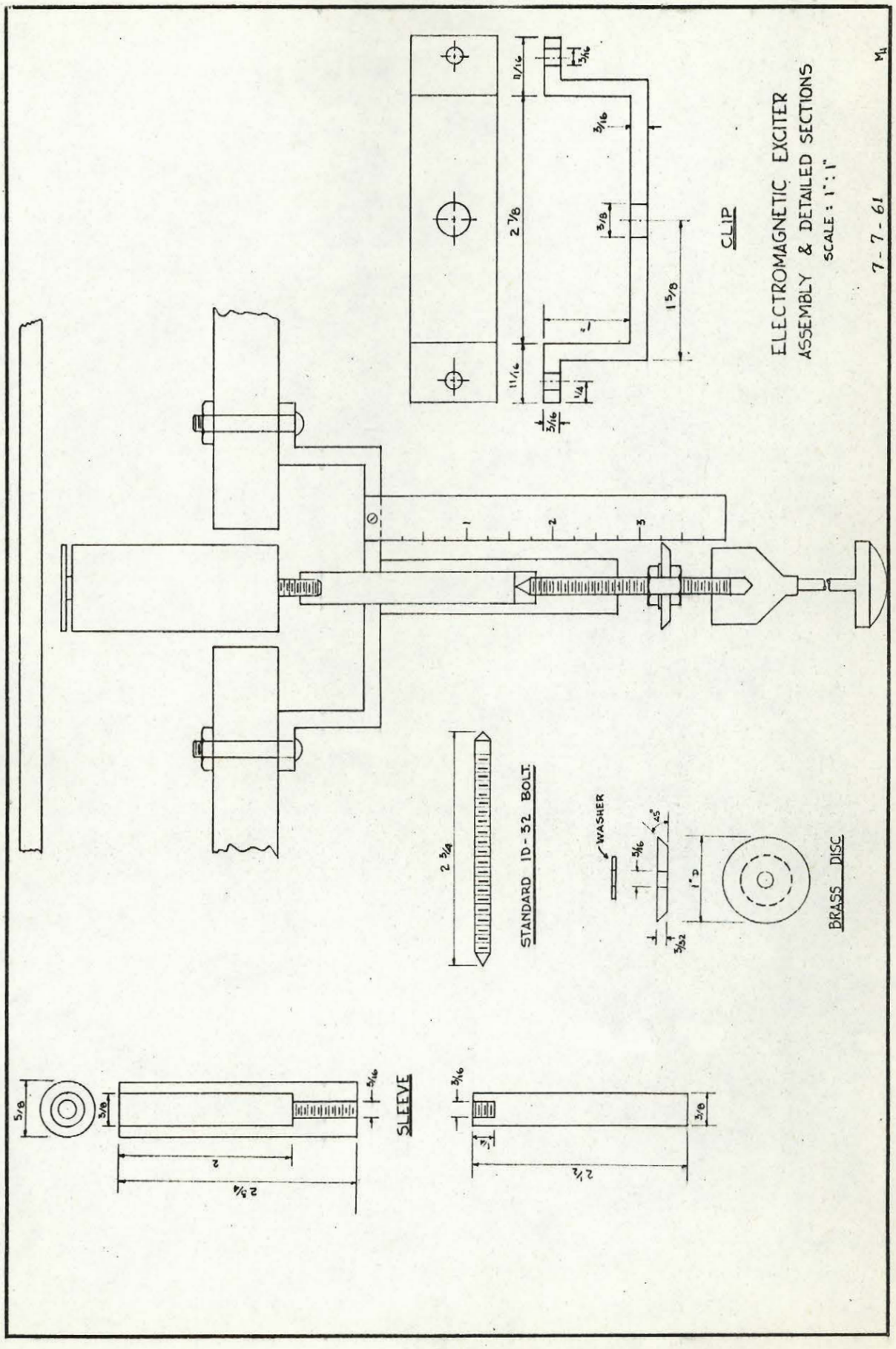
ELECTROMAGNETIC EXCITER
ASSEMBLY & DETAILED SECTIONS
SCALE : 1" : 1"
7-7-61
M4
CLIP
STANDARD ID-32 BOLT
WASHER
BRASS DISC
SLEEVE

Figure (7)

D. Damping Materials

The damping materials tested are listed below on a group basis:

Group I

Type	Material	Form
Bituminous	A	Liquid
	B	Tape
	D	Viscous
	G	Viscous
	H	Viscous

Group 2

Water-based	I,C-3,C-6	Liquid, pad
	J,C-4,C-7	ditto
	K,C-5,C-8	ditto

Group 3

Synthetic	F	Viscous

Group 4

Epoxy	C-1, C-2	Pad

Group 5

Others	E	Viscous

3.3 Physical Arrangement of Equipment

The equipment was arranged in four groups:

1. The Complex Modulus Equipment,Photograph (2).
2. The Geiger Plate Test Equipment, Photograph (3).
3. The Ventilation Duct Equipment, Photograph (4).
4. The Coating Equipment, Photograph (6).

The Microphone Amplifier and the Level Recorder were shared between Groups 1 and 2. Group 4 equipment was located in ventilated areas and near cleaning facilities. Equipment for Group 3 was located in an acoustics laboratory essentially free from floor vibrations and excessive ambient noises.

As mentioned previously, the plates used in this project were made of hot-rolled rather than cold-rolled steel. This constitutes the only major deviation from the equipment used for the original Geiger Test.

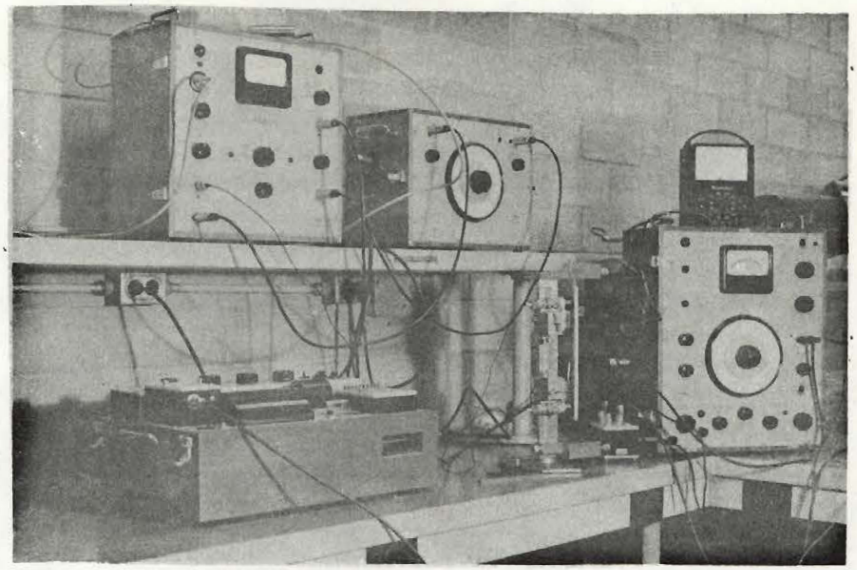

Photograph (2): Experimental arrangement of the Complex-Modulus Test.

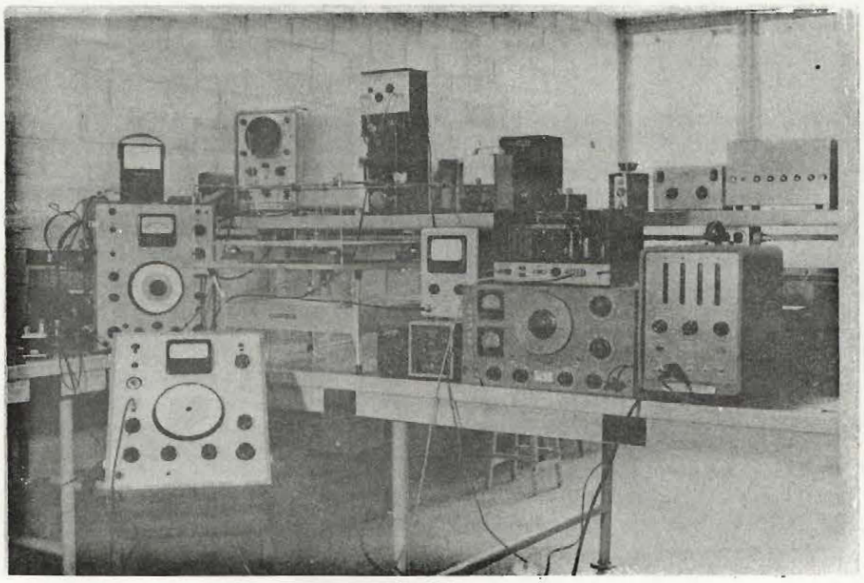

Photograph (3): Experimental arrangement of the Geiger Plate Test.

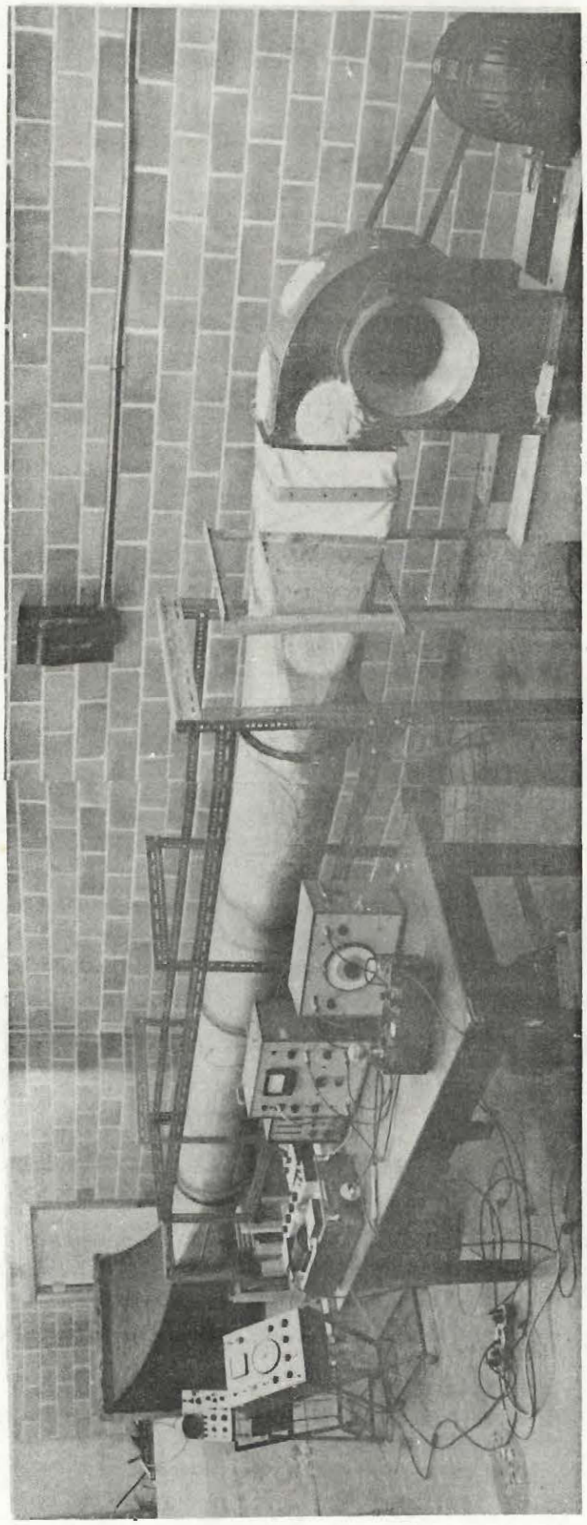

Photograph (4): Ventilation Duct Model

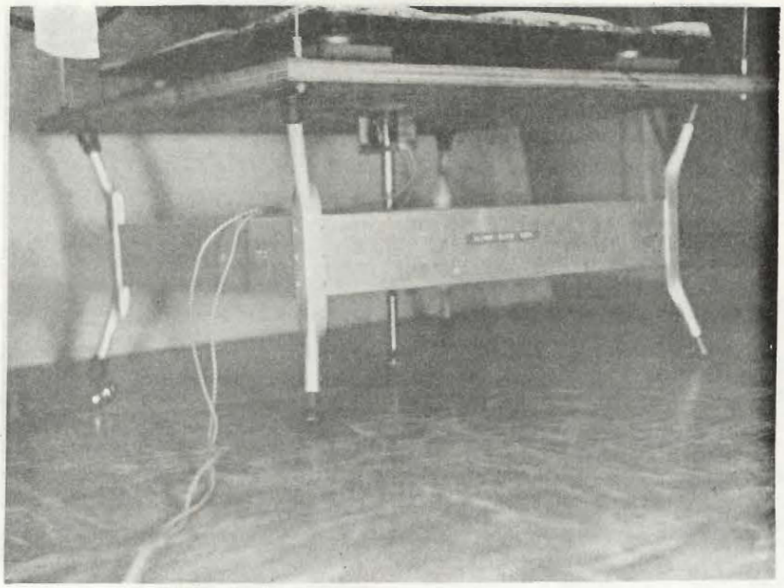

(a)

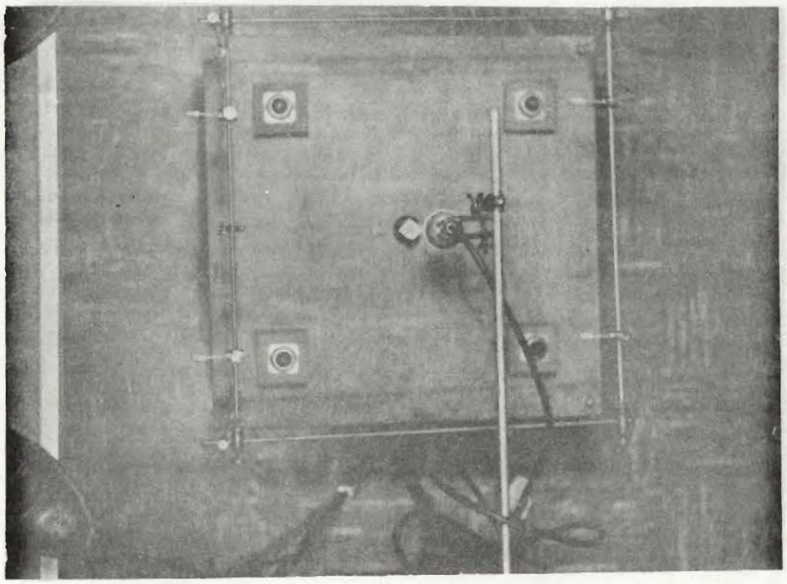

(b)

Photograph (5): (a) Geiger-plate stand supporting one plate - side view.

(b) Same as (a) with the plate removed - top view.

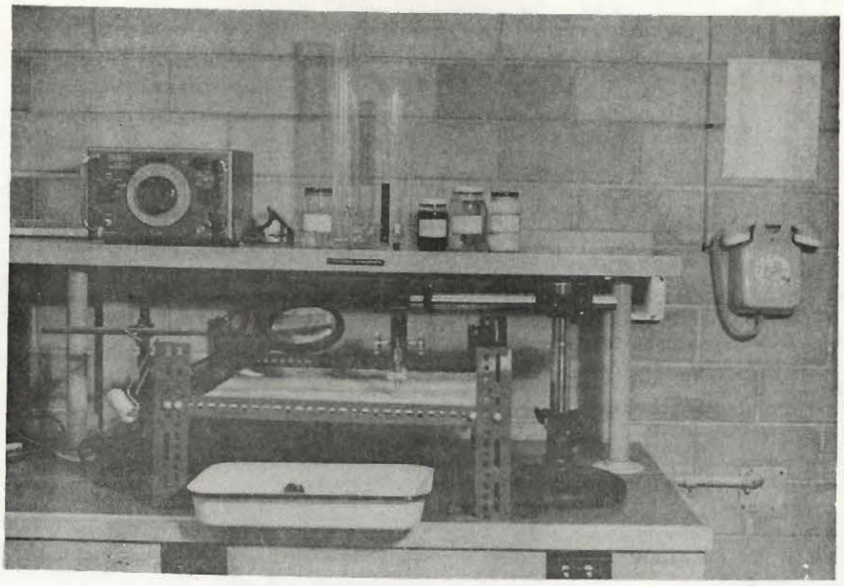

(a)

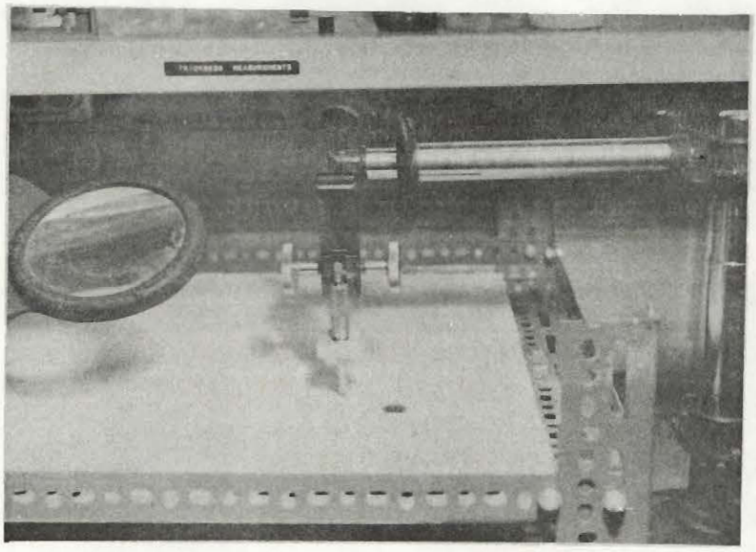

(b)

Photograph (6): (a) Arrangement for coating the Geiger plates.

(b) Shows a micrometer for measuring the coating-layer thickness and a Magnifying glass for examining the uniformity of the layer surface.

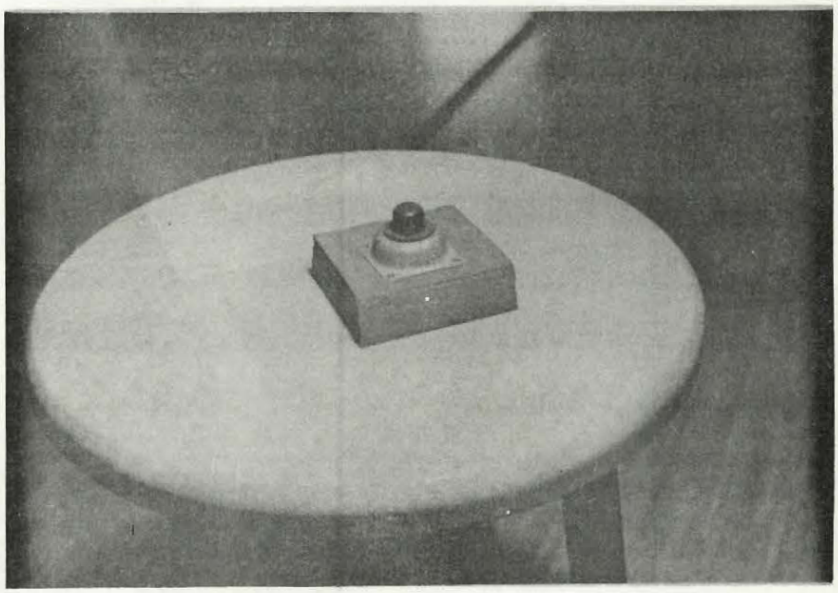

(a)

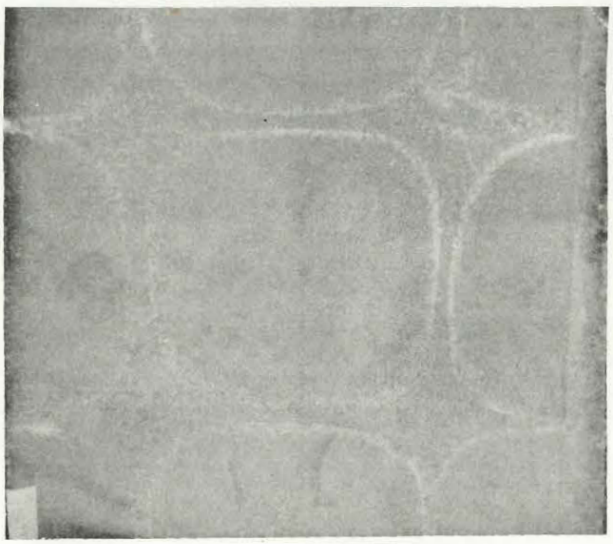

(b)

Photograph (7): (a) elastic support for the Geiger plates.
(b) node contours of Plate 2.

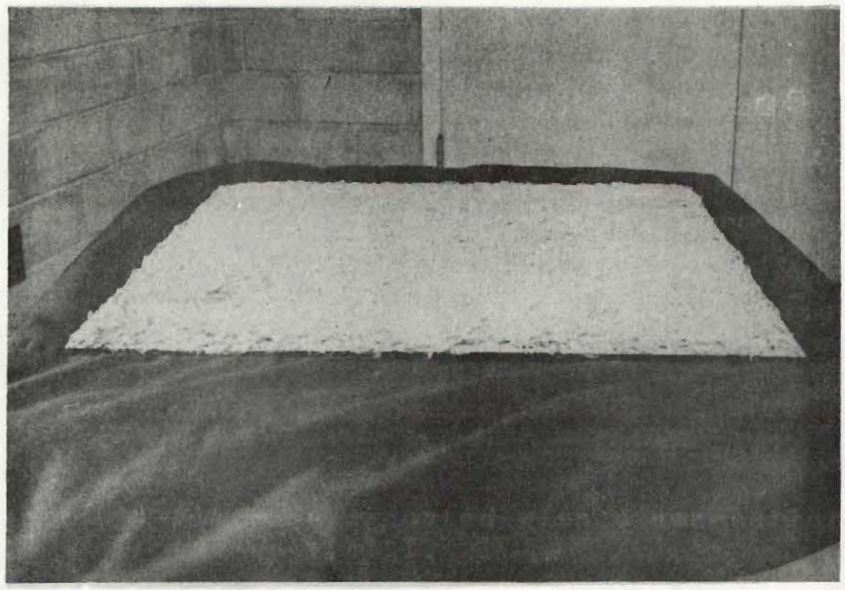

Photograph (9): Plate 2 coated with damping material E.

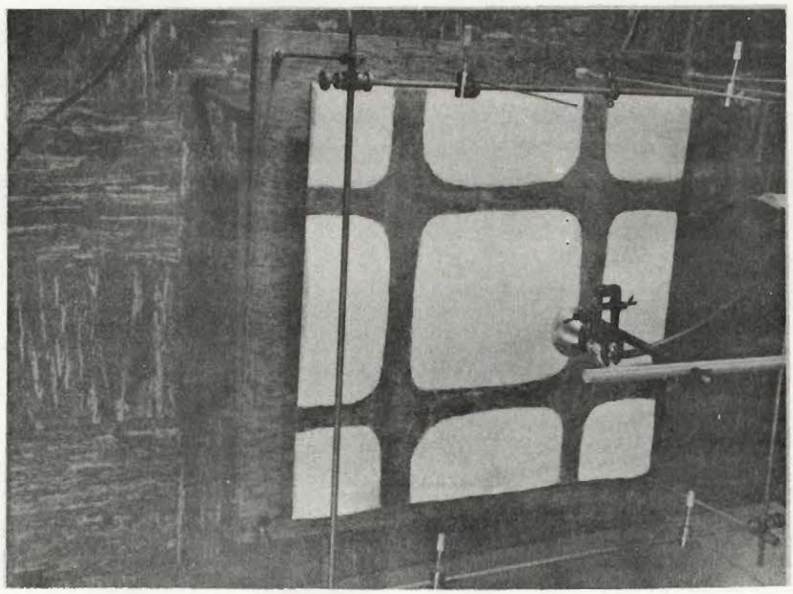

Photograph (10): Plate No.1 coated with a non-uniform thickness of material I.

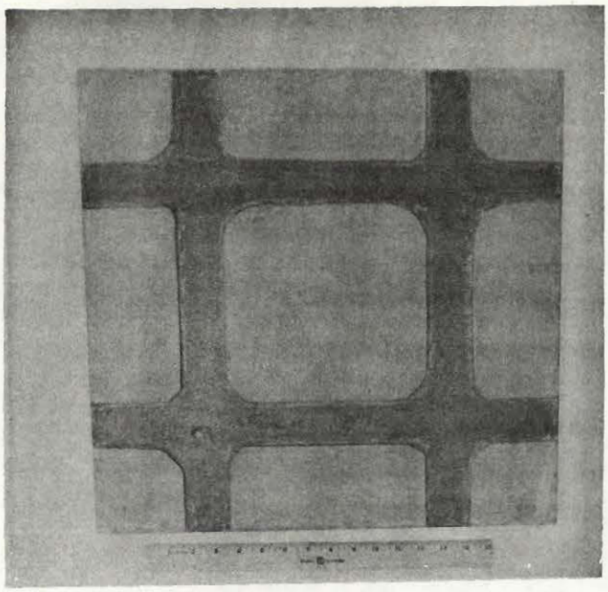

(a)

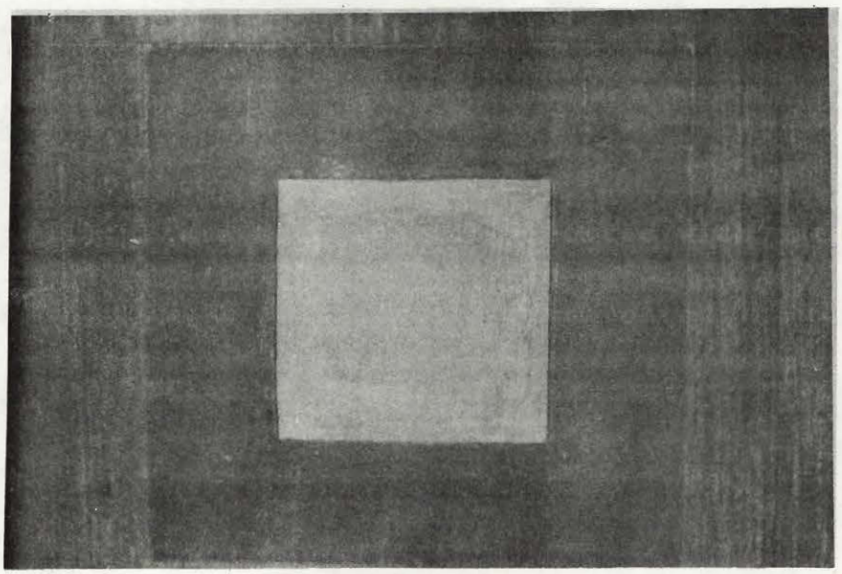

(b)

Photograph (11): Plate No.1 partially coated with material F.

(a) material on node lines is removed.
(b) 24.4% of the plate area coated.

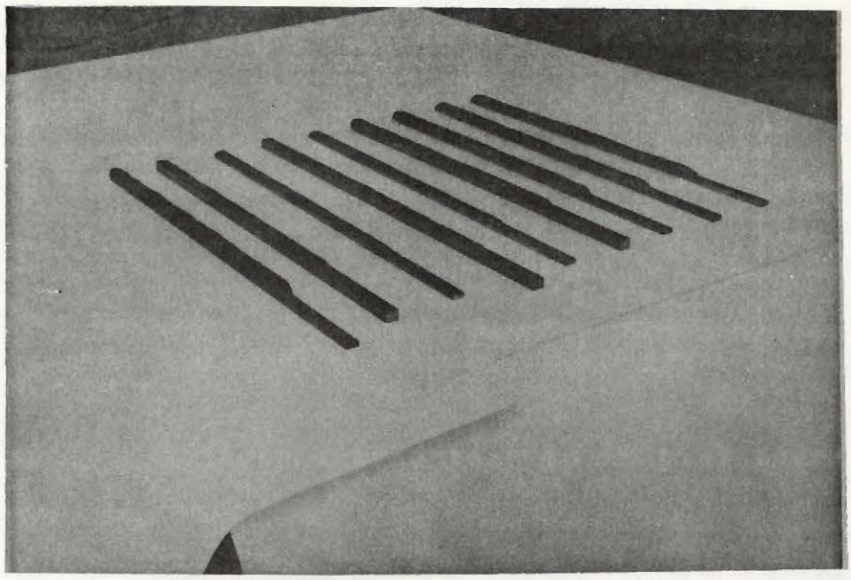

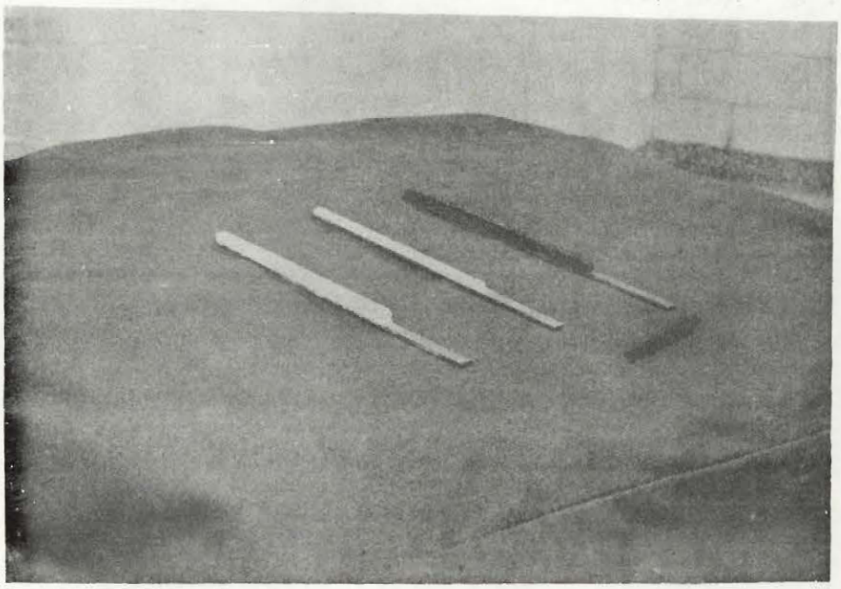

Photograph (12): Shows sample bars in initial coating stages.

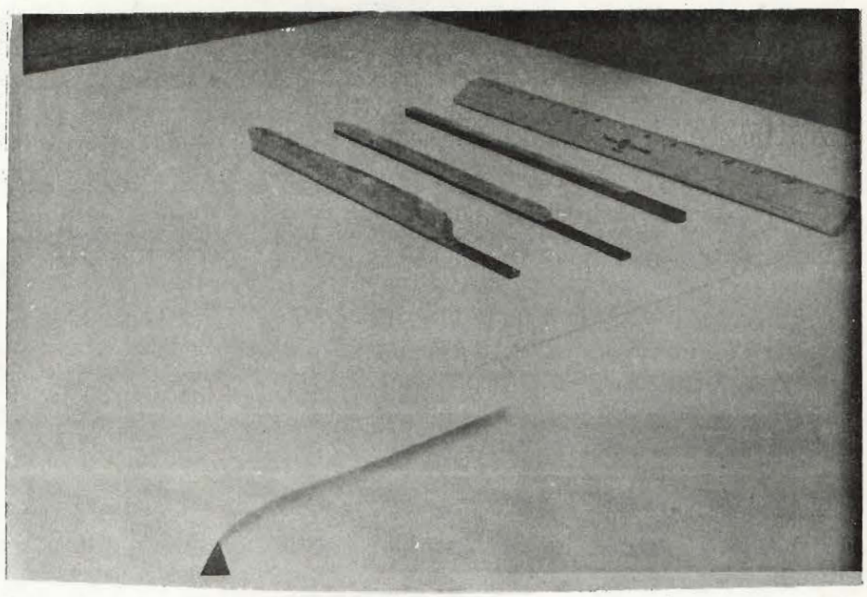

(a)

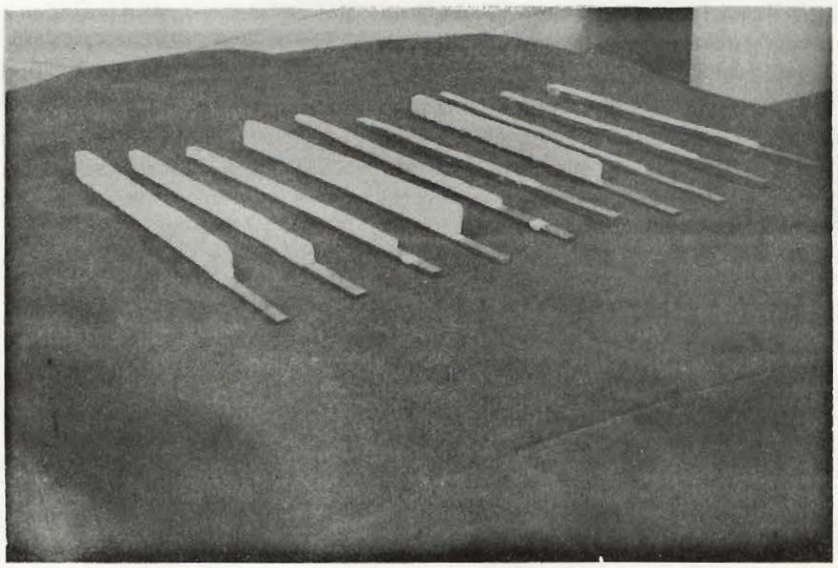

(b)

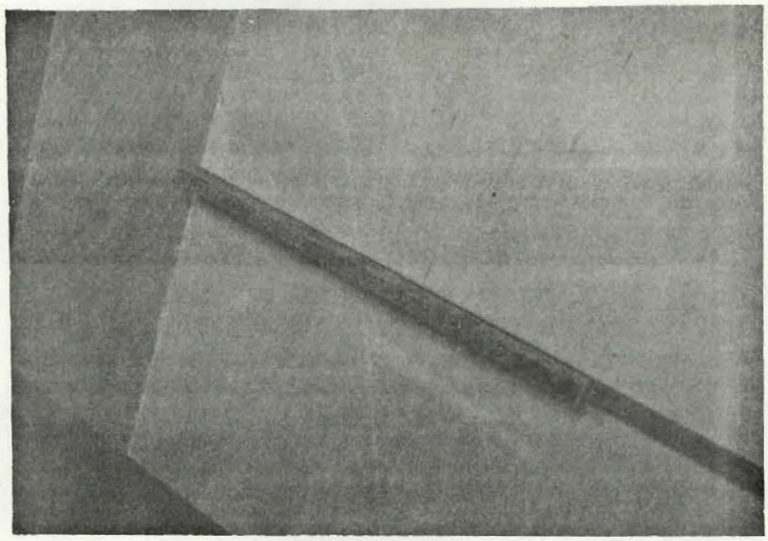

(c)

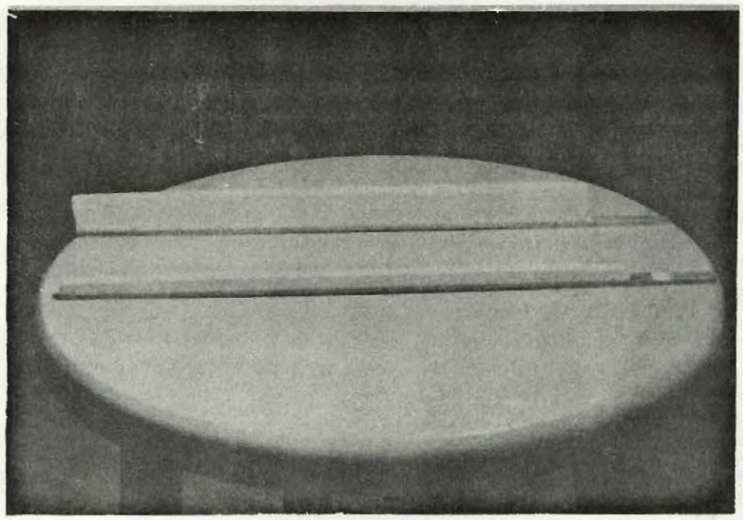

(d)

Photograph (13): Shows sample bars coated with different materials and thicknesses and ready for test on the bending wave apparatus.

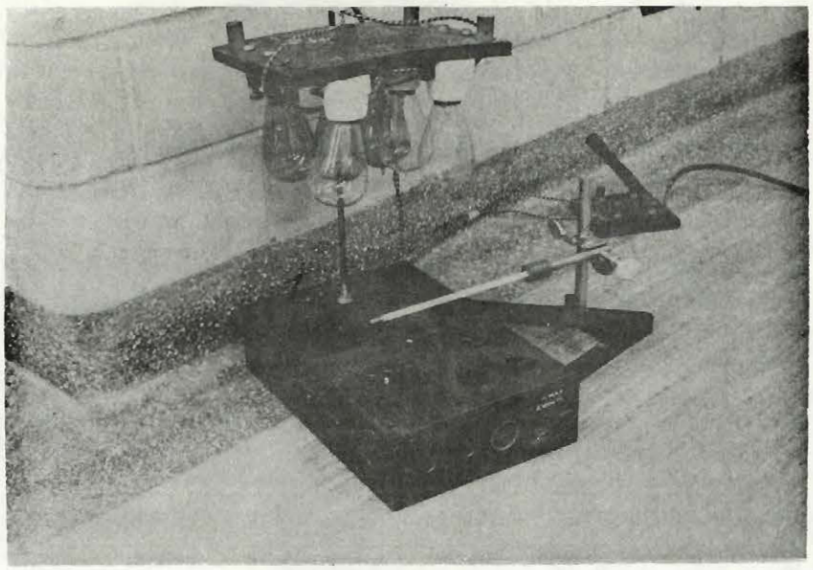

Photograph (14): Heater-lamps used for drying some damping materials coated on sample bars.

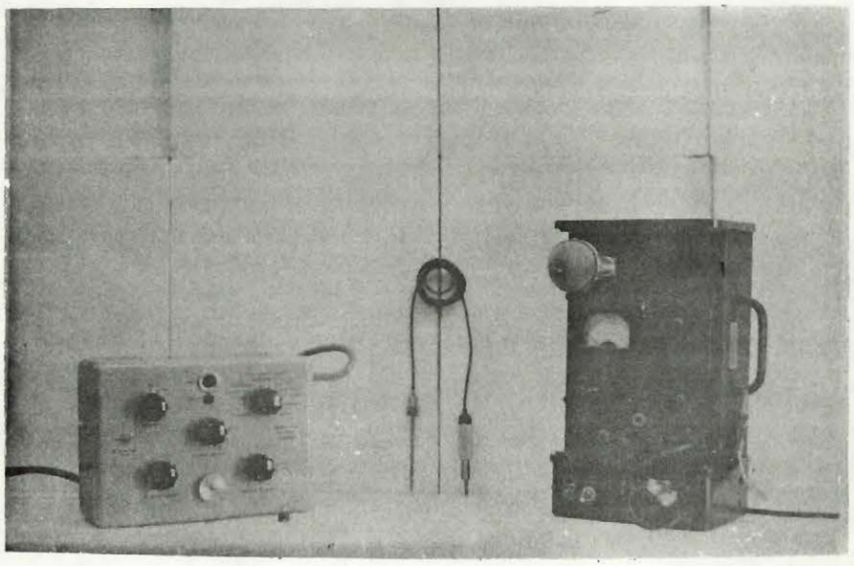

Photograph (15): Left to right - preamplifier, accelerometer and sound level meter used for velocity and acceleration measurements on the ventilation duct surface.

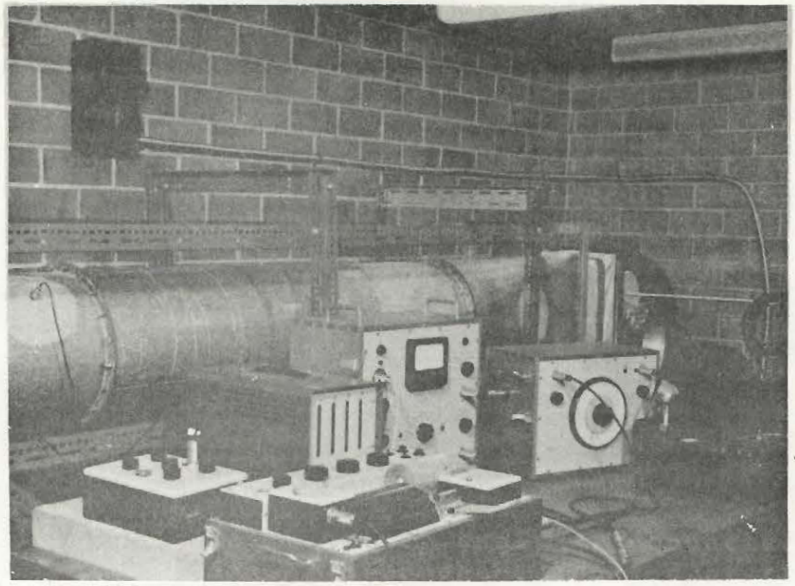

Photograph (16): Shows some coated areas on the fan-housing and duct-shell with accelerometer connected to the measuring equipment.

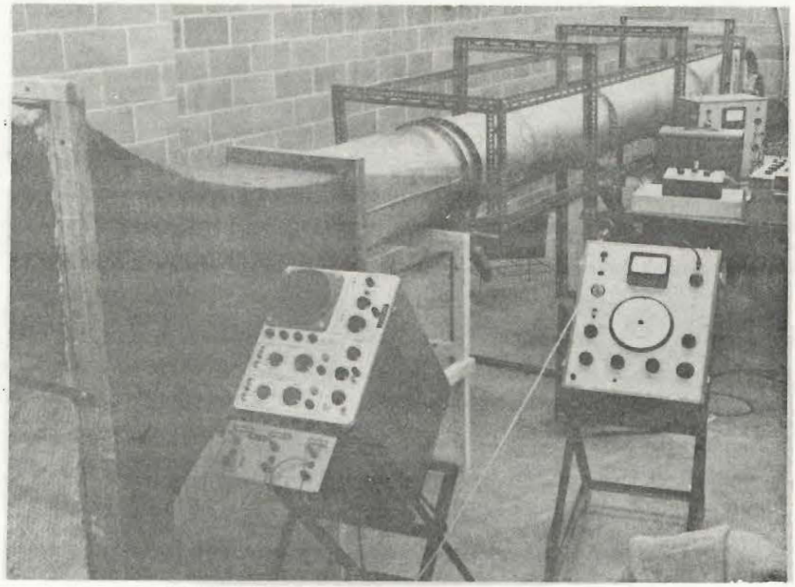

Photograph (17): Shows the frequency analyzer connected to the condenser microphone located at the throat of the exponential acoustic horn.

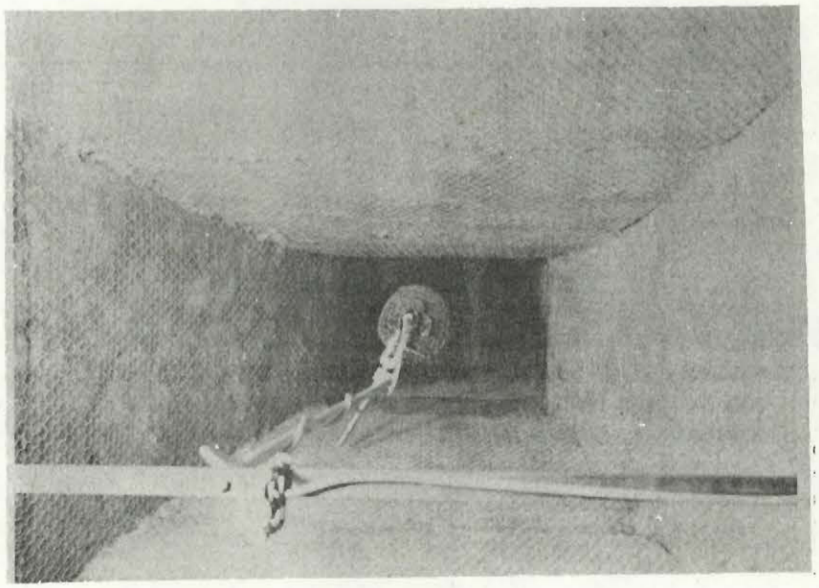

Photograph(18): The circular holes visible in the background were used to create air turbulence. Located in front of these is the egg crate straightener. In the forefront is the condenser microphone located at the throat of the exponential horn.

CHAPTER 4

EXPERIMENTAL PROCEDURES

4.1 General

This chapter outlines the manner in which the results presented in Chapter 5 were obtained.

The testing procedures described here include the adjustment of the measuring equipment, the preparation of the samples and the actual testing. This is supplemented by photographs and illustrations.

4.2 The Geiger Plate Test

Figure (8) is a block diagram showing the connections of the measuring equipment. Experience proved that the following items were of vital importance for obtaining accurate measurements:-

1. Oscillator stability: This will ensure constant driving force once the plate is vibrating in resonance.

2. Power-Amplifier response: The gain of the amplifier must be flat over the frequency range 100-250 cycles/second.

3. Accurate location of the plate nodes: This is important for accurate support of the plate over any number of tests. These nodes must be symmetrical and clearly marked on the plate surface.

4. Lossless elastic supports: The supports for the plate at its four selected nodes must introduce no damping during the test. Any appreciable stiffness in the supports gives losses which cannot be accounted for.

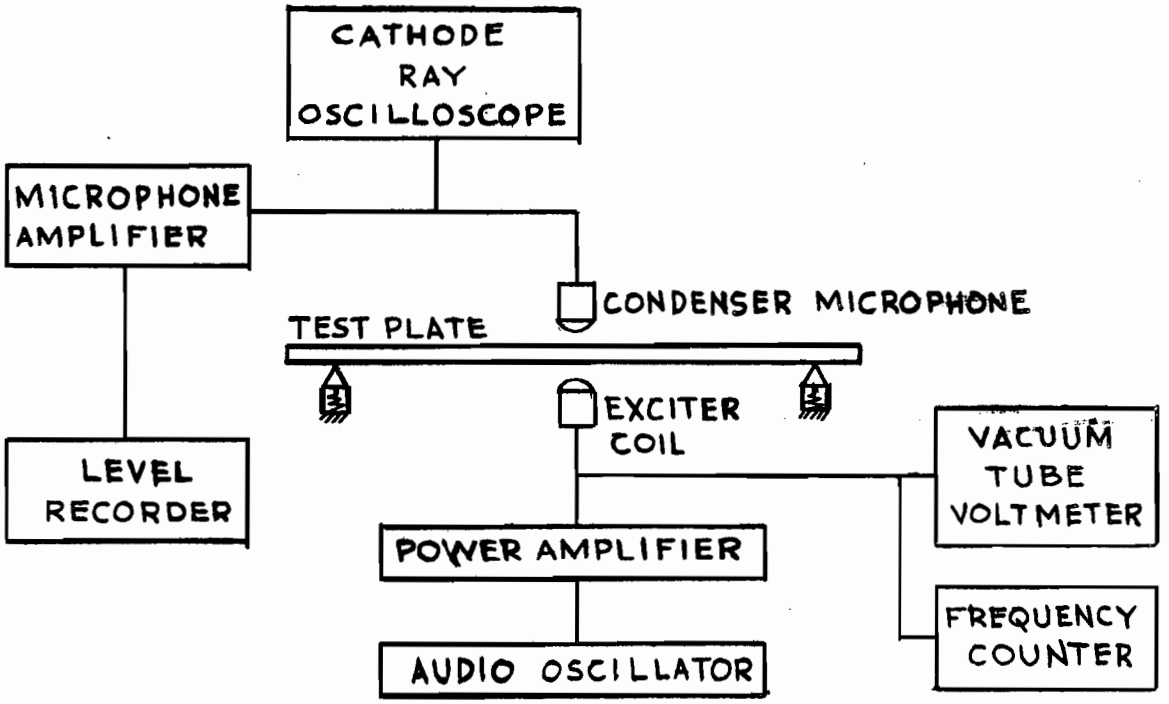

(a) GEIGER PLATE TEST

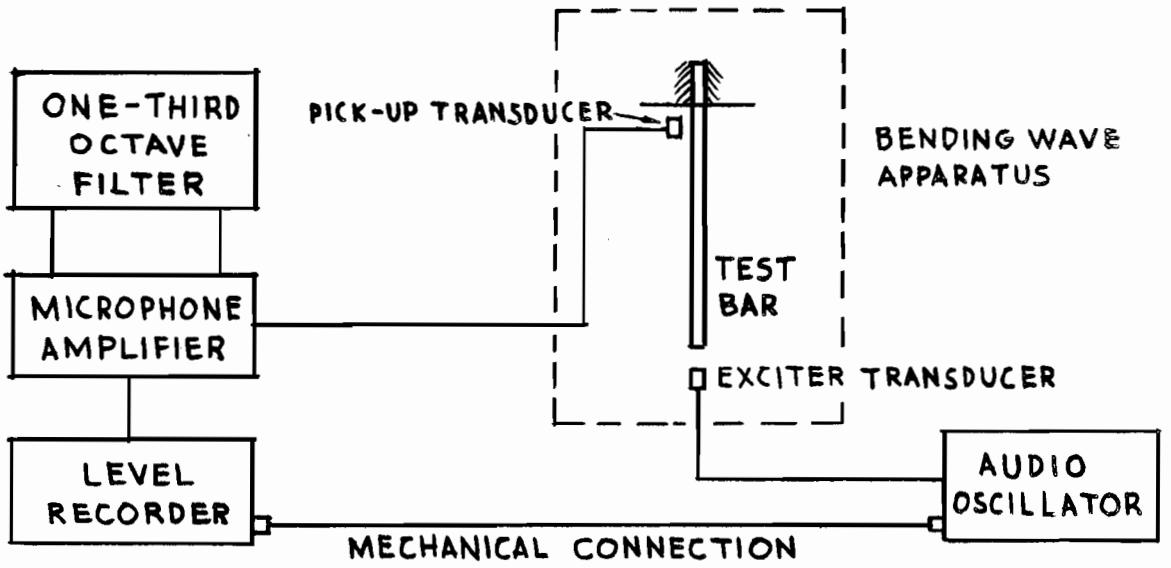

(b) COMPLEX MODULUS TEST

Fig.(8) - SCHEMATIC DIAGRAM OF THE MEASURING EQUIPMENT

5. Suitable capacity of the driving coil: The coil must induce sufficient flux to drive the plate into resonance. The vibration amplitude due to the fundamental frequency must be large enough to generate a sound tone 15-20 db higher than ambient noise level. Extremely large vibration amplitudes are not suitable for this test.

6. Accurate positioning of the transducers: The condenser microphone must remain at an optimum height (5 inches) above the centre of the plate. The driving coil should be at optimum distance below the centre of the plate. A large separation between the coil and the plate will increase the reluctance of the air gap, while a small separation might cause physical contact at resonance. Provision for adjusting this separation was necessary.

7. Accurate positioning of the test plate: The test plate must remain simply supported and in a horizontal position. The plate stand should be as isolated from air streams and impulse noises etc. as possible.

Fortunately, the above requirements were carefully followed and were the basic reasons for the successful tests whose results are presented in Chapter 5.

The actual testing on the Geiger plates started by locating the node lines of the four test plates. This was done by spreading fine salt over the plate surface and tuning the

oscillator to the fundamental frequency of the plate. The new salt position was noted (see photograph (7)), and the node lines were symmetrically located and marked on the plate surface. This surface was then used to position the supports, while the other plate surface was availabe for coating.

Appendix A is a sample of the laboratory record. As shown, the readings are divided into the three following main groups:

(a) Physical constants of the steel plate and the damping layer. These give some parameters of the equivalent circuit (see Section 2.4), such as L_p, f_{op}, Q_p, τ, L, Q and f_o.

(b) Coil Input readings. This record is essential for the accuracy of repetitive tests.

(c) Acoustical readings: These give further parameters of the equivalent circuit such as T_p, δ_p, T and δ.

4.3 The Complex Modulus Test

The settings and adjustments of the equipment shown in Figure (8b) are given in the Instructions supplied by the Manufacturer[18]. These include the following:

---

[18] Bruel & Kjaer, Instructions and Applications for Types 1014, 2603, 2304, 1609 and 3930.

1. Adjustment of the oscillator for the zero-frequency.
2. Sensitivity check of the microphone amplifier.
3. Optimum settings (potentiometer, paper speed and writing speed) of the level recorder.
4. Synchronization of the recording-paper speed on the Level Recorder with that of the frequency sweep of the Beat Frequency Oscillator and the one-third octave filter.

Two important settings remained to be determined, however, since they were not given by the manufacturer:

First: When tracing the vibration resonance curves for a sample bar, one needs to know how fast the frequency sweep should be. If the frequency sweep is too fast and the response time of the bar is long, the resonant frequencies cannot be determined accurately. Thus the resonance curves cannot be traced since the oscillator and the paper speed (on the level recorder) must have been synchronized previously. This happened frequently when testing heavily coated bars. Hence, it was decided to record at a low speed of 0.1 millimeters/second. A trace using this speed is shown in Photograph (8). Another advantage of using low recording speed is to allow the vibration amplitude due to one mode to decay before the next mode. A fast speed would amount to recording a superposition of the amplitudes due to the two modes.

Second: The correct voltage across the exciter transducer: A relatively high voltage would drive the test bar into its destruction region. The measured damping is then very much higher than the correct one. Also high voltages might damage the 1500 ohm coil in the transducer. For these reasons it was decided to keep the voltage below 10 volts for lengthy tests, while for short periods, 30 volts was considered safe.

The correct settings of the recording speed and exciter voltage were necessary to carry out the Frequency Response Method (see Section 1.3). This method was used at the beginning of each test to determine the resonant frequencies and the vibration-amplitude vs. frequency response of the sample.

Once the equipment was ready for measurements the testing procedure was done in the following steps:

1. The sample bar was mounted on the Bending Wave Apparatus. The top end of the bar was rigidly clamped leaving a free length of ten inches approximately. (The apparatus was designed to test bars of twelve inches maximum and five inches minimum free length). The exciter transducer was then positioned near the free end of the bar, while the pick-up transducer was positioned as close to the clamped end as possible*. By making the free length of the bar

*The ideal location for the pick-up transducer was opposite the clamped end of the bar. Any damping, due to the magnetic field of the transducer then had no effect at a node.

equal to ten inches, the transducers were separated by a distance sufficient to minimize their cross-talk level.

Before the transducers were rigidly clamped in their selected positions along the bar, the separation of their heads from the bar surface was adjusted. The optimum separation recommended by the manufacturer was 1/8 inch and equal for both transducers. However, this separation was critical and had to be selected for each particular test, and had to be large enough to prevent the permanent magnetic field (from the transducers) from damping the oscillations and hence disturbing the measurement. Conversely, the separation had to be small enough, especially in the case of highly damped bars, so that the detected signal could be recorded with the available gain of the amplifier.

2. The reverberation-time method was then carried out. The bar was driven at its fundamental resonant frequency and the driving force was removed once the vibration amplitude reached a steady value. The slope of the recorded decay curve was a measure of the decay time and the decay rate.

3. The bar was then coated and the above procedure repeated. The free length of the bar and the positions of the transducers were maintained.

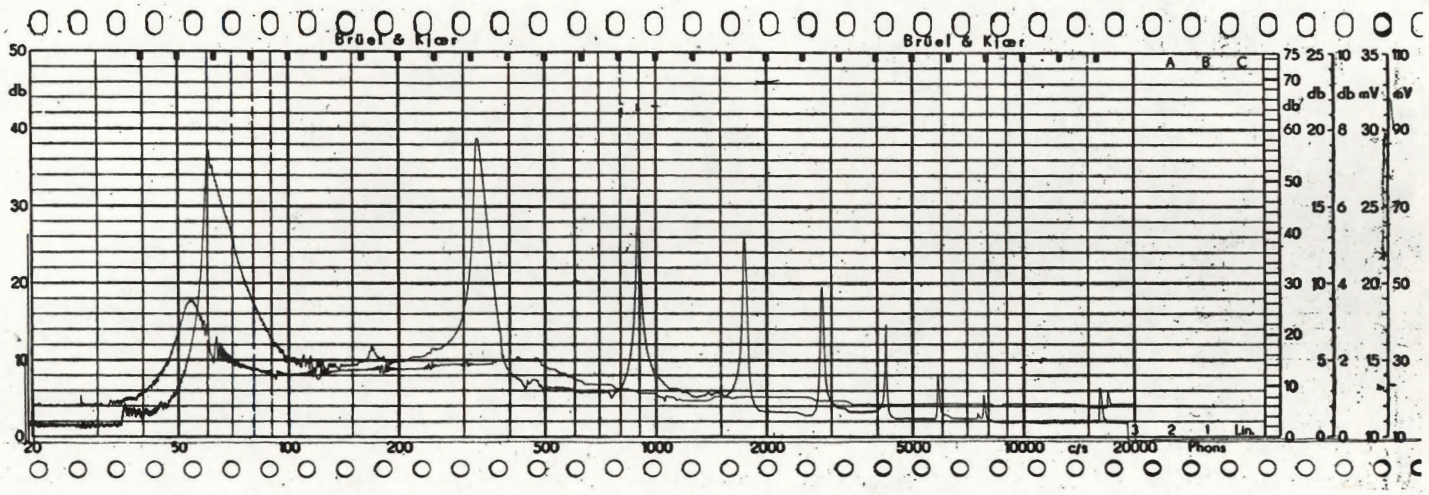

Photograph (8): Frequency Response of
Bar No.44

Top: Uncoated bar.
Bottom: Bar coated

4. The procedure was also repeated for various coating thicknesses and for higher order modes.

In order to obtain the loss factor and the dynamic modulus of elasticity of the coating material, certain calculations were necessary.

A sample of such calculations using data from the Complex Modulus test is shown in Appendix B.

4.4 Preparation of the Samples

The process of coating plates and bars was quite simple. However, continuous attention was necessary to ensure that the coating layers were quite adequate with regard to the thickness, adhesion and uniformity.

The process followed logical steps which are summarized below:

1. The steel sample, plate or bar, was cleaned to remove any undesirable spots of dirt or grease. The physical dimensions and mass of the sample bar were noted. Also its decay rate was obtained, following the procedure stated in Section 4.3.
2. The sample plate was positioned on the table shown in Photograph (6). This table was made for the purpose of holding the plates in a horizontal position during the coating process. This was important to prevent the damping material from sagging non-uniformly to the sides, and also for thickness measurements. The sample bar was also positioned in a simple mould to simplify the coating process.

3. The damping material was applied to one surface of the sample and spread uniformly.
4. For some damping materials forced drying was used. This was done for coated bars only, using the heater lamps shown in Photograph (14).

   When coating the plate with pads (Material C - see Chapter 5), a thin cement layer was used to ensure proper adhesion.
5. In the final stage of the process, the surface of the coating was smoothed. The thickness and mass of the coating layer were obtained. Photographs (9), (10), (11), (12) and (13) show some coated bars and plates.

   Coated plates were supported in their stand accurately. Bars were also clamped rigidly in the Bending Wave Apparatus.

It is left to Chapter 5 to present the results of the experimental measurements.

CHAPTER 5

EXPERIMENTAL RESULTS

5.1 General

The results of the tests on eleven materials are presented in this chapter and an interpretation of these results suggested. Some of the implications of these results are pointed out and further experimentation proposed.

5.2 Presentation of the Results

The results are divided into the following two main groups:

FIRST

(A) Evaluation of the damping properties of each material using the Geiger and Complex Modulus methods. These are presented in the form of graphs and tables.

(B) Results regarding the optimum coating procedure of these materials for maximum damping efficiency. These include the optimum area and shape of the coating layer.

SECOND - Results related to the testing methods. These are:

(A) Breakdown of the Complex Modulus Method.

(B) Possible improvement of both methods.

5.2.1 Results of the Uniform-Thickness Tests

The damping properties of the eleven tested materials for uniform thicknesses and room temperature were tabulated and plotted in the following order:

1. Resonance curves (Figures (9) to (27)). These curves were obtained from the Geiger Plate Tests, and their running parameter was the layer thickness τ. These curves were used to find the Q-factor of the coated plate at the particular values of τ.
2. Curves showing the reduction in the radiated sound pressure level vs. the coating layer thickness τ and mass L_g. These results were derived from the resonance curves, (see Figures (27) to (29)).
3. Resonant frequency vs. τ (Figures (29) to (34)).
4. Decay Rate vs. Frequency: (Figures (34) to (44)).
5. Decay Rate vs. τ (Figures (44) to (52)).
6. Loss-factor and imaginary modulus of elasticity vs. ξ and μ for material F (Figure (52)). Also the loss-factor vs. the ratio a for material F (Figure (53)).
7. Tables derived from Figures (9) to (53). (See Tables 1-8).

MATERIAL "A"

MANUFACTURER'S DATA

COLOUR:	Black
SOLIDS CONTENT:	85% basically asphalt
LBS/GALLON:	13.7
VISCOSITY:	300,000 c.p.s.
SAE COLD SLAM:	90% adhesion
SAE FLOW RATE:	60 sec/quart
DRYING RATE:	
Dry to touch -	30 minutes
Firm -	4 hours
BAKING SCHEDULE:	Material can be force-dried at temperatures up to 300°F.
SOUND DEADENING:	
Decay rate at 0°F. -	16 db/sec.
70°F. -	15 db/sec.
100°F. -	5.8 db/sec.
PRICE:	$0.45 per gallon (3.28 cents per lb.).

MATERIAL "B"

MANUFACTURERS' DATA

COLOUR:	Aluminum foil - Grey: Mastic - Black (basically asphalt)
FT/ROLL:	50
DIMENSIONS:	1 - 1/2" wide, 3/32" thick.
APPLICATION:	Direct, preferably in specific patterns at the points of maximum vibration.
ADHESION:	Permanent. Tape has selected adhesive spacers to create a positive sound wave interruption.
SERVICE TEMPERATURE:	-20°F to 400°F.
DECAY RATE:	
At 0.1 lbs/sq.ft. 84 cps:	23 db/sec. at 0°F. 25 db/sec. at 30°F. 24 db/sec. at 80°F.
At 0.1 lbs/sq.ft.160 cps:	31 db/sec. at 0°F. 32 db/sec. at 30°F. 30 db/sec. at 80°F.
At 0.1 lbs/sq.ft.281 cps:	31.5 db/sec. at 0°F. 33 db/sec. at 30°F. 30.5 db/sec. at 80°F.
PRICE:	$0.09 per foot. ($0.68 per lb.).

MATERIAL "D"

MANUFACTURERS' DATA

COLOUR:	Black
CONTENT:	A special blend of treated asphalt with fine cork particles producing a dry film of 65% cork and 5% mica and asbestos fibre filler by volume.
AVERAGE NON-VOLATILE:	66% by volume.
VISCOSITY:	Coarse paste.
LBS/GALLON	7.6
COVERAGE RANGE:	20-25 gallons per 100 sq.ft. (0.32" -).40" wet film thickness)
DRYING TIME:	
Touch -	6 hours
Through -	36 hours. (Minimum of five days drying time between coatings).
SERVICE TEMPERATURE LIMITS:	-20°F to 200°F.
APPLICATION:	Spray or trowel.
SOLVENT FOR CLEAN-UP:	Mineral Spirits.
FLAMMABILITY:	Wet - flash point 100°F. Dry - burns.
PRIMER:	Oxide-Chromate
PRICE:	$1.45 per imperial gallon (19.1 cents per lb.).

MATERIAL "E"

MANUFACTURERS' DATA

COLOUR:	Grey
CONTENTS:	Granulated cork
AVERAGE NON-VOLATILE:	57% by volume
VISCOSITY:	Soft paste
LBS/GALLON:	10
COVERAGE RANGE:	15-20 gallons per 100 sq.ft. (0.25" - 0.375" wet film thickness)
DRYING TIME:	
Touch -	6 hours
Through -	36 hours. (Minimum 5 days drying time between layers).
SERVICE TEMPERATURE LIMITS:	$0^{\circ}F.$ - $180^{\circ}F.$
APPLICATION:	Spray or trowel
SOLVENT FOR CLEAN-UP:	Water
FLAMMABILITY:	Wet - non-flammable Dry - fire-resistive
PRIMER:	Chromate Phosphate Vinyl Primer
PRICE:	$7.40 per imperial gallon (74.0 cents per lb.)

MATERIAL "F"

MANUFACTURERS' DATA

COLOUR:	Vista Green
CONTENT:	Epoxy and other natural and synthetic high polymers with suitable fillers.
TYPICAL APPLICATION:	Wet weight per sq.ft. = 0.024" thick layer on 20-22 gauge steel, applied by spray or trowel to sheet metal.
DENSITY, WET:	1.5
THERMAL CONDUCTIVITY: (K factor)	0.175 B.T.U./hr./ Sq.ft./^{o}F/ft.
SHRINKAGE ON DRYING:	25% to 28%
CURING TIME:	48 hours at room temperature, approximately 30 mins, at 250^{o}F.
MINIMUM DRYING TEMPERATURE:	50^{o}F.
DECAY RATE:	45 db/sec, at 80^{o}F.
FLAMMABILITY:	Non-flammable.
PRICE:	$14.25 per gallon ($1.10 per lb.).

MATERIAL "G"

MANUFACTURERS' DATA

COLOUR:	Black
CONTENT:	Asphalt, non-abrasive fillers in a non-toxic petroleum blend.
SOLIDS CONTENT:	82% minimum.
APPLICATION:	Spray
DRYNESS:	This is a three-stage deadener with different type drying rates, rapid, medium, slow.
SAGGING AIR DRY:	No sag on a 12" x 12" cold rolled steel panel, at 0.5 lbs/ sq.ft. dry weight.
SAGGING ON HEATING:	No sag on a 12" x 12" cold rolled steel panel at 0.5 lbs/sq.ft. at temperatures of up to 350°F.
COLD RESISTANCE:	No evidence of cracking with 25 inch-pounds impact force applied twice to the panel cooled to -10°F and coated up to 1/8" thick layer.
FLASH POINTS:	Type 1 - 0°F (Rapid dry) Type 2 - 40 - 60°F (medium dry) Type 3 - 100°F (slow dry)
SOUND DEADENING:	Applying 0.5 lbs (dry) material/sq.ft. the sound decay is not less than 8 db/sec. from 0-100°F. not less than 14 db/sec. at 70°F.
VISCOSITY:	Core penetrometer method. ASTM D217-44T Limits 330-350°F.
SETTLING:	30 days minimum time.
PRICE:	$0.60 per gallon. (6 cents per lb.).

MATERIAL "H"

MANUFACTURERS' DATA

COLOUR:		Black
COMPOSITION:		Oxidized mid-continent asphalt, asbestos fibre and magnesium silicate - 58% petroleum naphtha (boiling range 190 - 250°F) - 42%
WEIGHT/GALLON:		8 pounds
FLASH POINT, CLOSED CUP:		27°F.
VISCOSITY:		350-370 core penetration, 150 grams.
APPLICATION:		By spray or trowel.
DRYING TIME:		1- 4 hours when applied 1/16" thick.
DRY FILM PROPERTIES:		
(a) Heat Resistance	-	may be baked or used at temperatures of at least 275°F without danger of sagging or running.
(b) Cold Resistance	-	adhesion and toughness good at at least -10°F in slam test.
(c) Chemical Resistance	-	withstands water, dilute acids and alkalis. Film is resoluble when soaked in oil, naphtha, or gasoline.
FLAME RESISTANCE:		Burns under direct flame.
PRICE:		$0.70 per gallon (8.75 cents per lb.).

MATERIAL "I"

MANUFACTURERS' DATA

COLOUR:	Off-white
TOTAL SOLIDS CONTENT:	63%
VISCOSITY:	Pasty
DENSITY:	Wet - 1.5 Dry - 1.3
SHRINKAGE ON DRYING:	27%
THERMAL CONDUCTIVITY: (K factor)	0.175 B.T.U./hr/sq.ft/^{o}F/ft.
DECAY RATE:	30 db/sec. at 55^{o}F. 70 db/sec. at 70^{o}F. 45 db/sec. at 75^{o}F. 40 db/sec. at 78^{o}F. 22 db/sec. at 100^{o}F.
APPLICATION RATE:	3 lb/minute.
TYPICAL APPLICATION	
THICKNESS ON 20/22 GAUGE STEEL:	3oz wet weight/sq.ft. - equivalent to 0.024" wet or 1.9 oz dry weight/sq.ft. - equivalent to 0.017" dry.
MAXIMUM THICKNESS PER COAT ON VERTICAL SURFACES:	3/16" wet
DRYING TIME FOR 0.024" WET COAT:	Approximately 20 minutes at 248^{o}F.
SAFE DRYING TEMPERATURES FOR 0.024" wet coat:	50^{o}F minimum; 302^{o}F maximum.
PRICE:	25 cents per lb.

MATERIAL "J"

MANUFACTURER'S DATA

COLOUR:	Off-white
TOTAL SOLIDS:	68%
VISCOSITY:	Pasty
DENSITY:	
Wet -	1.45
Dry -	1.35
SHRINKAGE ON DRYING:	27%
DECAY RATE:	55 db/sec at 72°F.
APPLICATION RATE:	3 lb/min.
TYPICAL APPLICATION:	3 oz wet weight/sq.ft.
THICKNESS ON 20/22 GAUGE STEEL:	Equivalent to 0.025" wet or 2 oz. dry weight/sq.ft. equivalent to 0.018" dry.
MAXIMUM THICKNESS PER COAT ON VERTICAL SURFACES:	1/8" wet
DRYING TIME FOR 0.025" WET COAT:	Approximately 45 minutes at 212°F.
DRYING TEMPERATURES:	50°F minimum, 212°F maximum.
PRICE:	30 cents/lb.

MATERIAL "K"

MANUFACTURER'S DATA

COLOUR:	Off-white
VISCOSITY:	Pasty
DECAY RATE:	46 db/sec. at 0.5 dry lb/sq.ft.
PRICE:	30 cents/lb.

No other data was available.

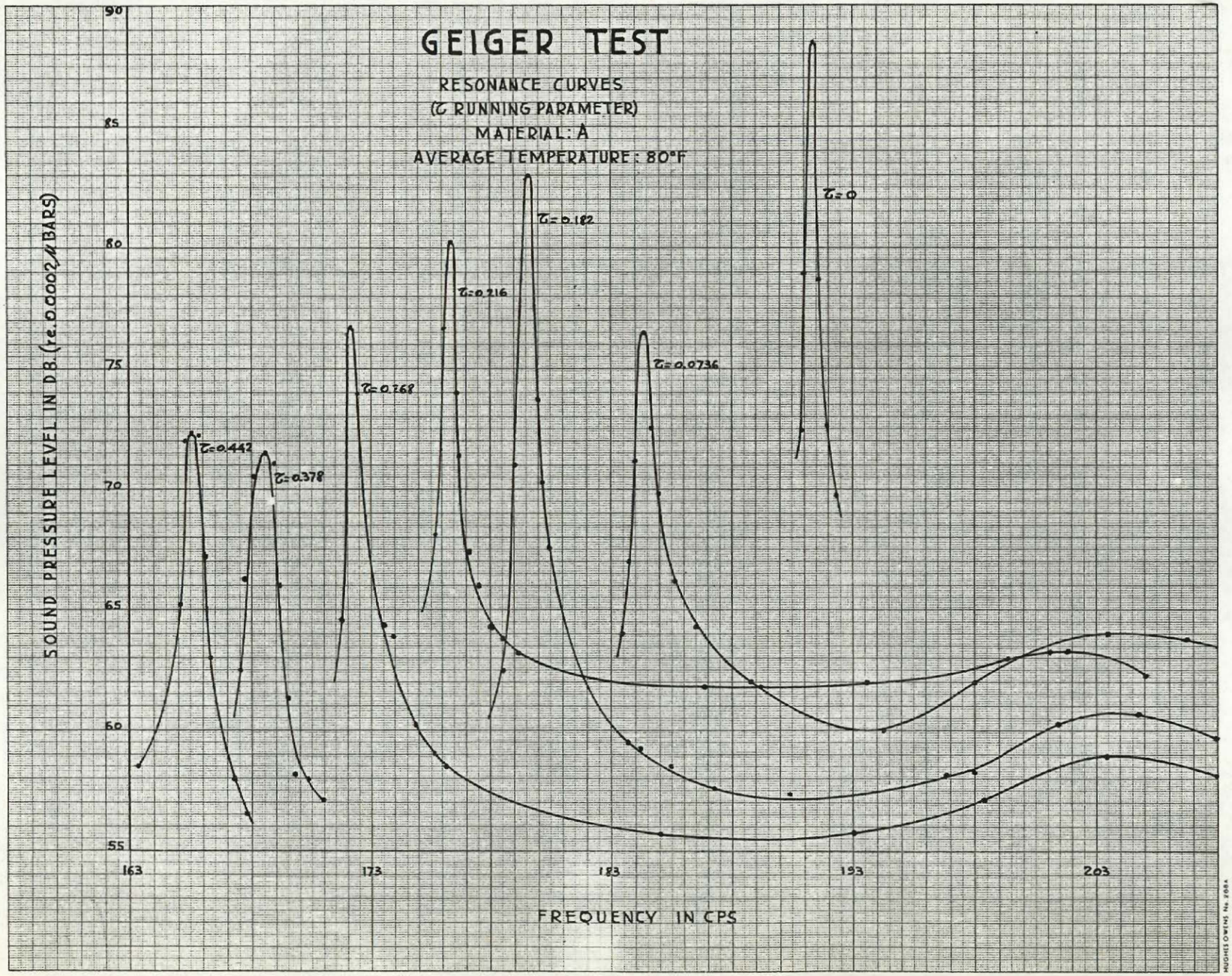
GEIGER TEST
RESONANCE CURVES
(τ RUNNING PARAMETER)
MATERIAL: A
AVERAGE TEMPERATURE: 80°F
SOUND PRESSURE LEVEL IN D.B. (re. 0.0002 μBARS)
90
85
80
75
70
65
60
55
τ=0.442
τ=0.378
τ=0.768
τ=0.216
τ=0.182
τ=0.0736
τ=0
163
173
183
193
203
FREQUENCY IN CPS

Figure (9)

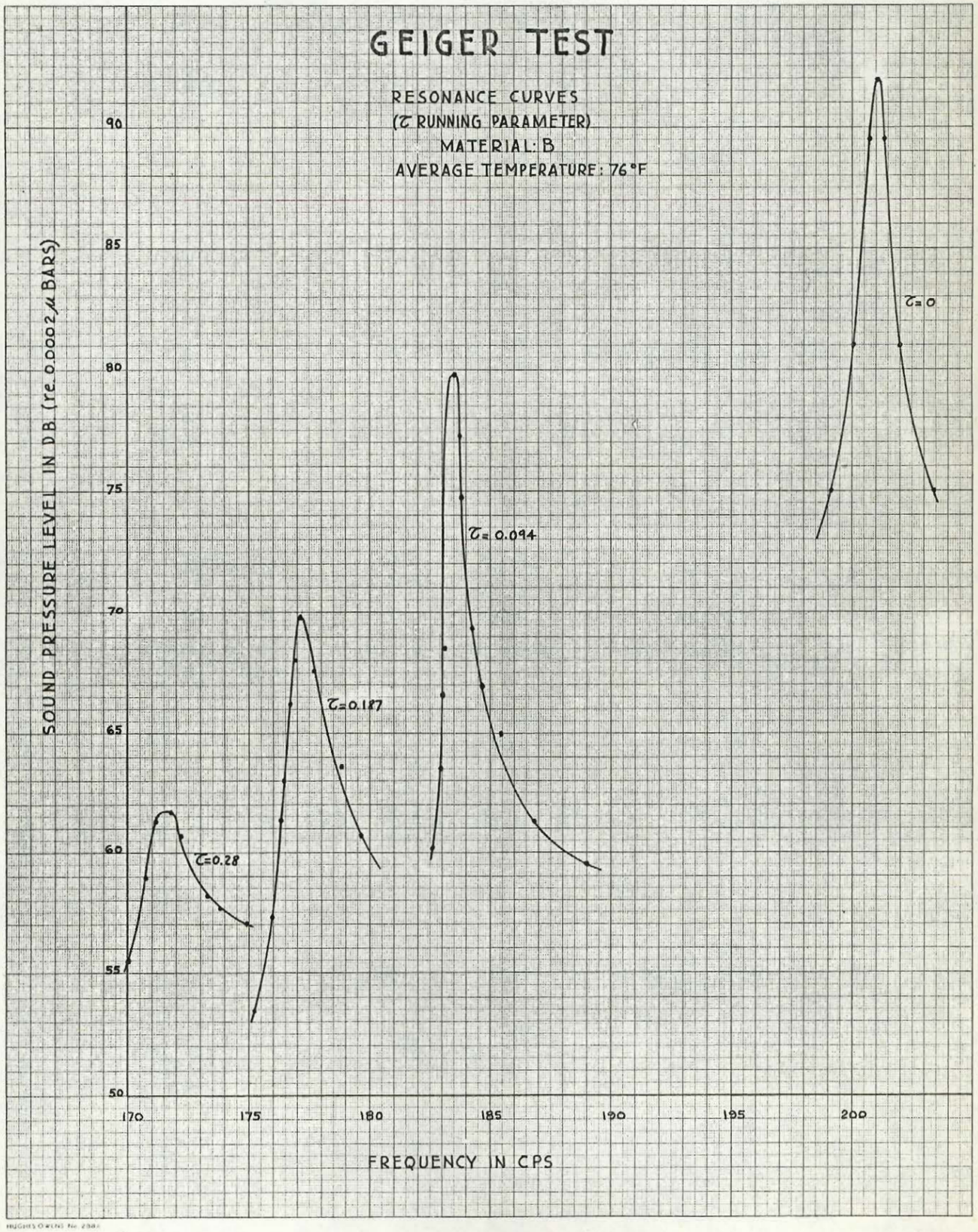
GEIGER TEST
RESONANCE CURVES
(τ RUNNING PARAMETER)
MATERIAL: B
AVERAGE TEMPERATURE: 76°F
SOUND PRESSURE LEVEL IN D.B. (re. 0.0002 μ BARS)
90
85
80
75
70
65
60
55
50
τ=0.28
τ=0.187
τ=0.094
τ=0
170
175
180
185
190
195
200
FREQUENCY IN CPS

Figure (10)

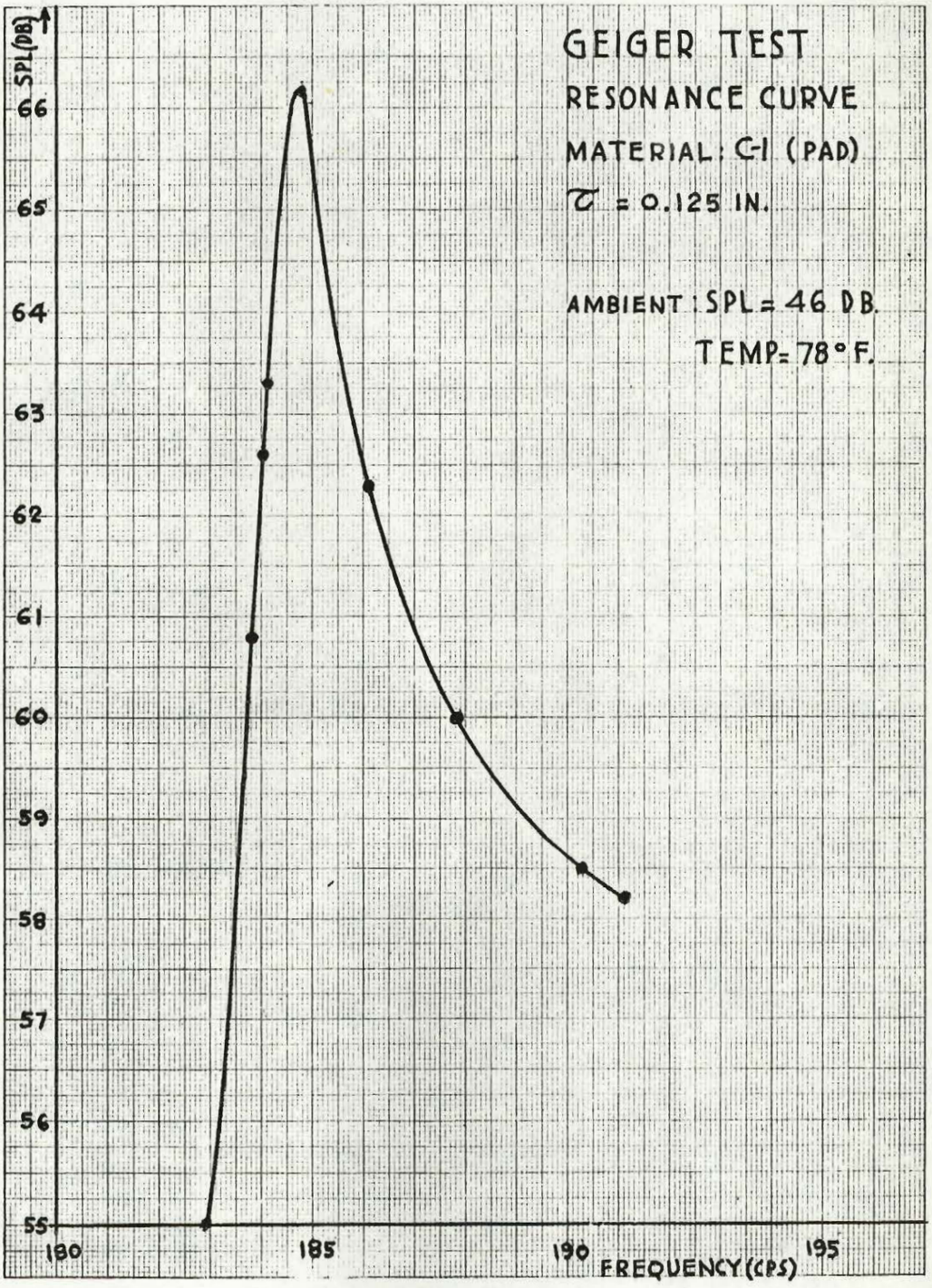
GEIGER TEST
RESONANCE CURVE
MATERIAL: C-1 (PAD)
τ = 0.125 IN.
AMBIENT: SPL = 46 DB.
TEMP = 78° F.
SPL (DB)
66
65
64
63
62
61
60
59
58
57
56
55
180
185
190
195
FREQUENCY (CPS)

Figure (11)

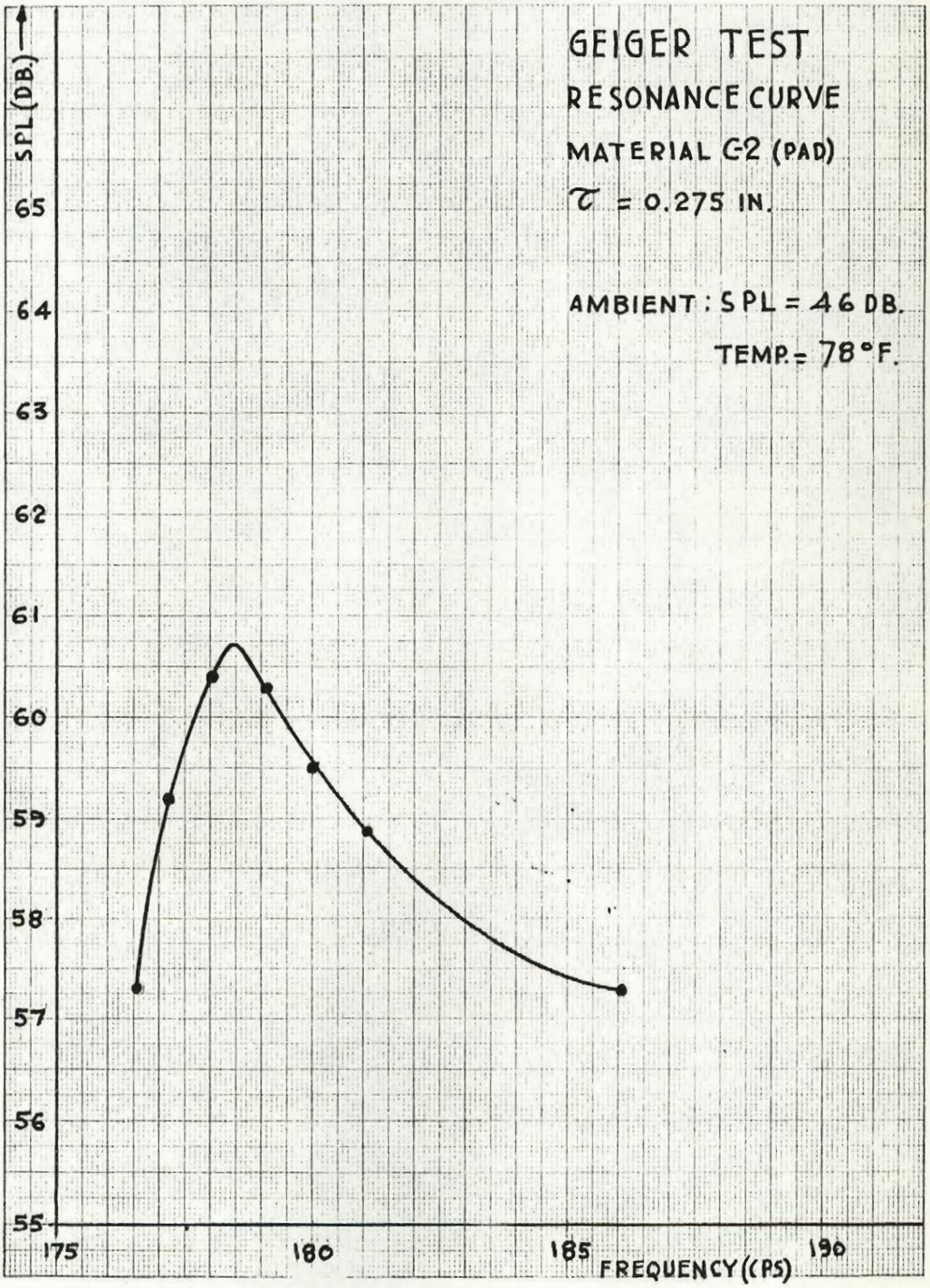
GEIGER TEST
RESONANCE CURVE
MATERIAL C-2 (PAD)
τ = 0.275 IN.
AMBIENT : SPL = 46 DB.
TEMP. = 78°F.
SPL (DB.)
65
64
63
62
61
60
59
58
57
56
55
175
180
185
190
FREQUENCY (CPS)

Figure (12)

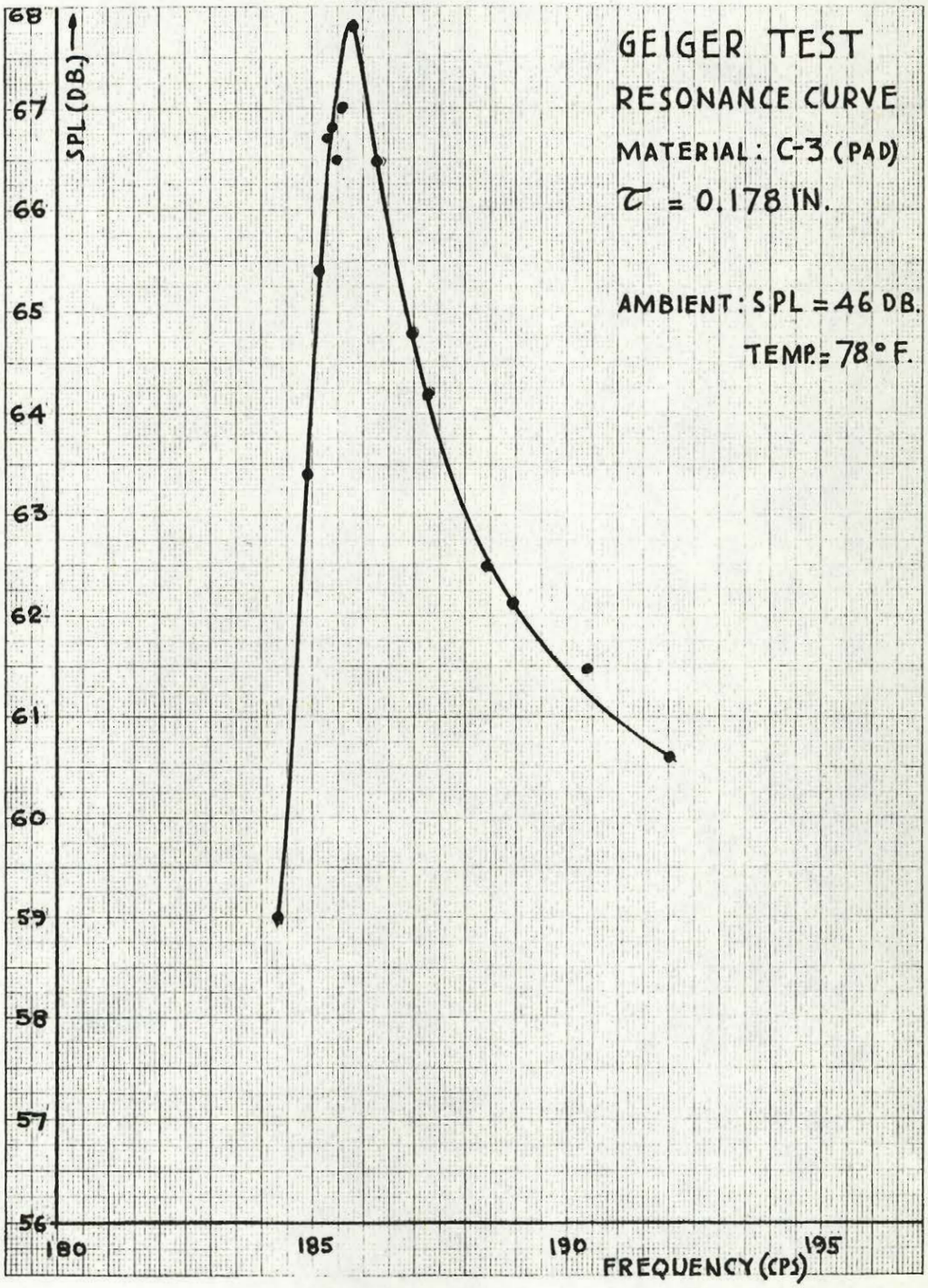
GEIGER TEST
RESONANCE CURVE
MATERIAL: C-3 (PAD)
τ = 0.178 IN.
AMBIENT: SPL = 46 DB.
TEMP. = 78° F.
SPL (DB.)
68
67
66
65
64
63
62
61
60
59
58
57
56
180
185
190
195
FREQUENCY (CPS)

Figure (13)

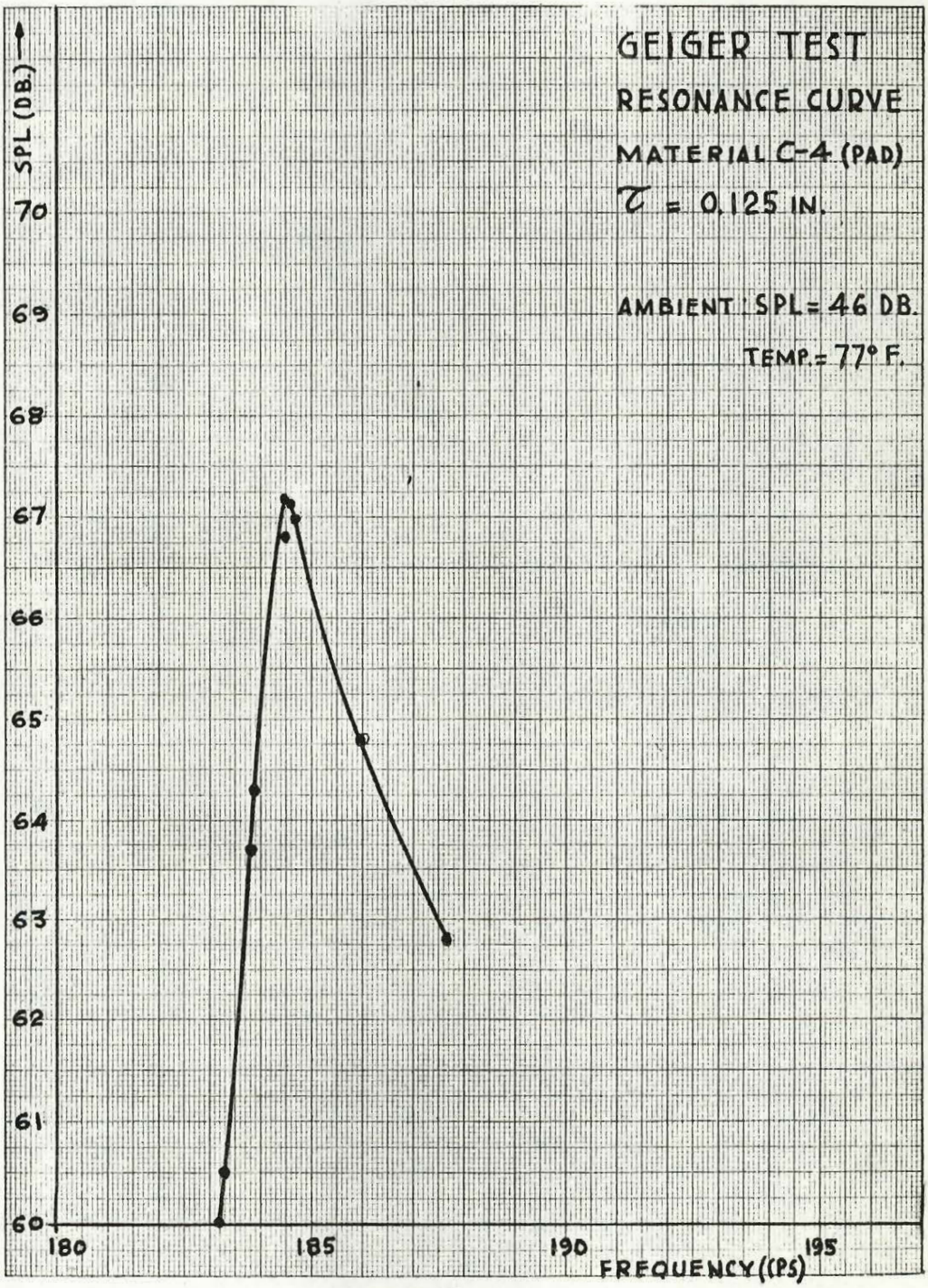
GEIGER TEST
RESONANCE CURVE
MATERIAL C-4 (PAD)
τ = 0.125 IN.
AMBIENT SPL = 46 DB.
TEMP. = 77° F.
SPL (DB.)
70
69
68
67
66
65
64
63
62
61
60
180
185
190
195
FREQUENCY (CPS)

Figure (14)

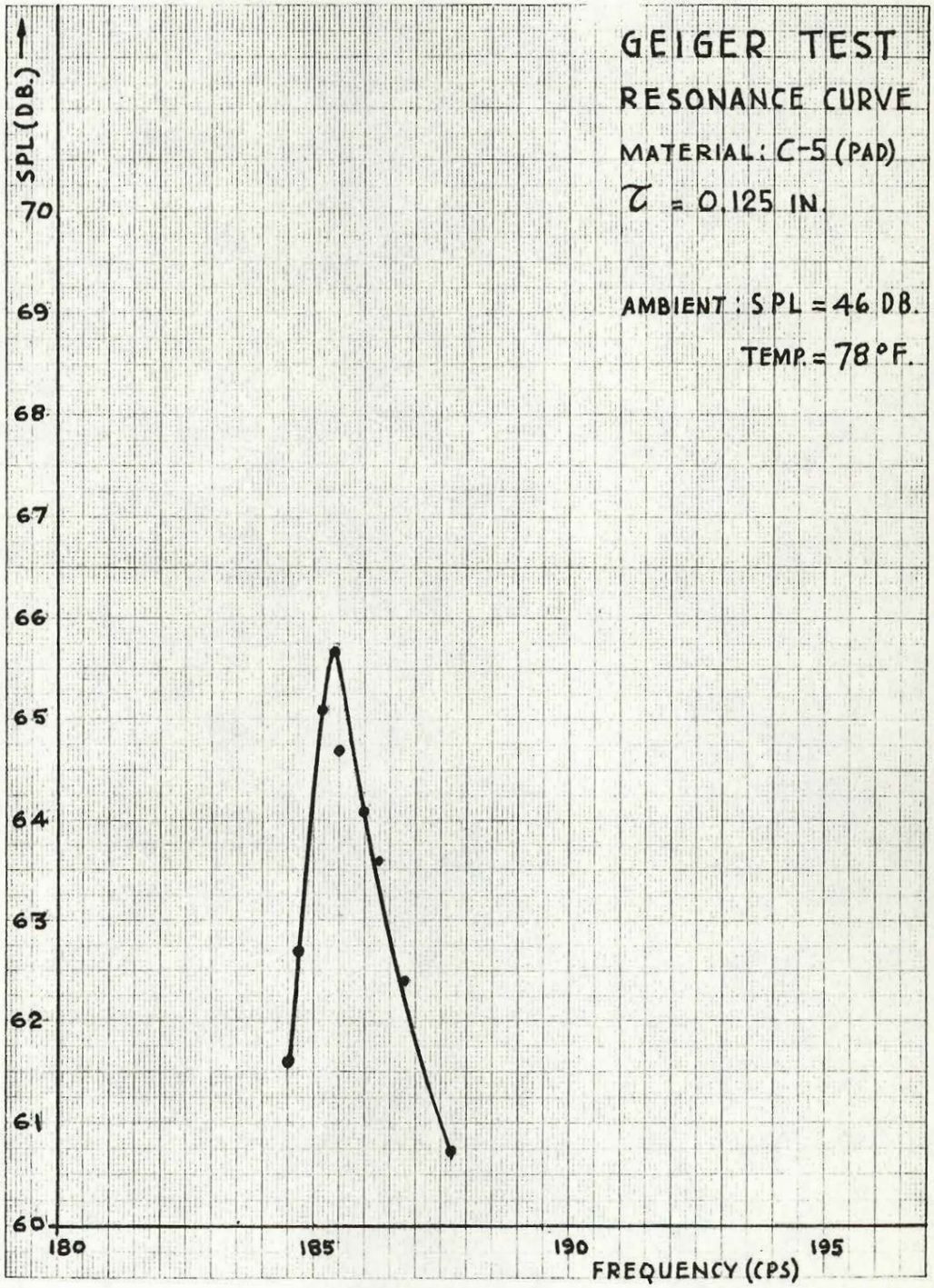
GEIGER TEST
RESONANCE CURVE
MATERIAL: C-5 (PAD)
τ = 0.125 IN.
AMBIENT: SPL = 46 DB.
TEMP. = 78°F.
SPL (DB.)
70
69
68
67
66
65
64
63
62
61
60
180
185
190
195
FREQUENCY (CPS)

Figure (15)

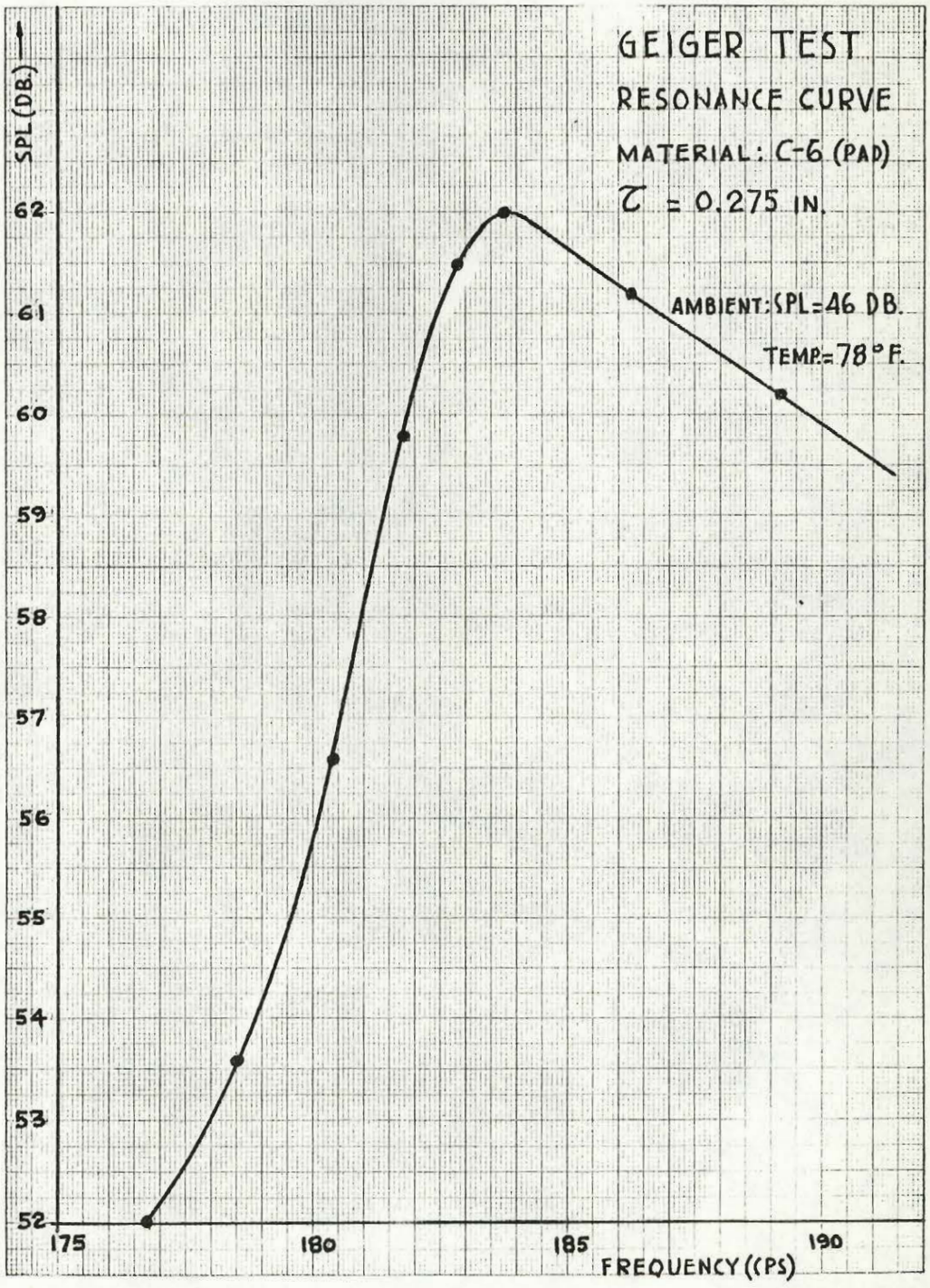
GEIGER TEST
RESONANCE CURVE
MATERIAL: C-6 (PAD)
τ = 0.275 IN.
AMBIENT: SPL=46 DB.
TEMP.=78° F.
SPL (DB.)
62
61
60
59
58
57
56
55
54
53
52
175
180
185
190
FREQUENCY (CPS)

Figure (16)

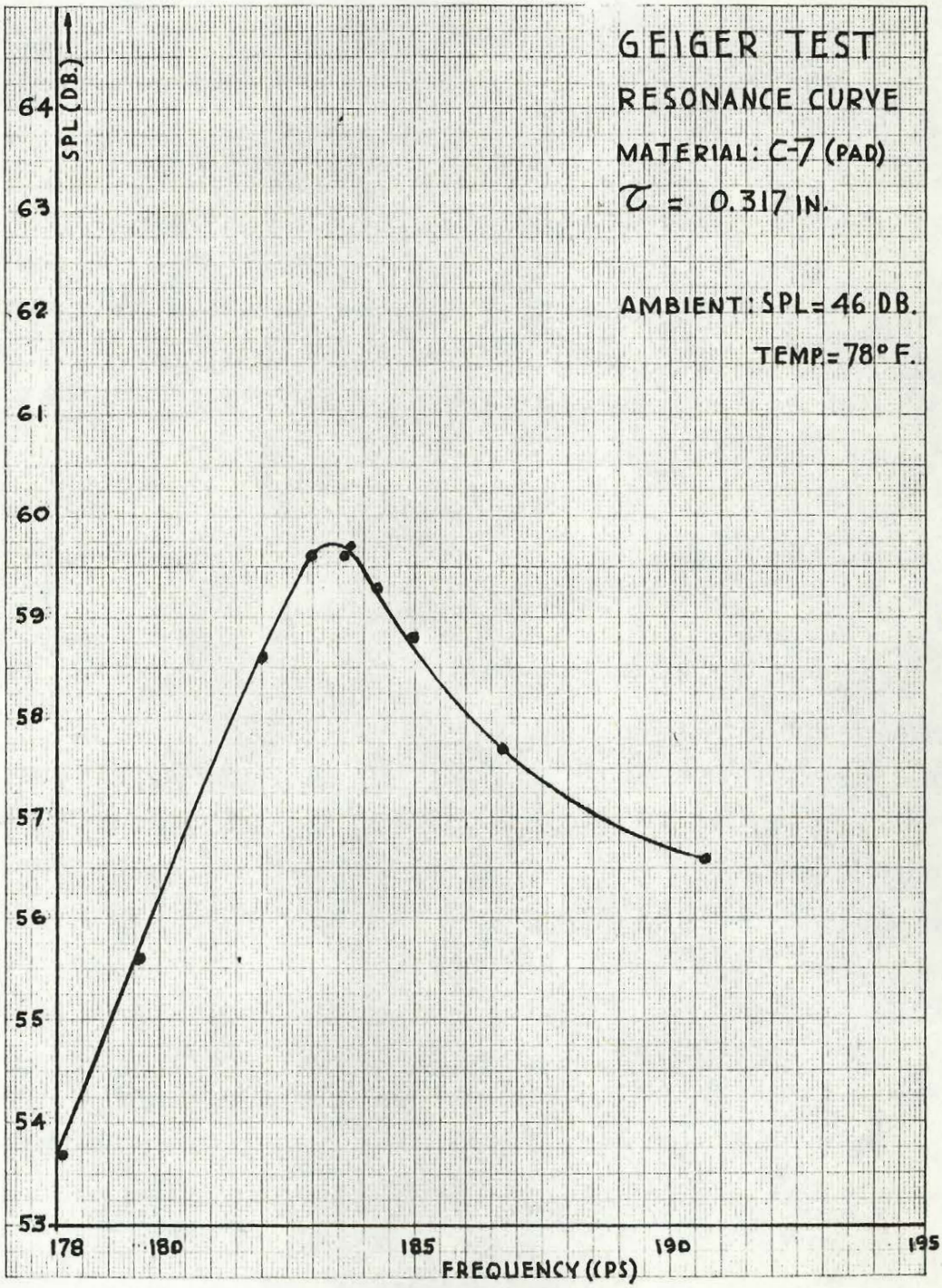
GEIGER TEST
RESONANCE CURVE
MATERIAL: C-7 (PAD)
τ = 0.317 IN.
AMBIENT: SPL = 46 DB.
TEMP. = 78° F.
SPL (DB.)
64
63
62
61
60
59
58
57
56
55
54
53
178
180
185
190
195
FREQUENCY (CPS)

Figure (17)

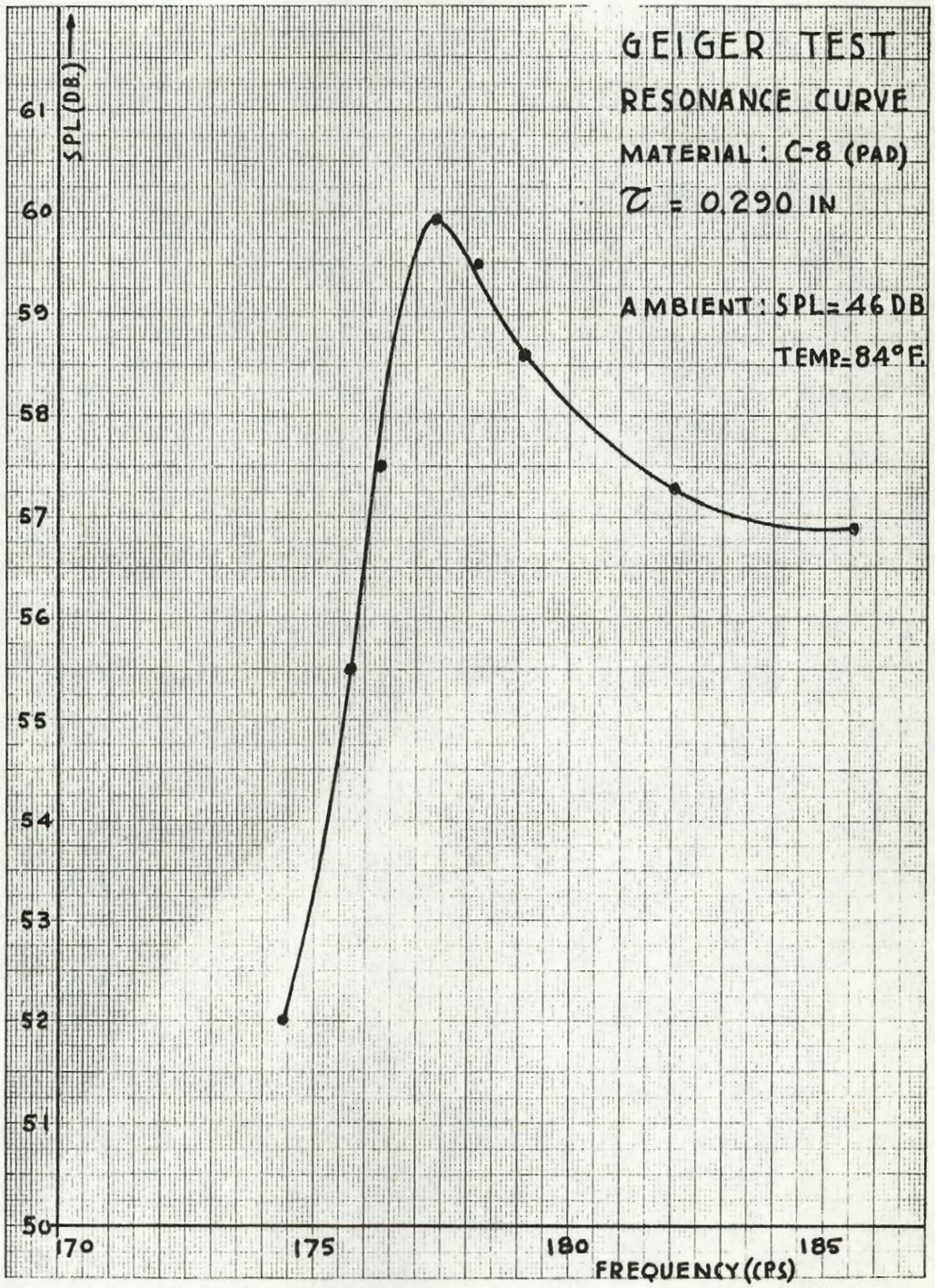
GEIGER TEST
RESONANCE CURVE
MATERIAL: C-8 (PAD)
τ = 0.290 IN
AMBIENT: SPL=46 DB
TEMP=84°F
SPL (DB.)
61
60
59
58
57
56
55
54
53
52
51
50
170
175
180
185
FREQUENCY (CPS)

Figure (18)

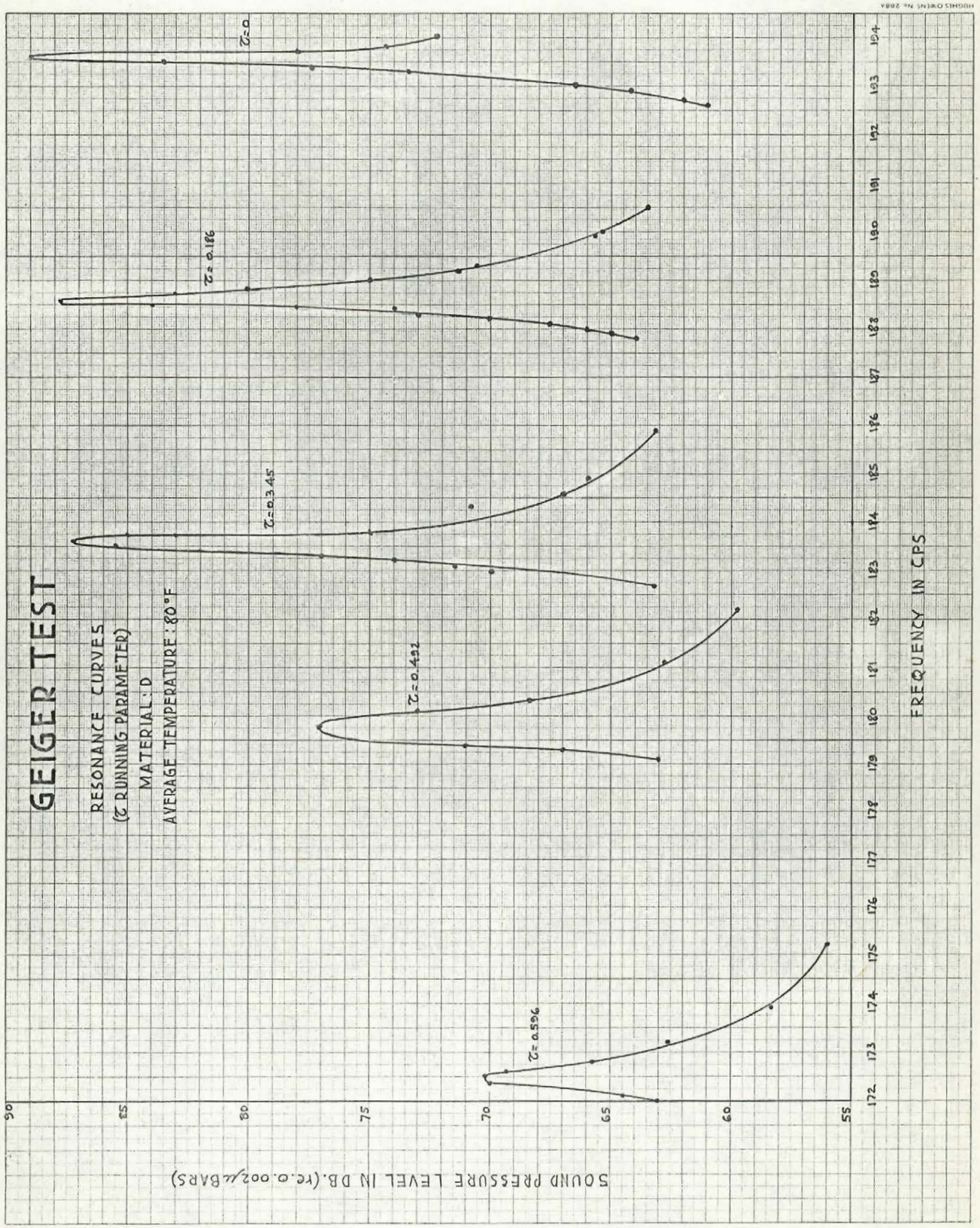
GEIGER TEST
RESONANCE CURVES
(ζ RUNNING PARAMETER)
MATERIAL: D
AVERAGE TEMPERATURE: 80°F
ζ=0.596
ζ=0.432
ζ=0.345
ζ=0.186
ζ=0
SOUND PRESSURE LEVEL IN DB. (re. 0.002 μBARS)
FREQUENCY IN CPS
90
85
80
75
70
65
60
55
172
173
174
175
176
177
178
179
180
181
182
183
184
185
186
187
188
189
190
191
192
193
194

Figure (19)

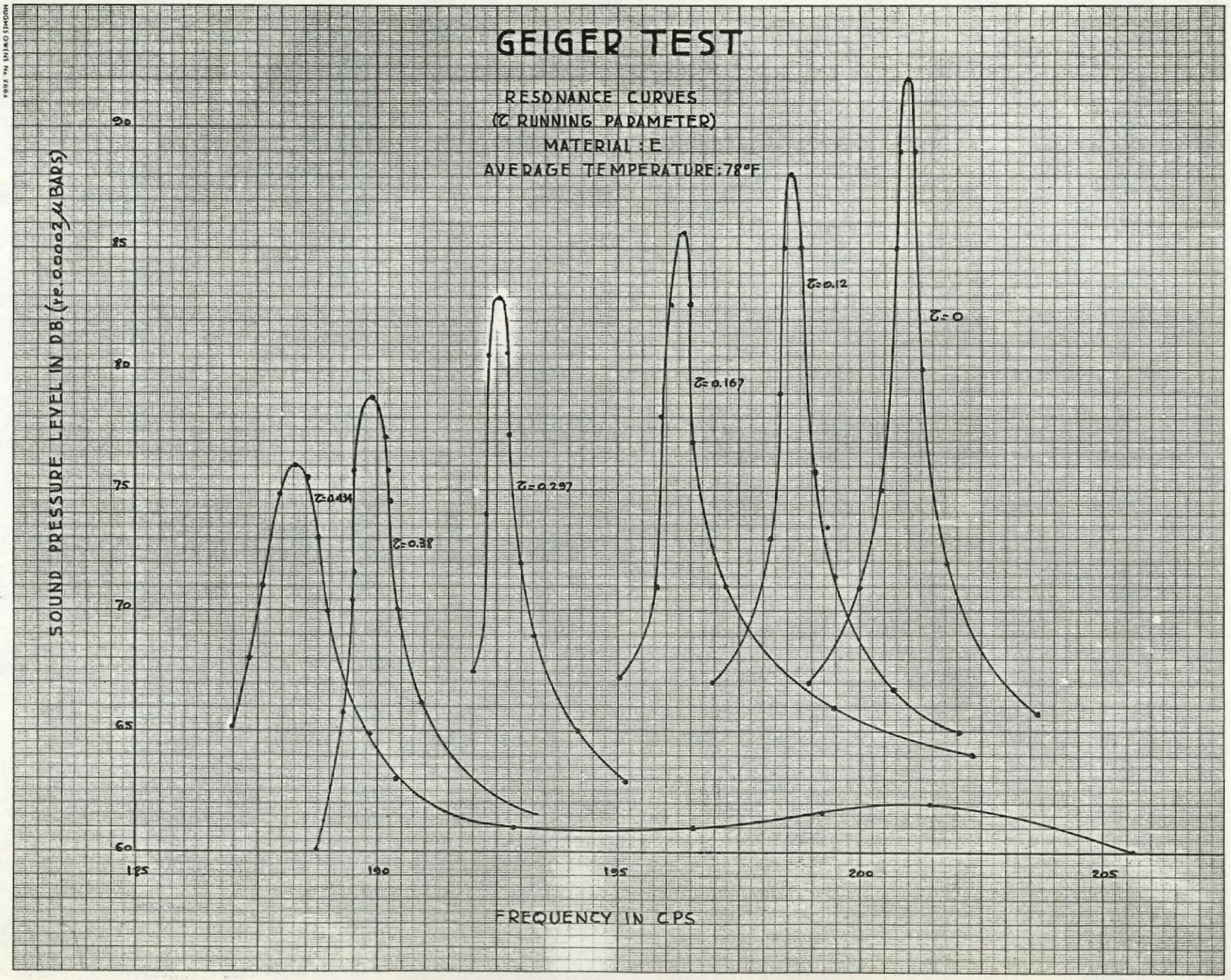
GEIGER TEST
RESONANCE CURVES
(Z RUNNING PARAMETER)
MATERIAL : E
AVERAGE TEMPERATURE: 78°F
SOUND PRESSURE LEVEL IN DB (re. 0.0002 μBARS)
20
85
80
75
70
65
60
Z=0.434
Z=0.38
Z=0.297
Z=0.167
Z=0.12
Z=0
185
190
195
200
205
FREQUENCY IN CPS

Figure (20)

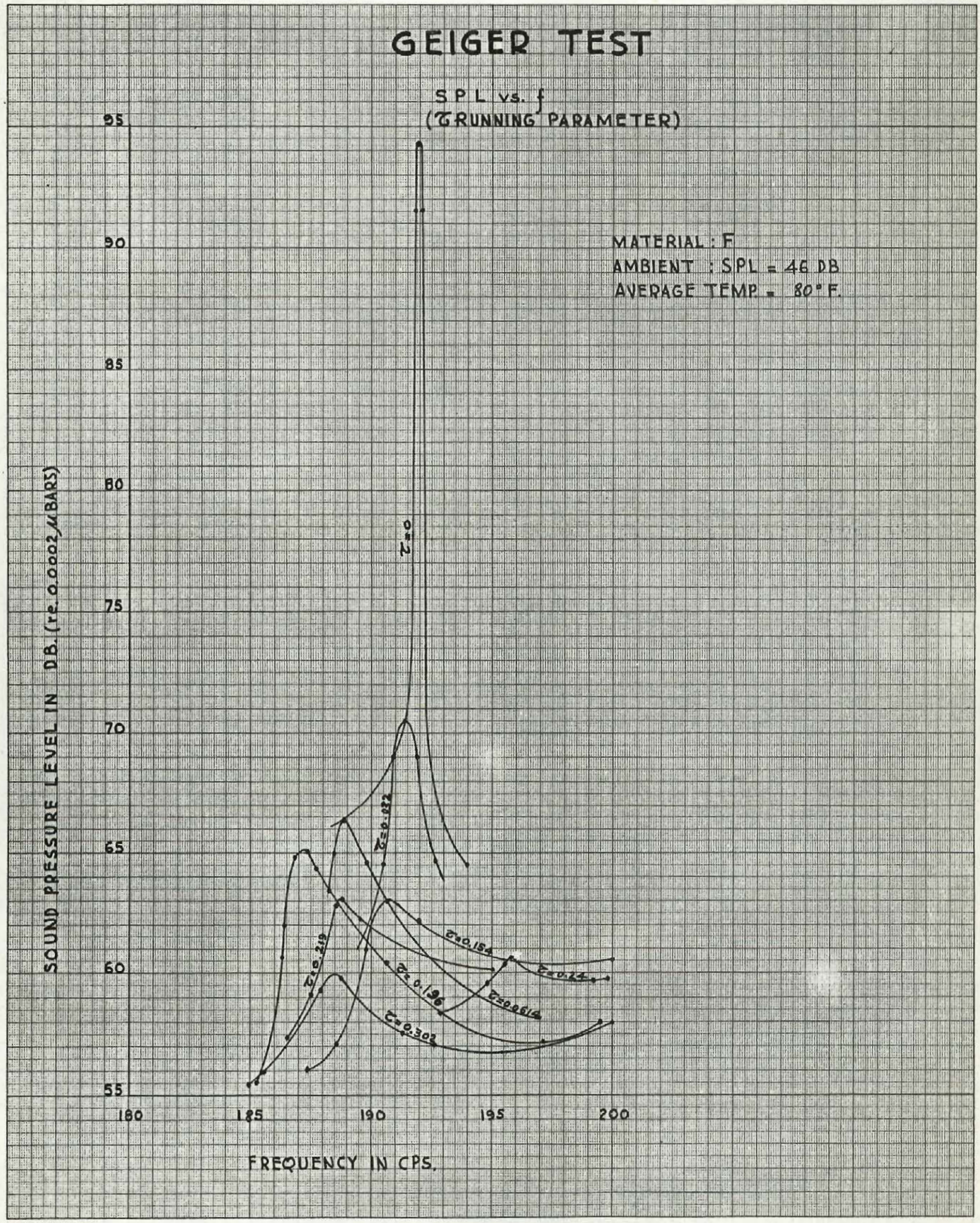
GEIGER TEST
SPL vs. f
(σ RUNNING PARAMETER)
MATERIAL : F
AMBIENT : SPL = 46 DB
AVERAGE TEMP = 80° F.
SOUND PRESSURE LEVEL IN DB. (re. 0.0002 μBARS)
95
90
85
80
75
70
65
60
55
180
185
190
195
200
FREQUENCY IN CPS.
σ=0
σ=0.122
σ=0.154
σ=0.14
σ=0.218
σ=0.136
σ=0.0614
σ=0.302
HUGHES OWENS No. 288A

Figure (21)

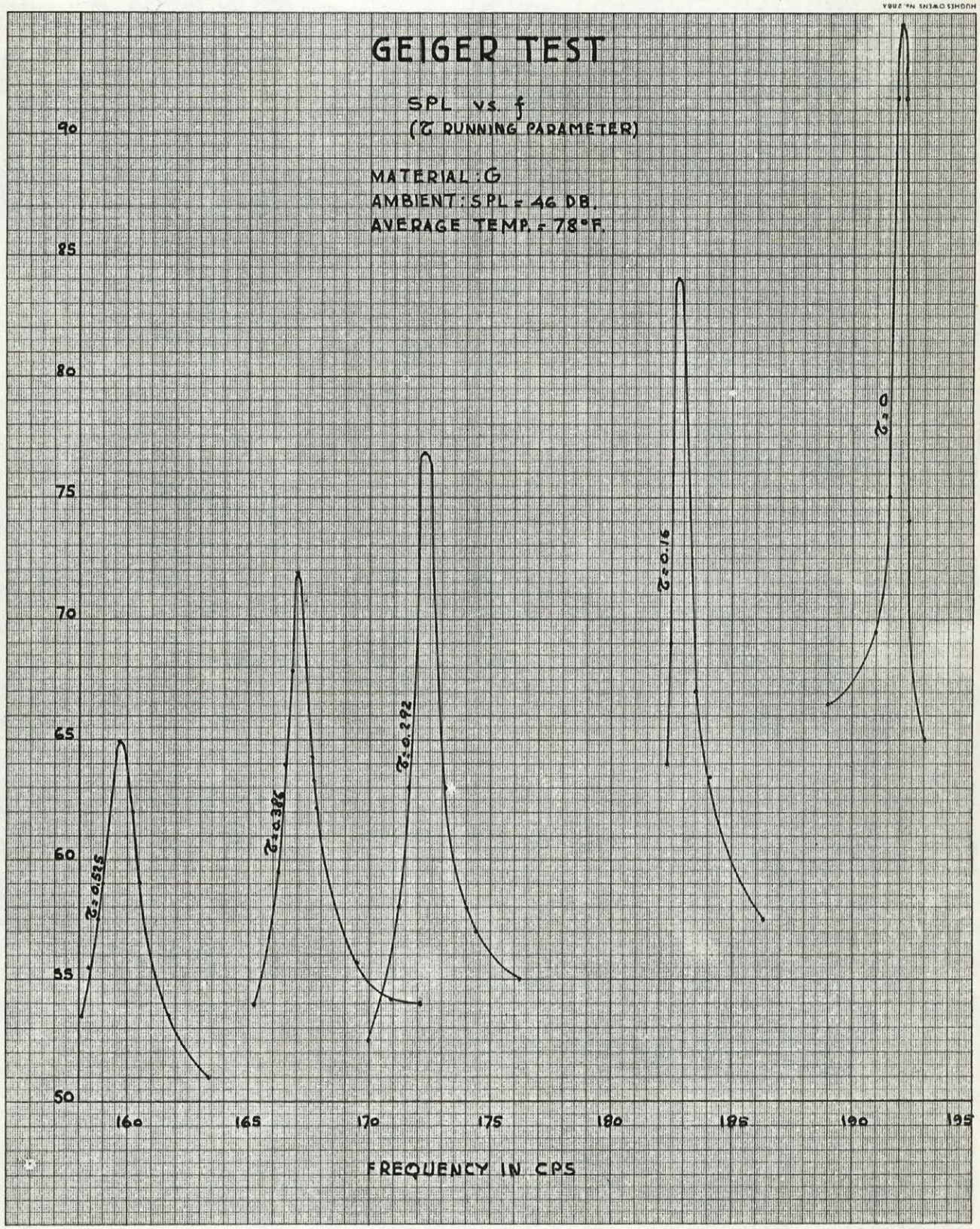
GEIGER TEST
SPL vs f
(Z RUNNING PARAMETER)
MATERIAL: G
AMBIENT: SPL = 46 DB.
AVERAGE TEMP. = 78°F.
90
85
80
75
70
65
60
55
50
160
165
170
175
180
185
190
195
FREQUENCY IN CPS
Z=0.525
Z=0.384
Z=0.282
Z=0.16
Z=0

Figure (22)

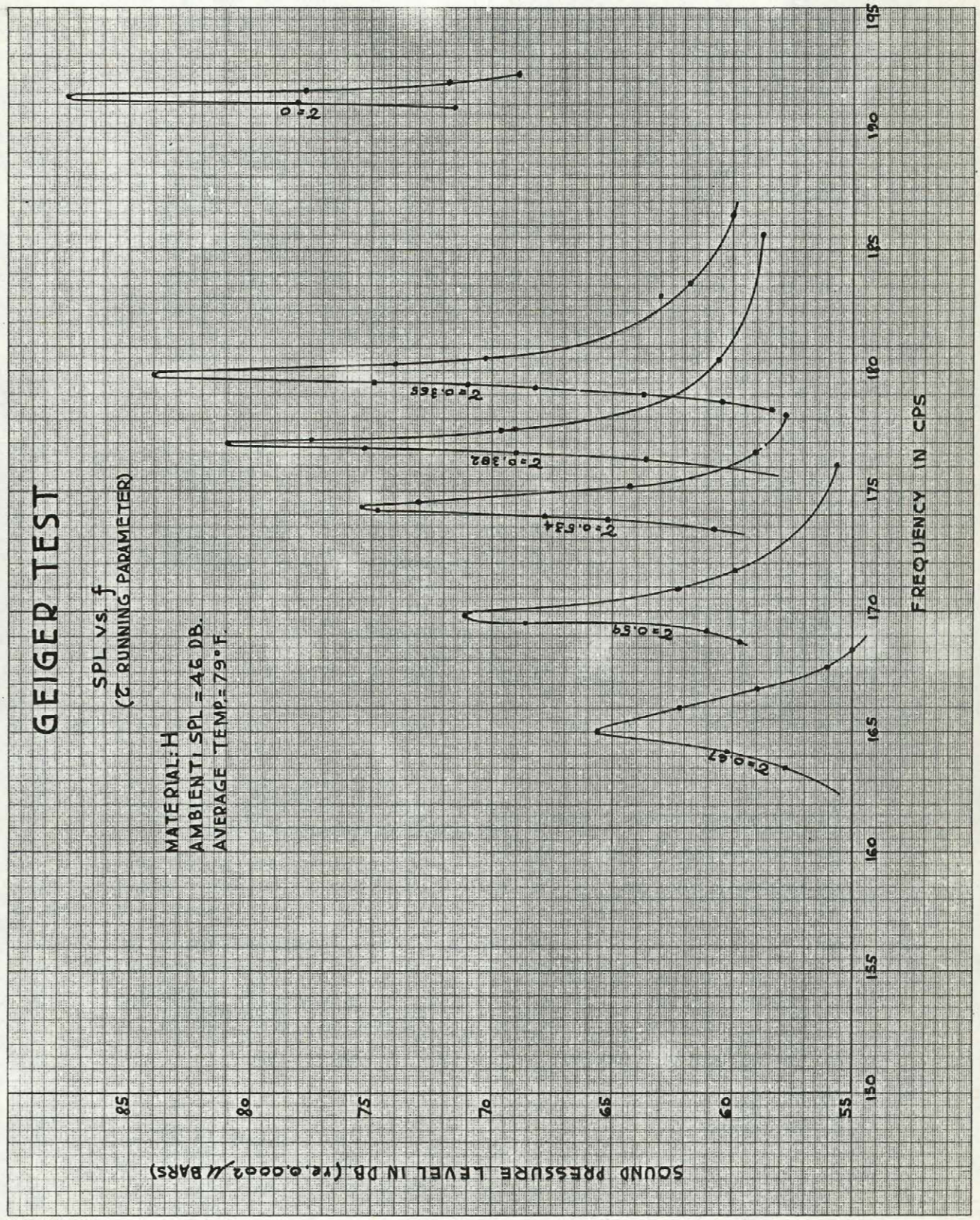
GEIGER TEST
SPL vs. f
(Z RUNNING PARAMETER)
MATERIAL: H
AMBIENT SPL = 46 DB.
AVERAGE TEMP. = 79°F.
SOUND PRESSURE LEVEL IN DB (re. 0.0002 μ BARS)
FREQUENCY IN CPS
85
80
75
70
65
60
55
130
135
140
145
150
155
160
165
170
175
180
185
190
195
Z = 0
Z = 0.365
Z = 0.382
Z = 0.634
Z = 0.59
Z = 0.67
Z = 0.67
HUGHES OWENS No. 288A

Figure (23)

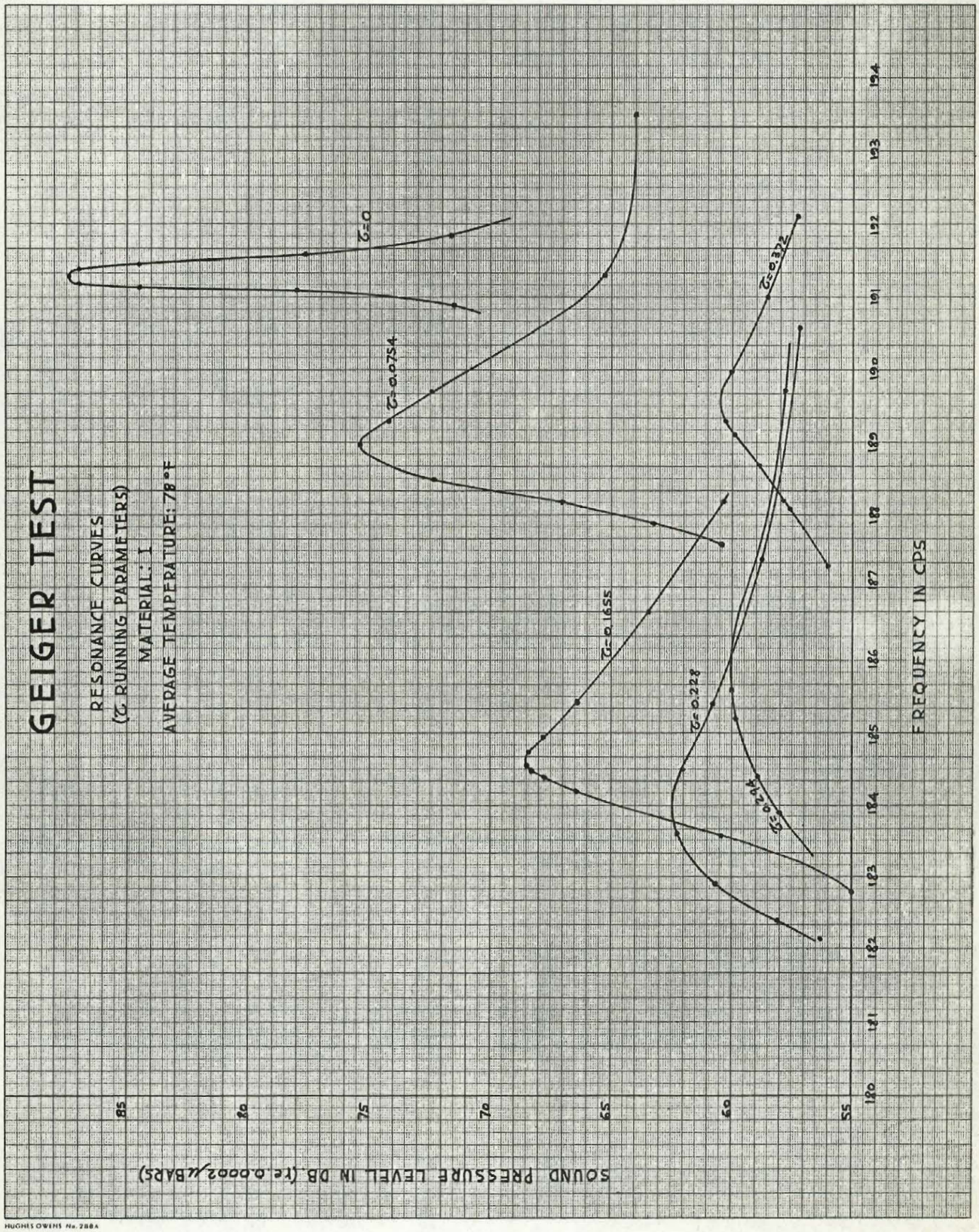
GEIGER TEST
RESONANCE CURVES
(σ RUNNING PARAMETERS)
MATERIAL: 1
AVERAGE TEMPERATURE: 78°F
SOUND PRESSURE LEVEL IN DB (re 0.0002 μBARS)
FREQUENCY IN CPS
σ=0
σ=0.0754
σ=0.1655
σ=0.223
σ=0.274
σ=0.32
85
80
75
70
65
60
55
120
121
182
123
184
185
186
187
188
189
190
191
192
193
194
HUGHES OWENS No. 288A

Figure (24)

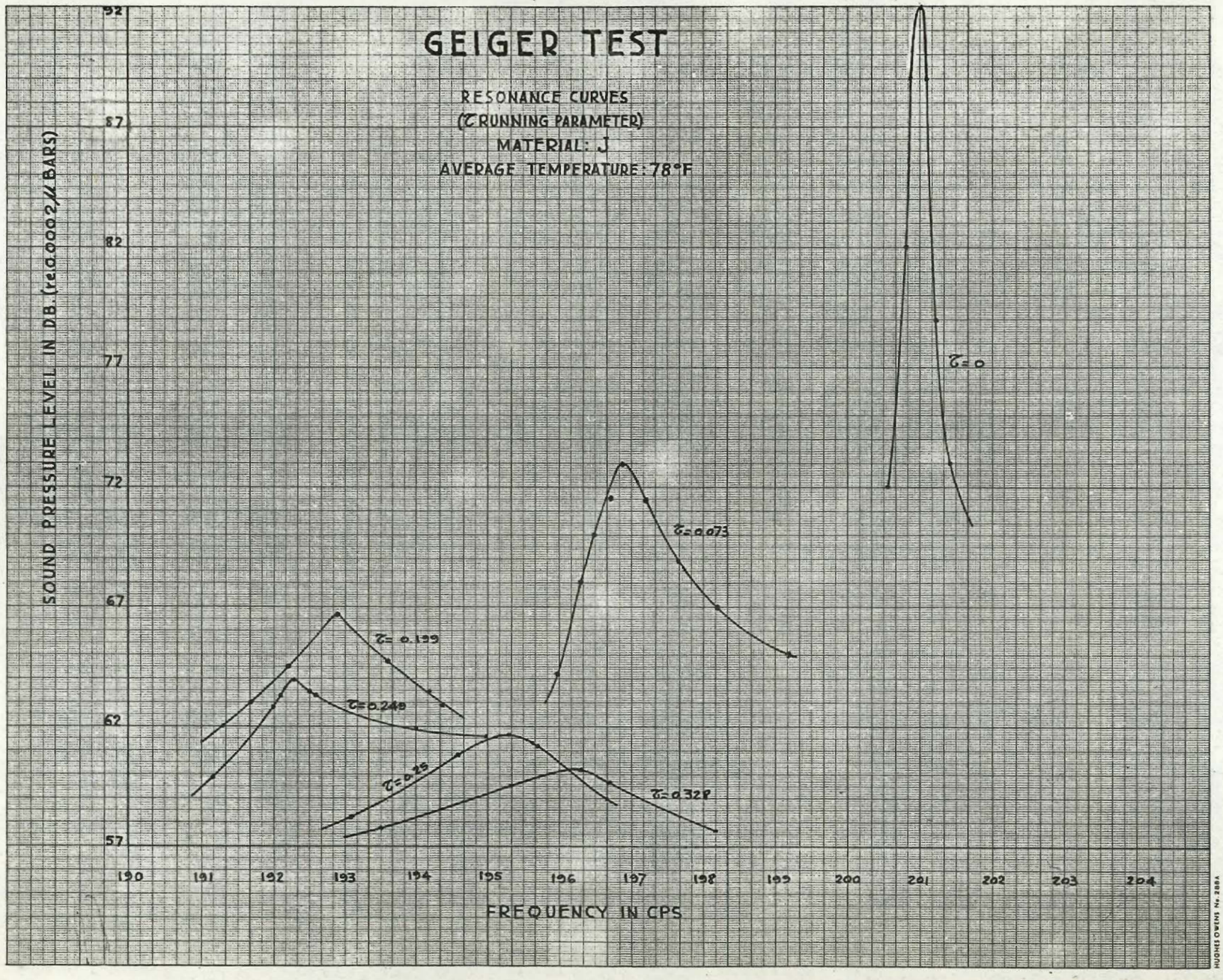
GEIGER TEST
RESONANCE CURVES
(τ RUNNING PARAMETER)
MATERIAL: J
AVERAGE TEMPERATURE: 78°F
SOUND PRESSURE LEVEL IN D.B. (re: 0.0002 μBARS)
92
87
82
77
72
67
62
57
τ=0
τ=0.073
τ=0.139
τ=0.248
τ=0.328
190
191
192
193
194
195
196
197
198
199
200
201
202
203
204
FREQUENCY IN CPS

Figure (25)

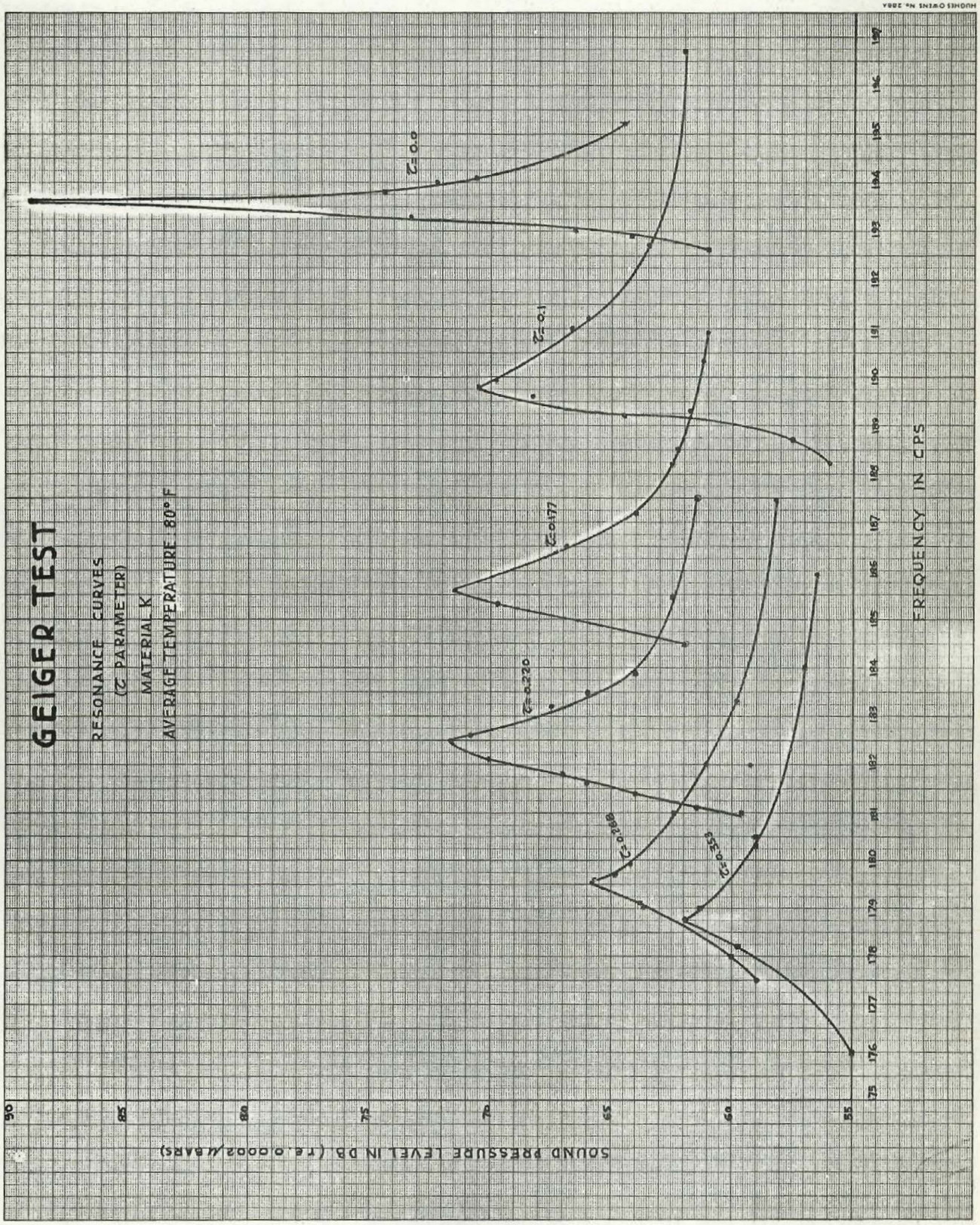
GEIGER TEST
RESONANCE CURVES
(Z PARAMETER)
MATERIAL K
AVERAGE TEMPERATURE 80° F
SOUND PRESSURE LEVEL IN DB (re 0.0002 μBARS)
FREQUENCY IN CPS
Z=0.0
Z=0.1
Z=0.177
Z=0.220
Z=0.268
Z=0.353
HUGHES OWENS No. 3884

Figure (26)

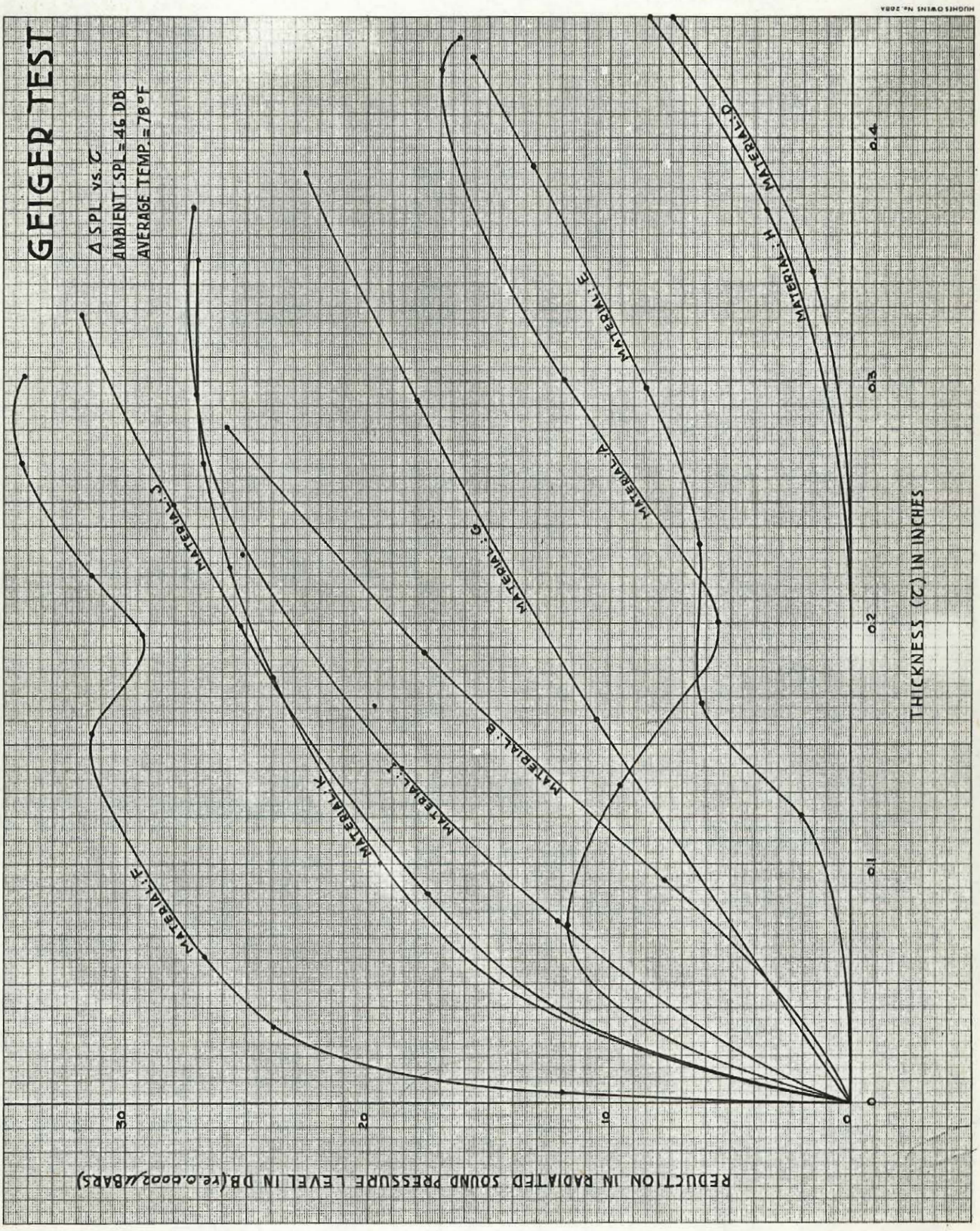
GEIGER TEST
Δ SPL vs. C
AMBIENT SPL = 46 DB
AVERAGE TEMP. = 78°F
REDUCTION IN RADIATED SOUND PRESSURE LEVEL IN DB (re. 0.0002 μBARS)
THICKNESS (C) IN INCHES
0
10
20
30
0.1
0.2
0.3
0.4
MATERIAL: D
MATERIAL: H
MATERIAL: E
MATERIAL: A
MATERIAL: G
MATERIAL: B
MATERIAL: I
MATERIAL: K
MATERIAL: F
MATERIAL: C

Figure (27)

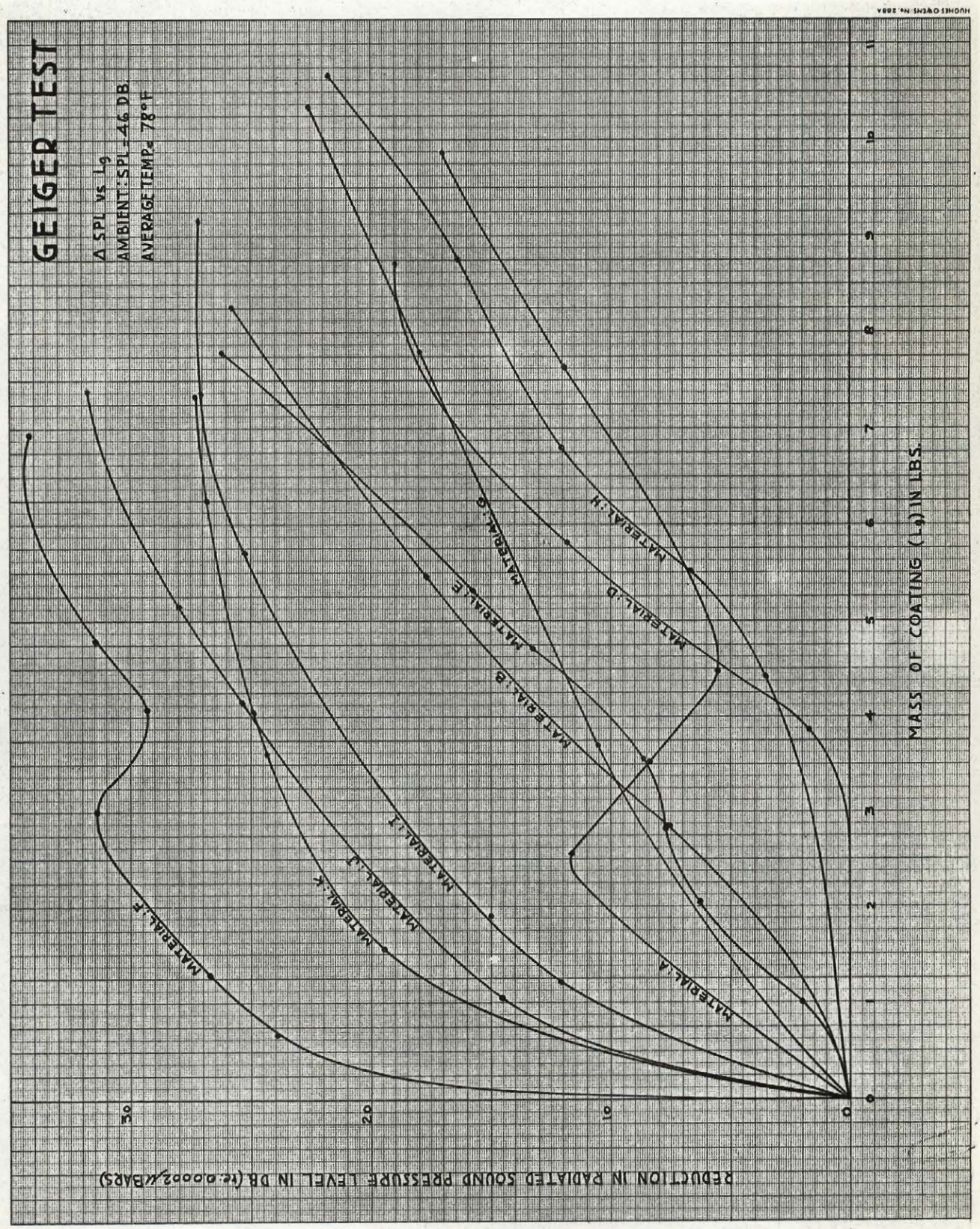
GEIGER TEST
Δ SPL vs L_g
AMBIENT SPL-46 DB
AVERAGE TEMP- 78°F
REDUCTION IN RADIATED SOUND PRESSURE LEVEL IN DB (re .0002 μBARS)
MASS OF COATING (Lg) IN LBS.
MATERIAL A
MATERIAL B
MATERIAL C
MATERIAL D
MATERIAL E
MATERIAL F
MATERIAL G
MATERIAL H
MATERIAL J
MATERIAL K
HUGHES DWGNS No. 2884

Figure (28)

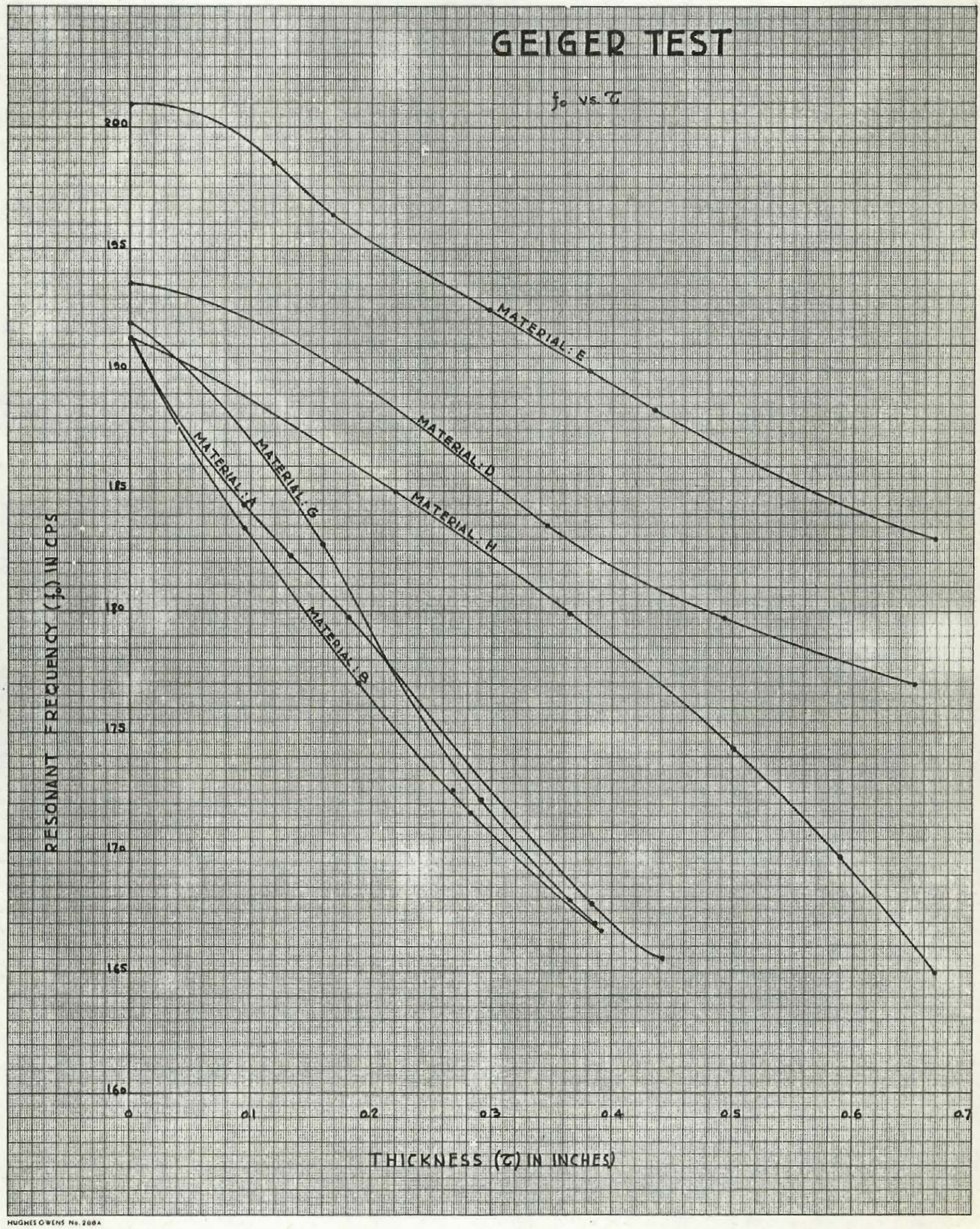
GEIGER TEST
f_o vs. τ
RESONANT FREQUENCY (f_o) IN CPS
200
195
190
185
180
175
170
165
160
0
0.1
0.2
0.3
0.4
0.5
0.6
0.7
THICKNESS (τ) IN INCHES
MATERIAL: E
MATERIAL: D
MATERIAL: H
MATERIAL: G
MATERIAL: A
MATERIAL: B
HUGHES OWENS No. 200A

Figure (29)

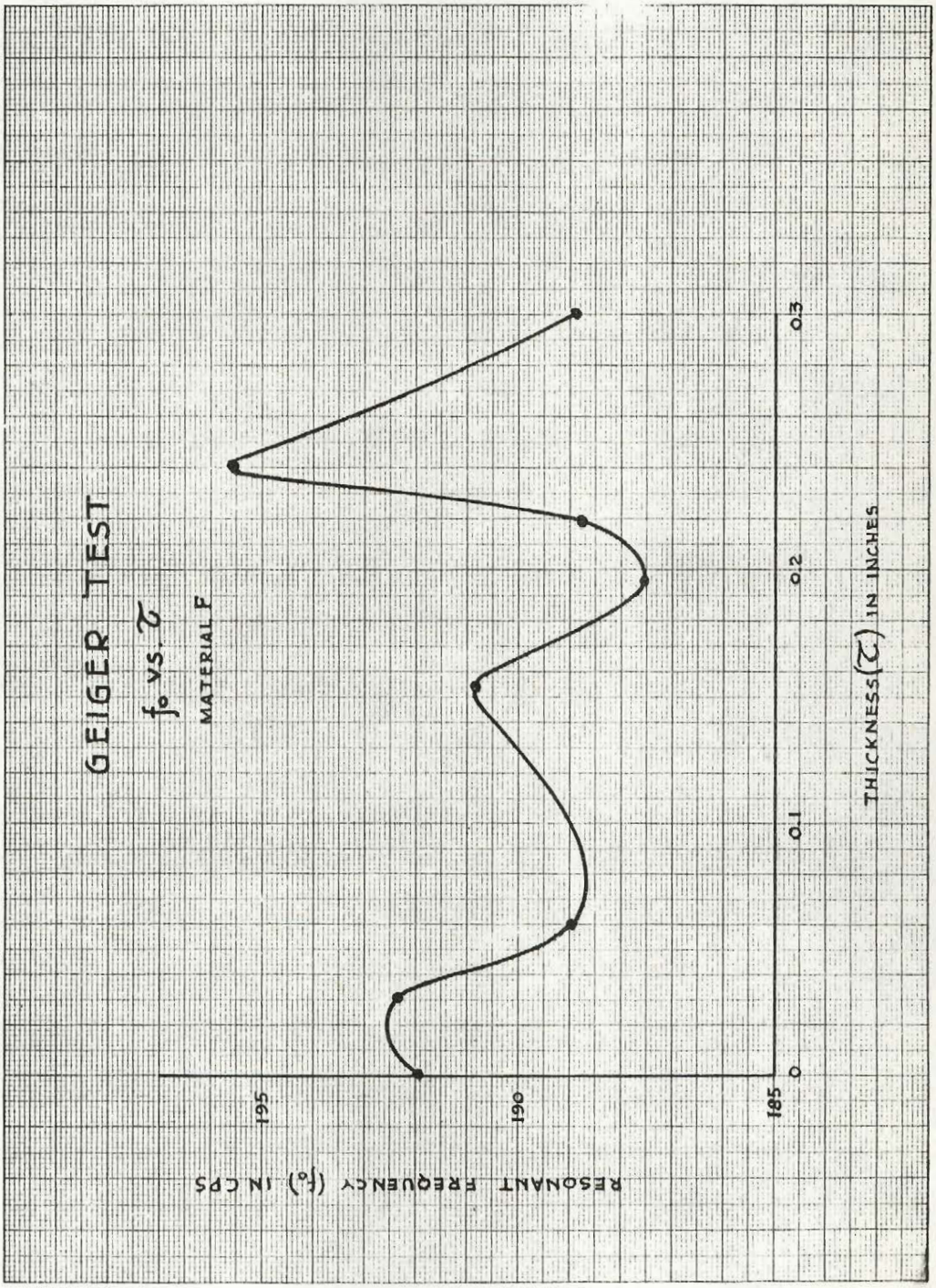
GEIGER TEST
f_o vs. τ
MATERIAL F
RESONANT FREQUENCY (f_o) IN CPS
195
190
185
0
0.1
0.2
0.3
THICKNESS(τ) IN INCHES

Figure (30)

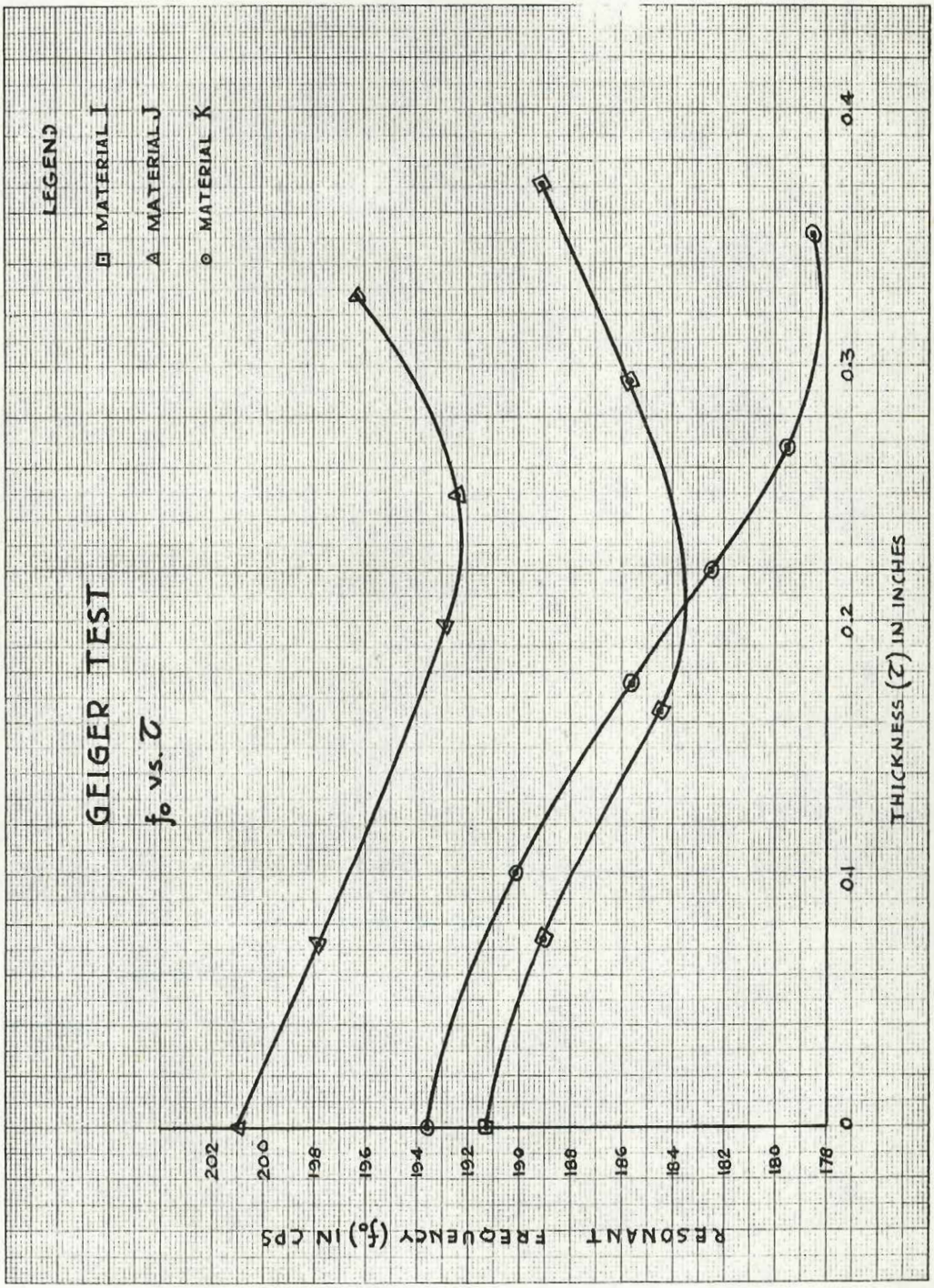
GEIGER TEST
f_o vs. Z
LEGEND
□ MATERIAL I
△ MATERIAL J
○ MATERIAL K
RESONANT FREQUENCY (f_o) IN CPS
202
200
198
196
194
192
190
188
186
184
182
180
178
0
0.1
0.2
0.3
0.4
THICKNESS (Z) IN INCHES

Figure (31)

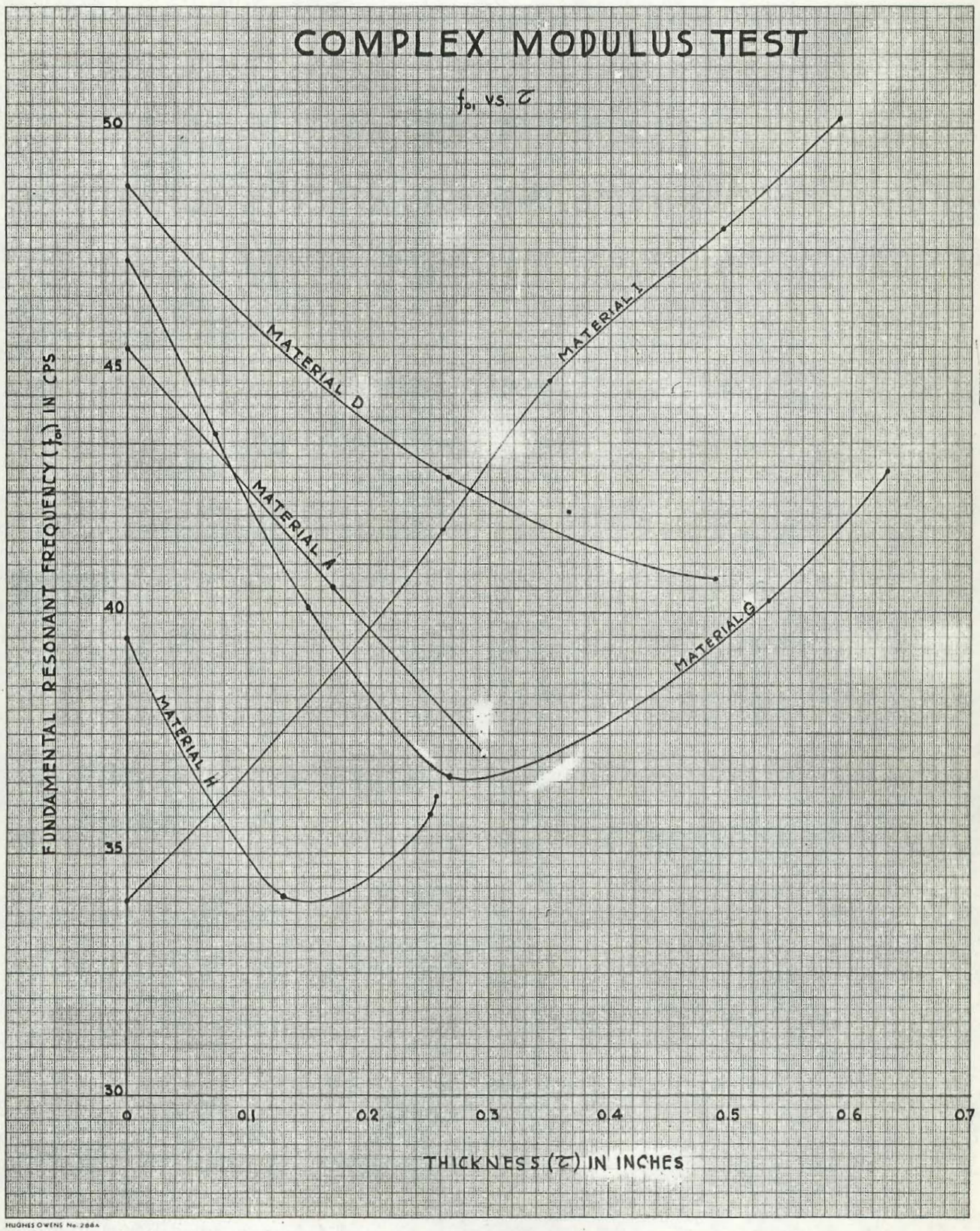
COMPLEX MODULUS TEST
f_{01} vs. τ
FUNDAMENTAL RESONANT FREQUENCY (f_{01}) IN CPS
50
45
40
35
30
0
0.1
0.2
0.3
0.4
0.5
0.6
0.7
THICKNESS (τ) IN INCHES
MATERIAL D
MATERIAL I
MATERIAL A
MATERIAL G
MATERIAL H
HUGHES OWENS No. 288A

Figure (32)

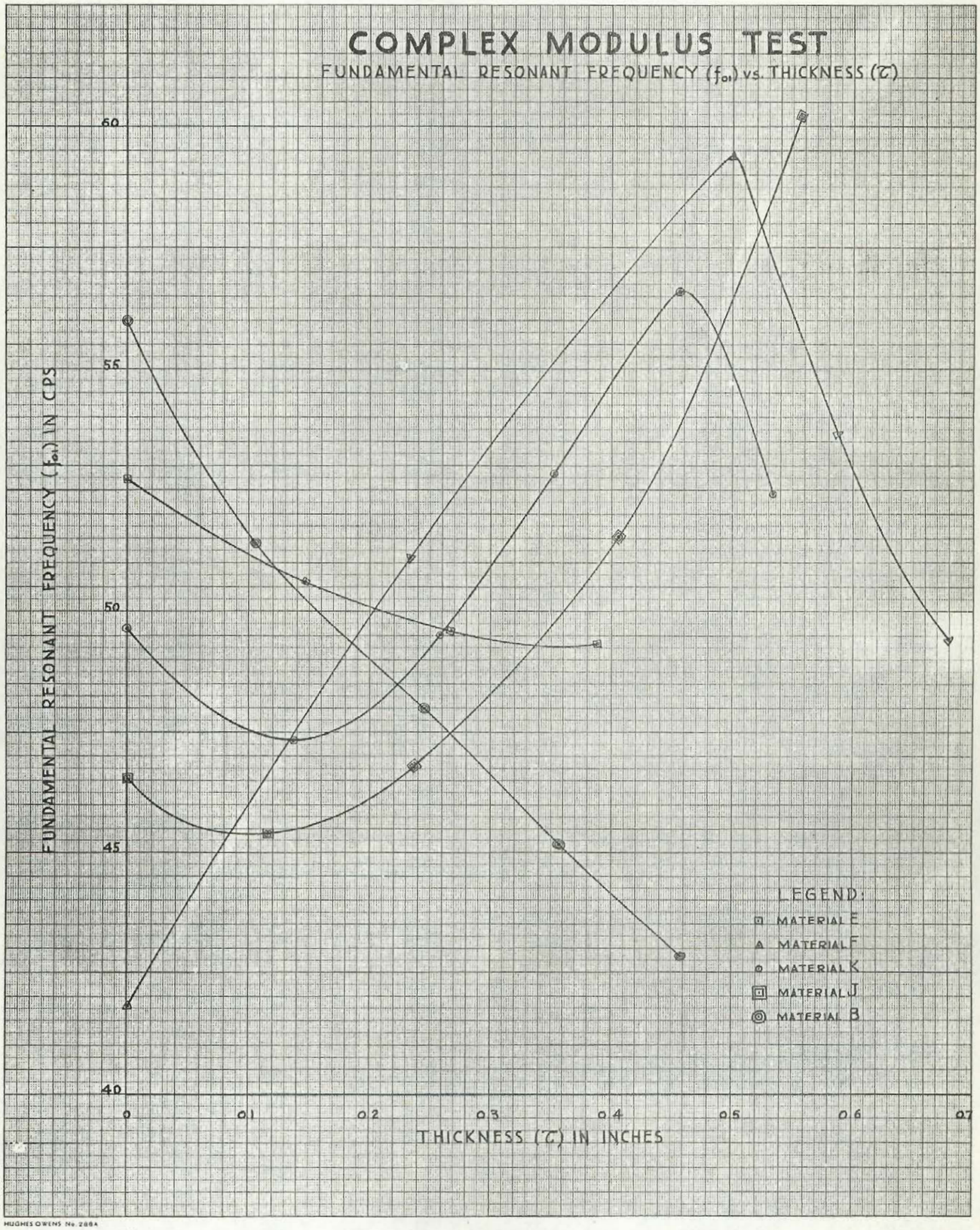
COMPLEX MODULUS TEST
FUNDAMENTAL RESONANT FREQUENCY (f_{o1}) vs. THICKNESS (T)
FUNDAMENTAL RESONANT FREQUENCY (f_{o1}) IN CPS
60
55
50
45
40
0
0.1
0.2
0.3
0.4
0.5
0.6
0.7
THICKNESS (T) IN INCHES
LEGEND:
MATERIAL E
MATERIAL F
MATERIAL K
MATERIAL J
MATERIAL B
HUGHES OWENS No. 288A

Figure (33)

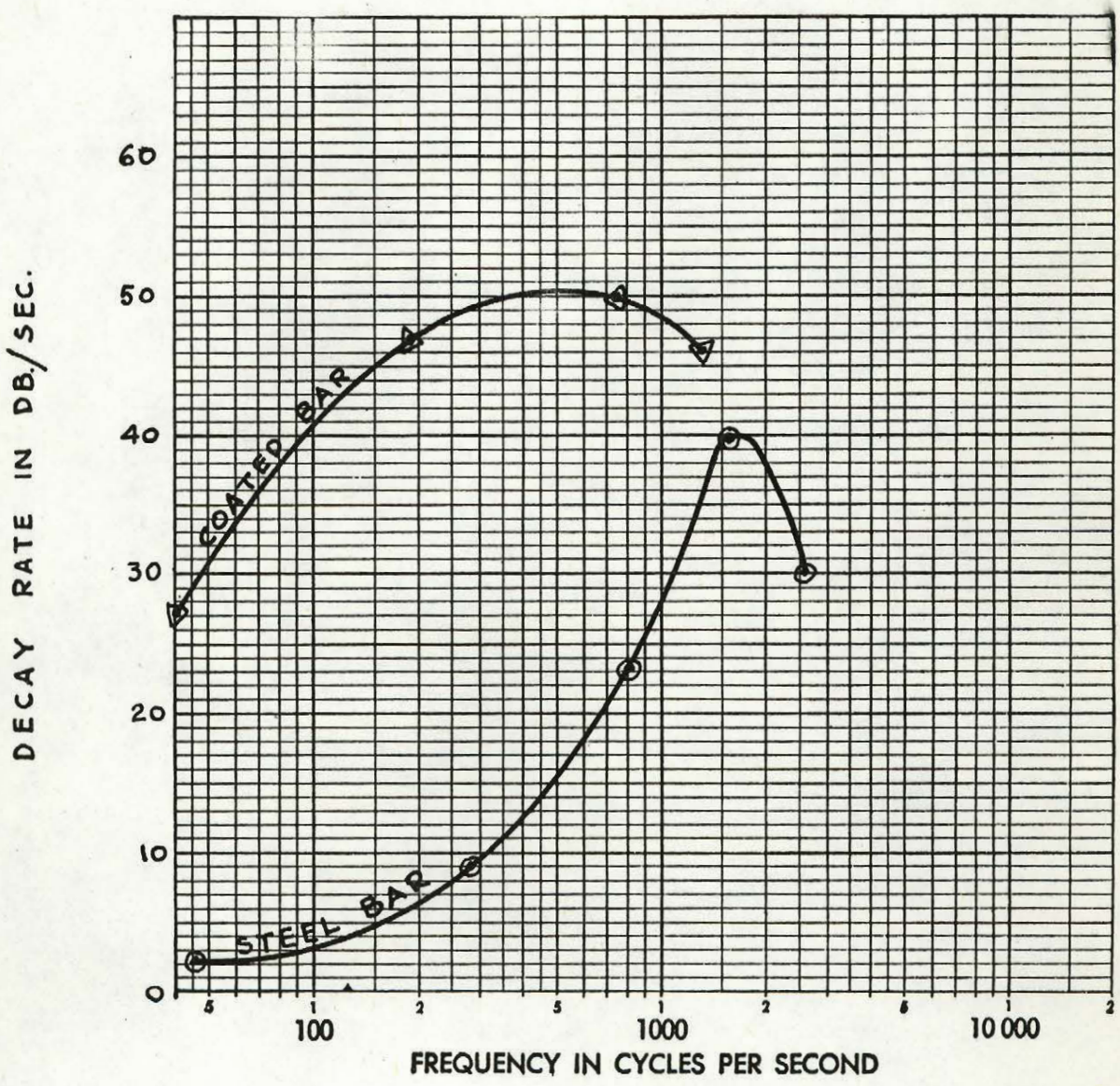

⊙ δ_p vs. f_{op}
△ δ vs. f_o
MATERIAL A

COMPLEX MODULUS TEST

Figure (34)

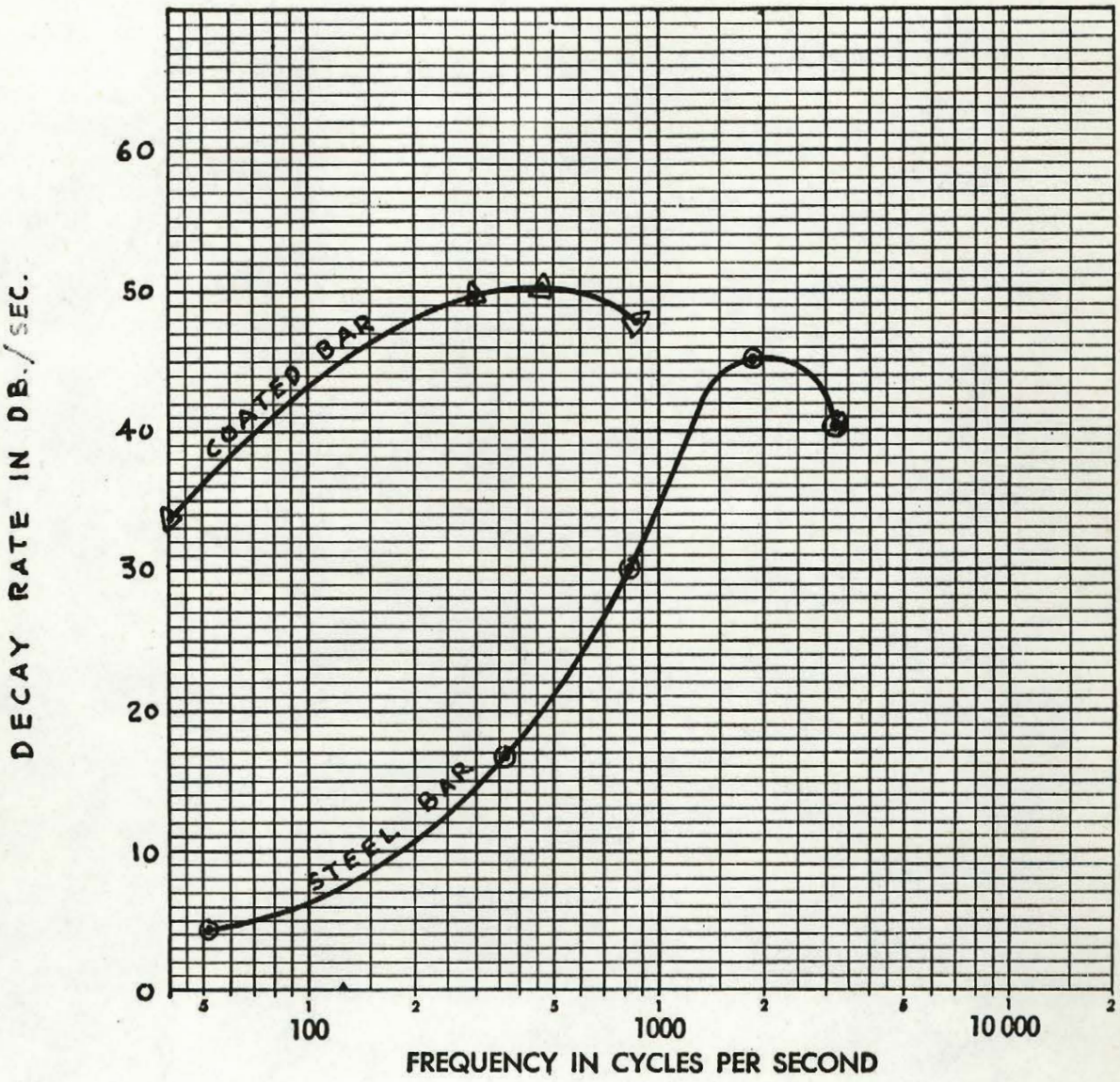

⊙ δ_p vs. f_{op}
△ δ vs. f_o
MATERIAL B

COMPLEX MODULUS TEST

Figure (35)

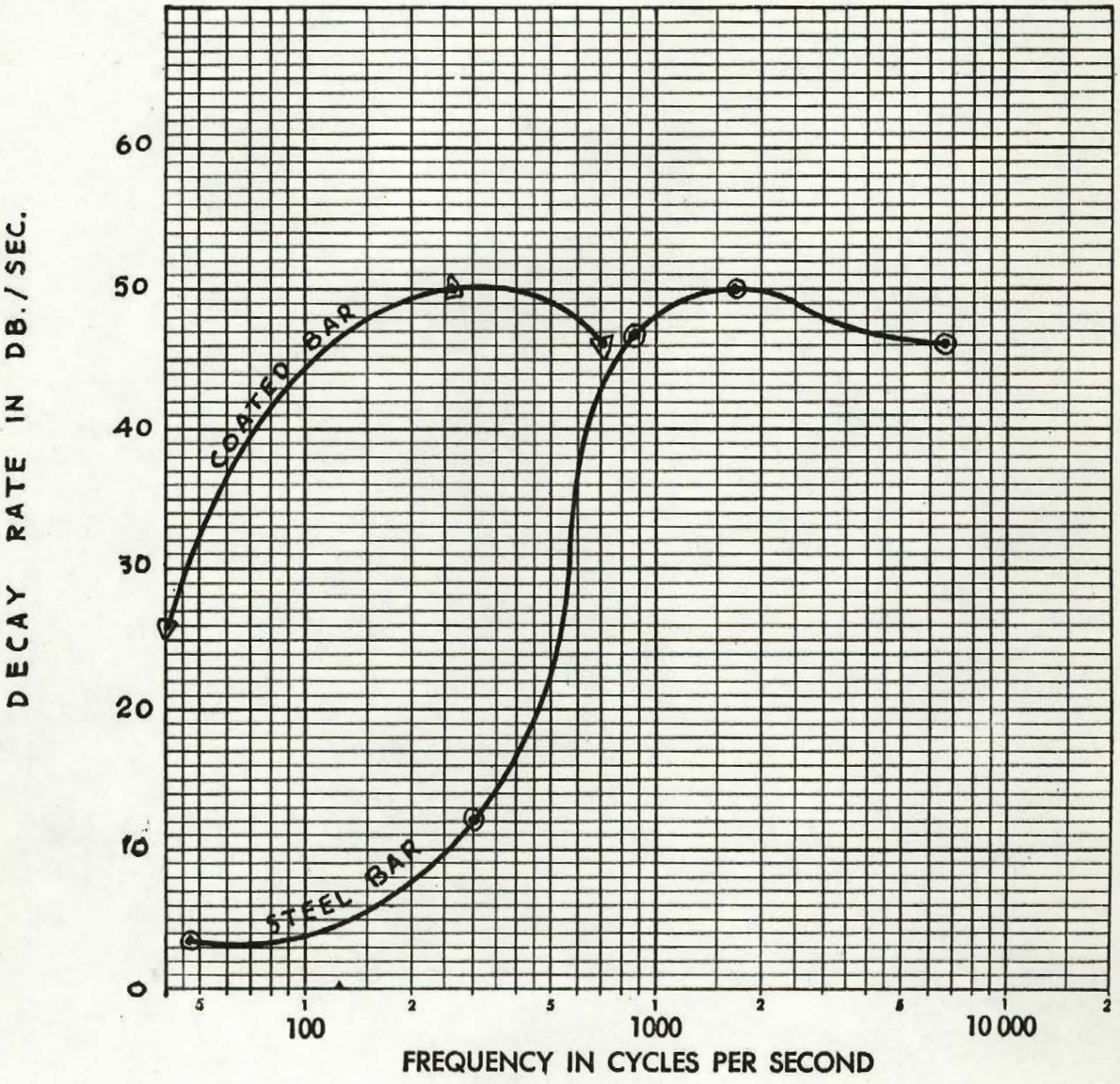

⊙ δ_p vs. f_{op}
△ δ vs. f_o
MATERIAL D

COMPLEX MODULUS TEST

Figure (36)

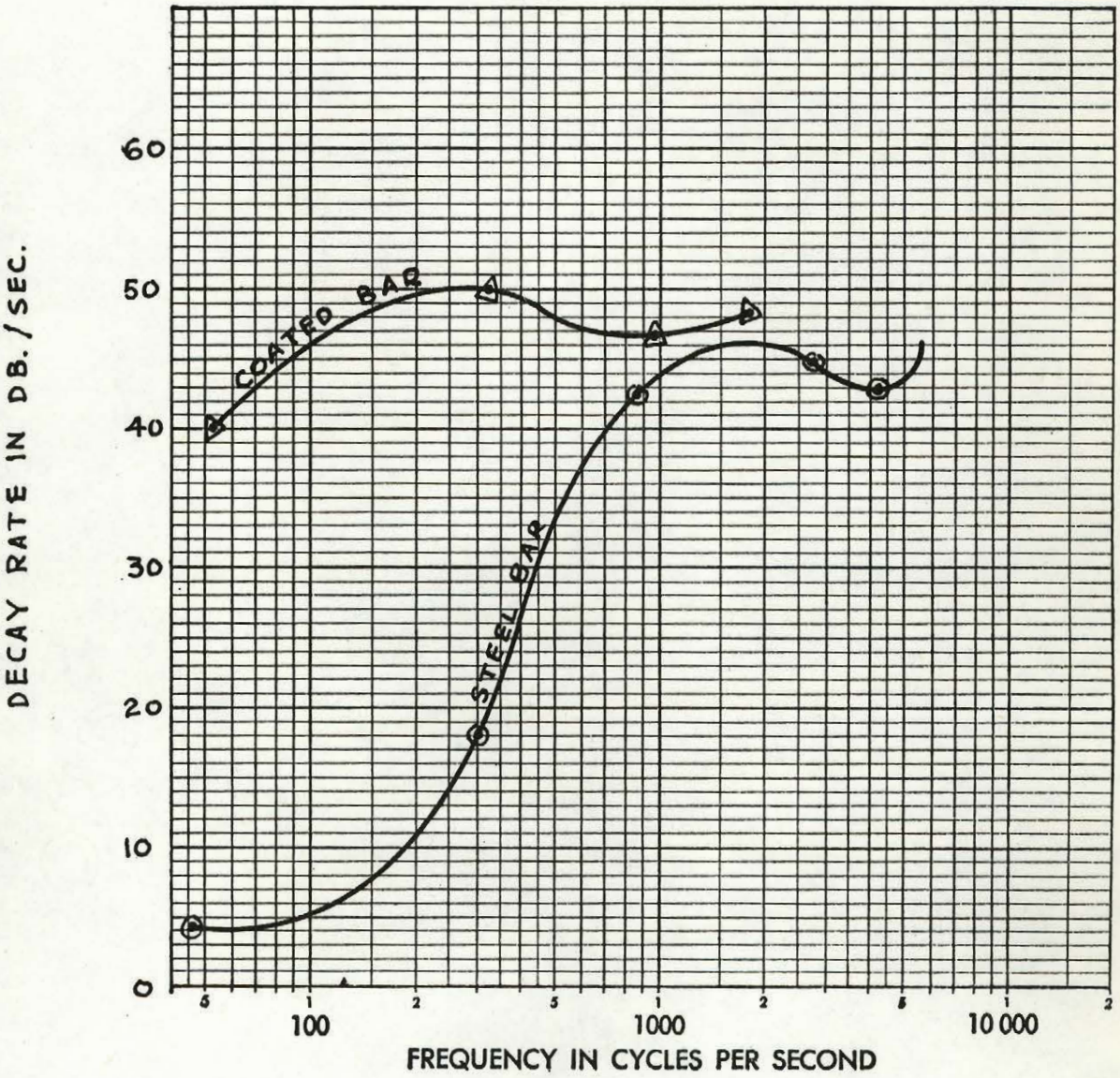

○ δ_p vs. f_{op}
△ δ vs. f_o
MATERIAL E

COMPLEX MODULUS TEST

Figure (37)

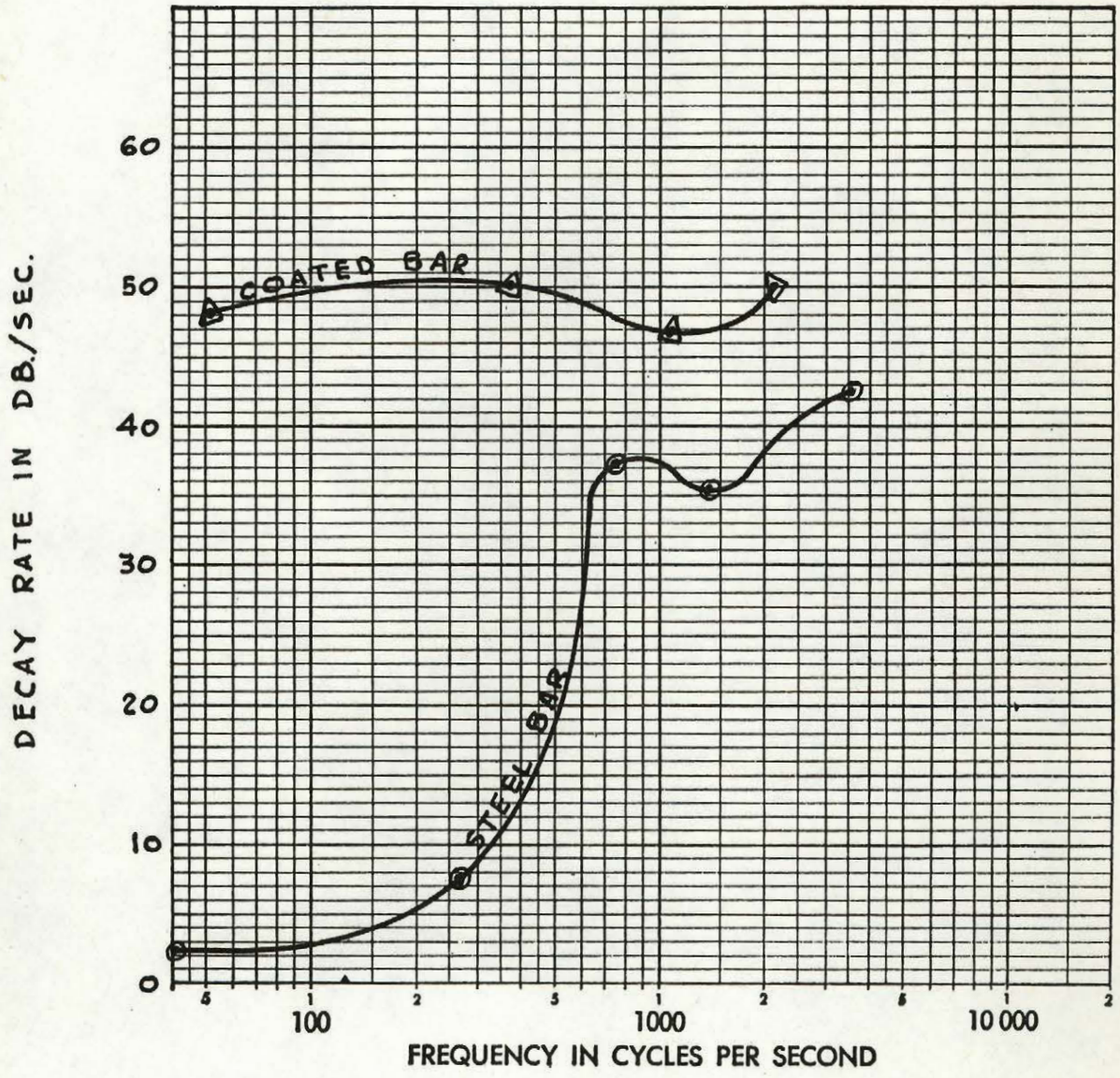

⊙ δ_p vs. f_{op}
△ δ vs. f_o
MATERIAL F

COMPLEX MODULUS TEST

Figure (38)

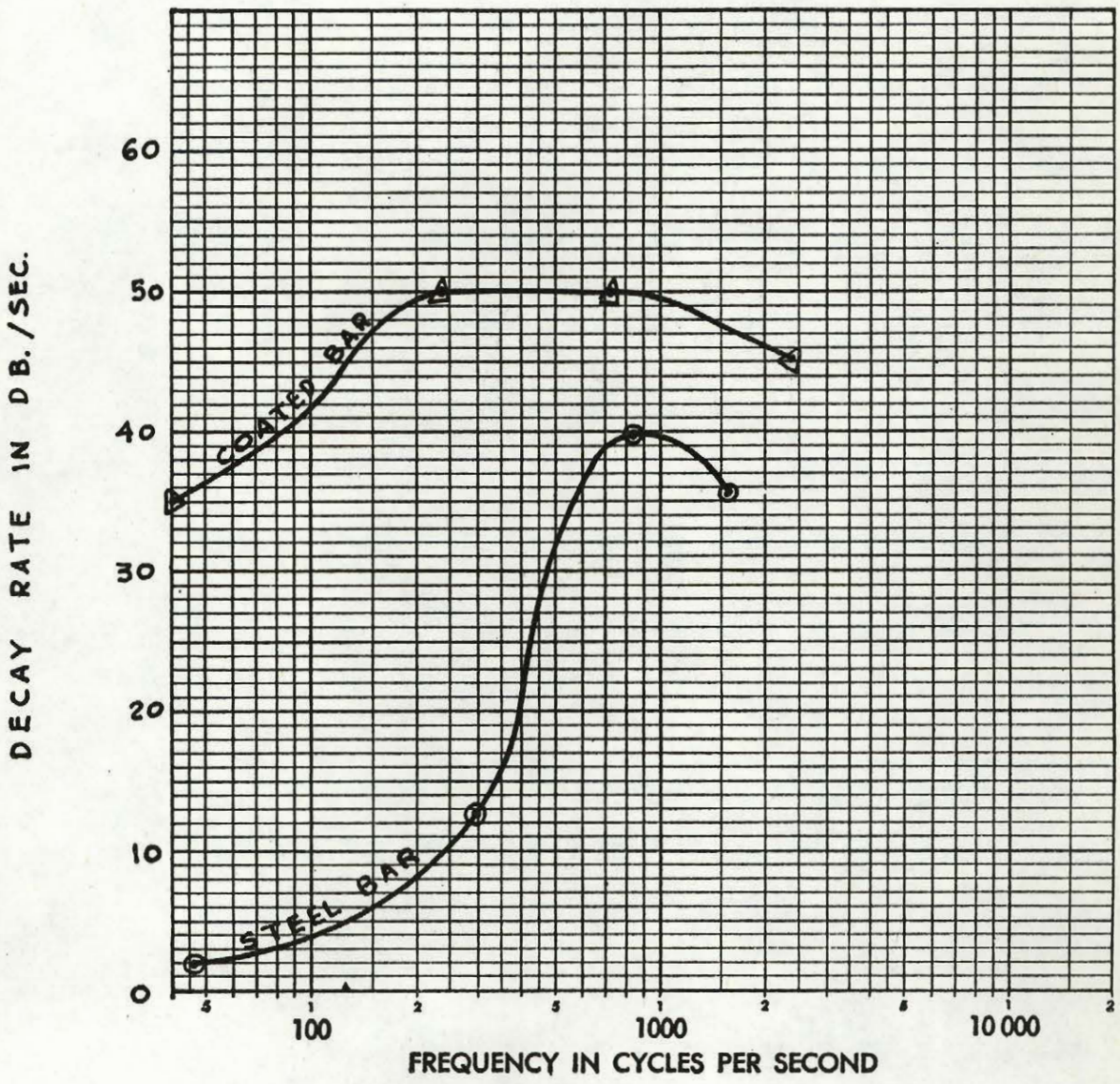

⊙ δ_p vs. f_{op}
△ δ vs. f_o
MATERIAL G

COMPLEX MODULUS TEST

Figure (39)

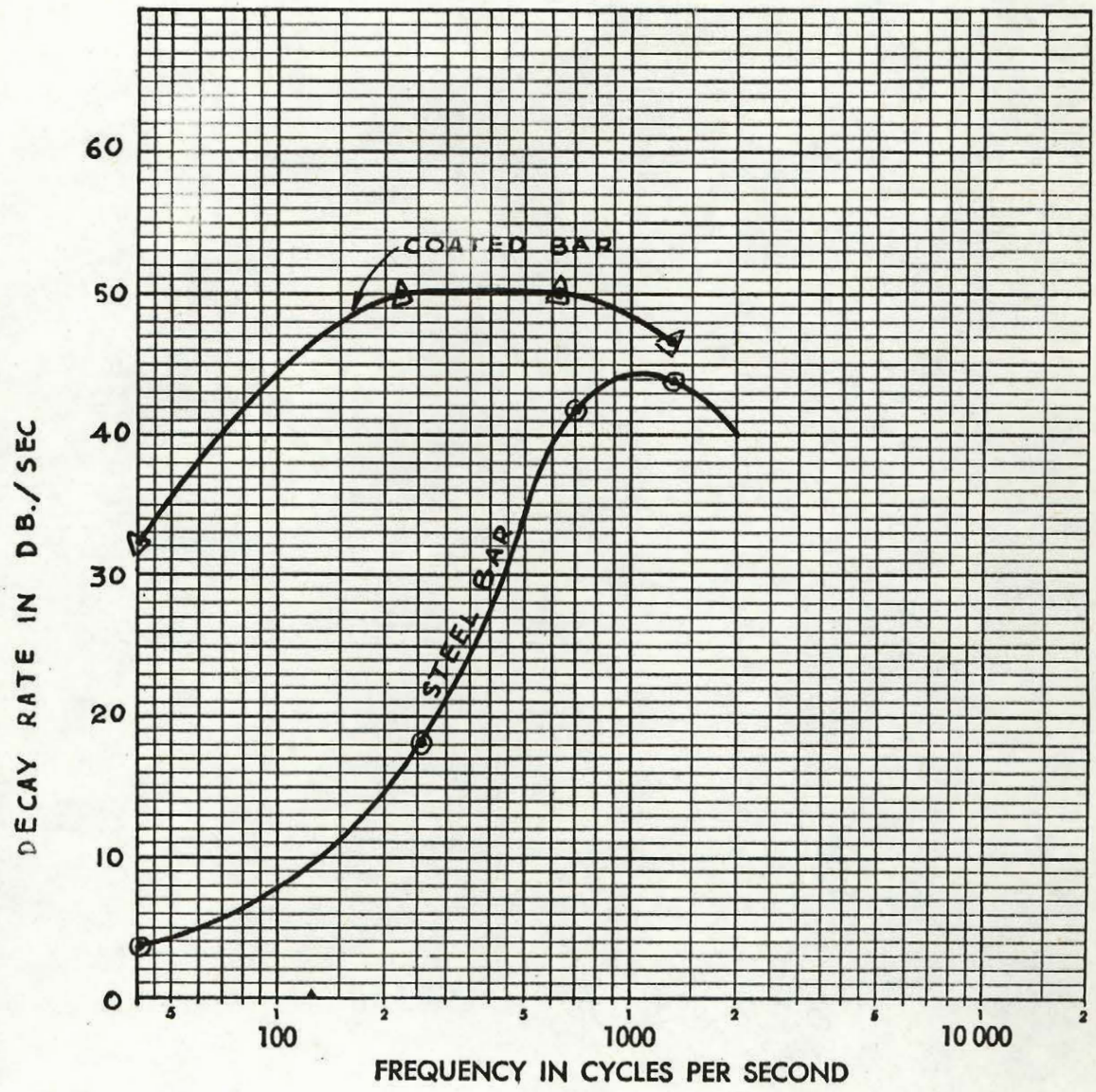

⊙ δ_p vs. f_{op}
△ δ vs. f_o
MATERIAL H

COMPLEX MODULUS TEST

Figure (40)

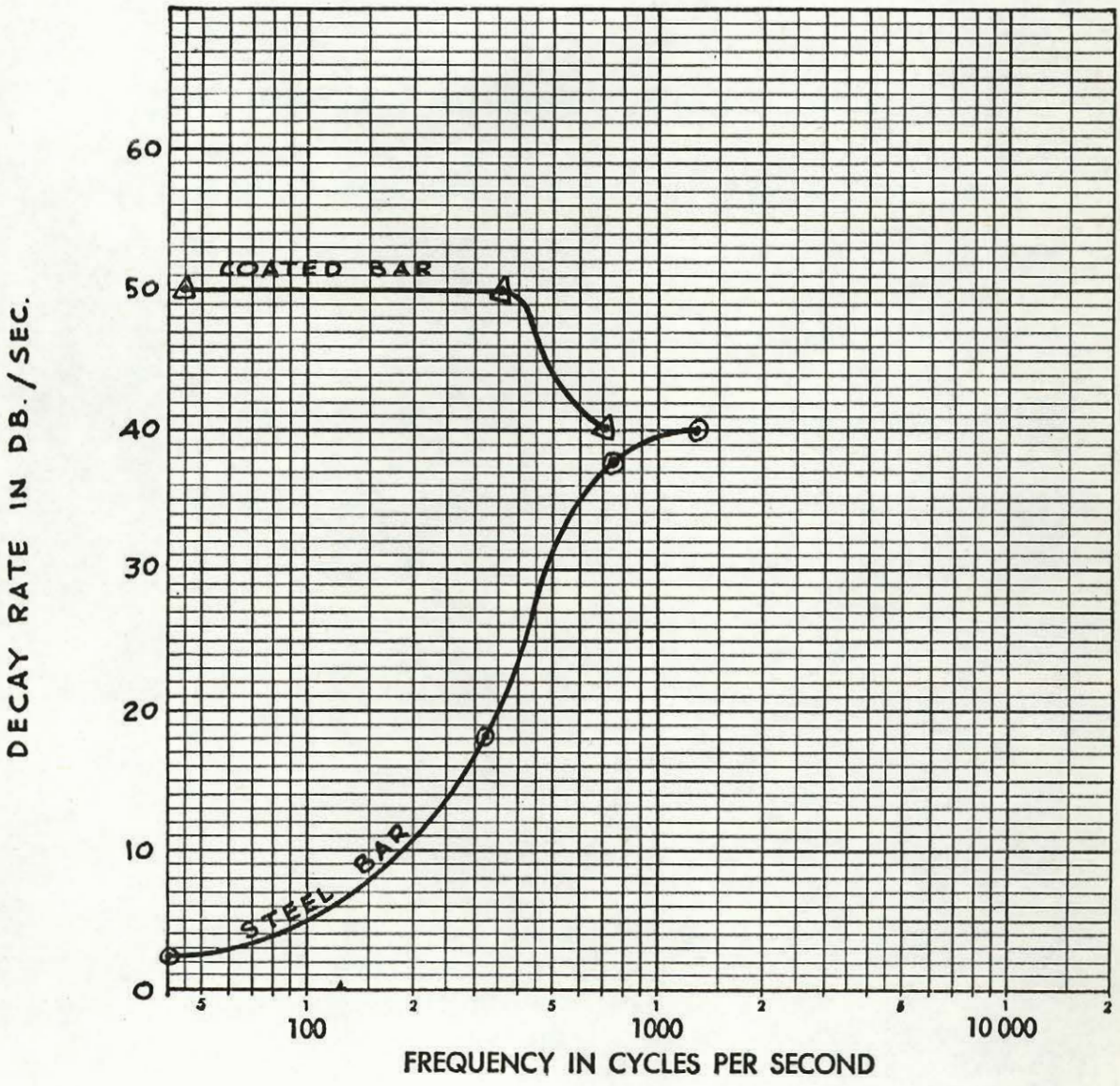

⊙ δ_p vs. f_{op}
△ δ vs. f_o
MATERIAL I

COMPLEX MODULUS TEST

Figure (41)

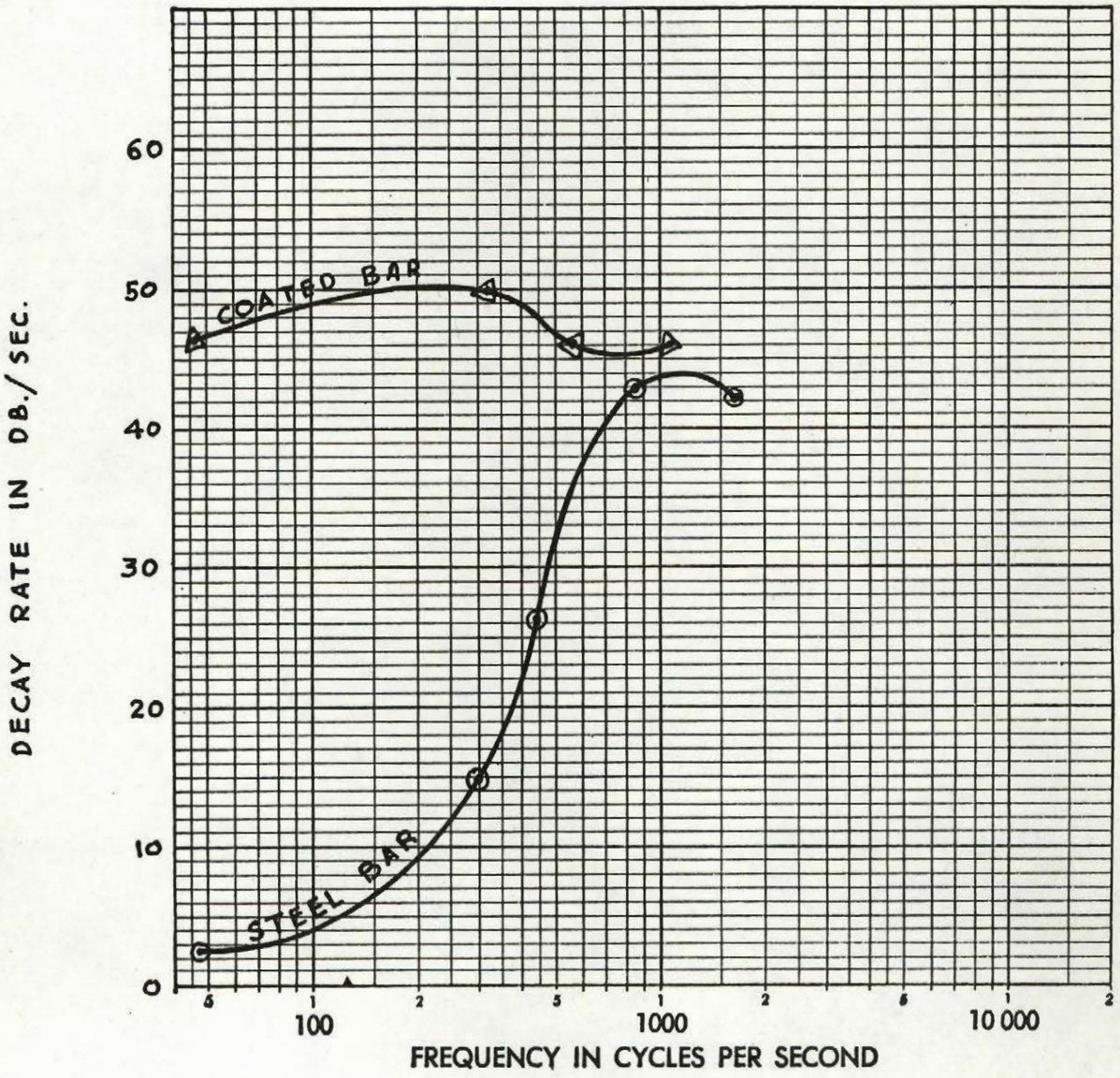

⊙ δ_p vs. f_{op}

△ vs. f_o

MATERIAL J

COMPLEX MODULUS TEST

(Figure 42)

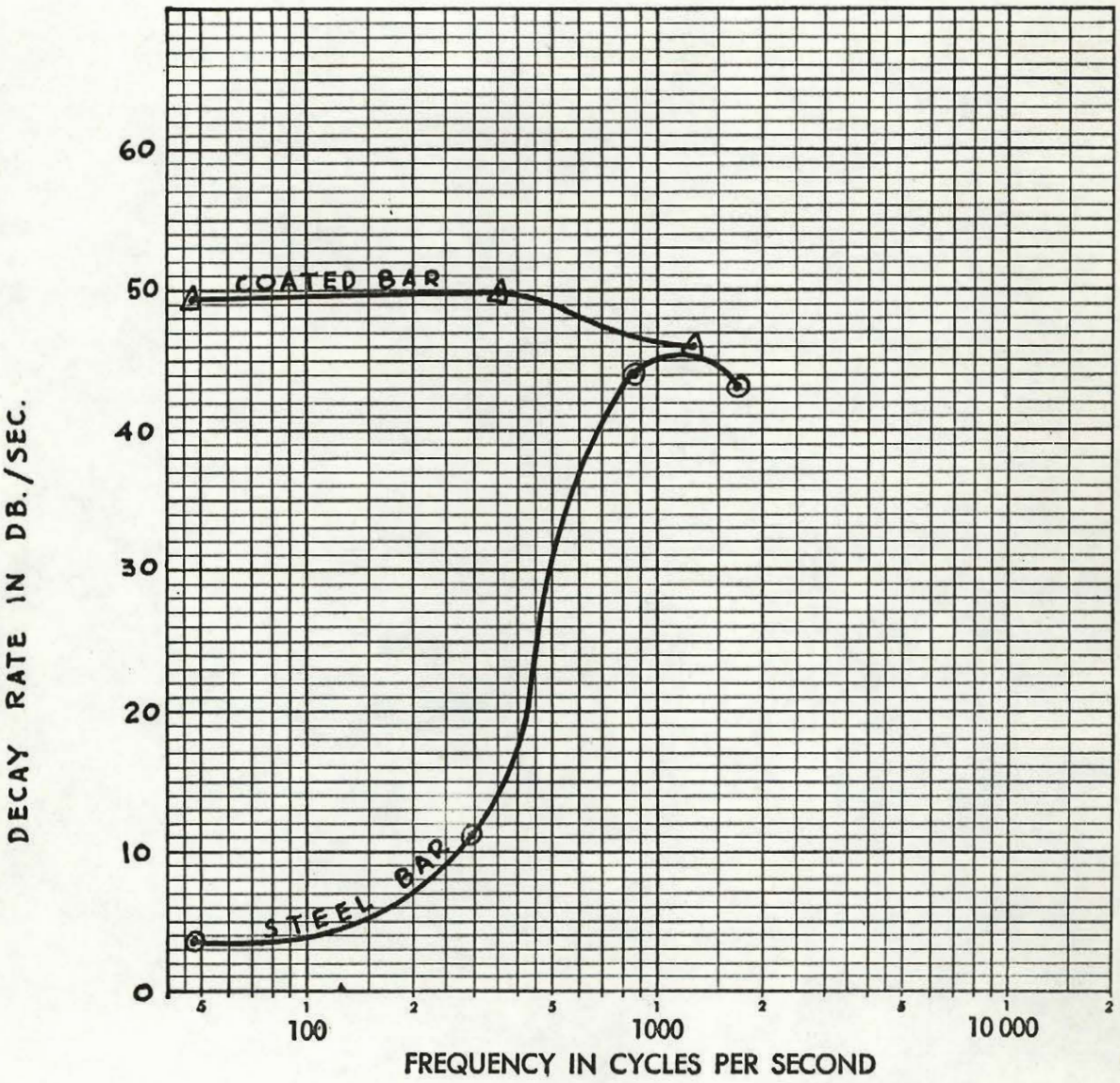

⊙ δ_p vs. f_{op}
△ δ vs. f_o
MATERIAL K

COMPLEX MODULUS TEST

Figure (43)

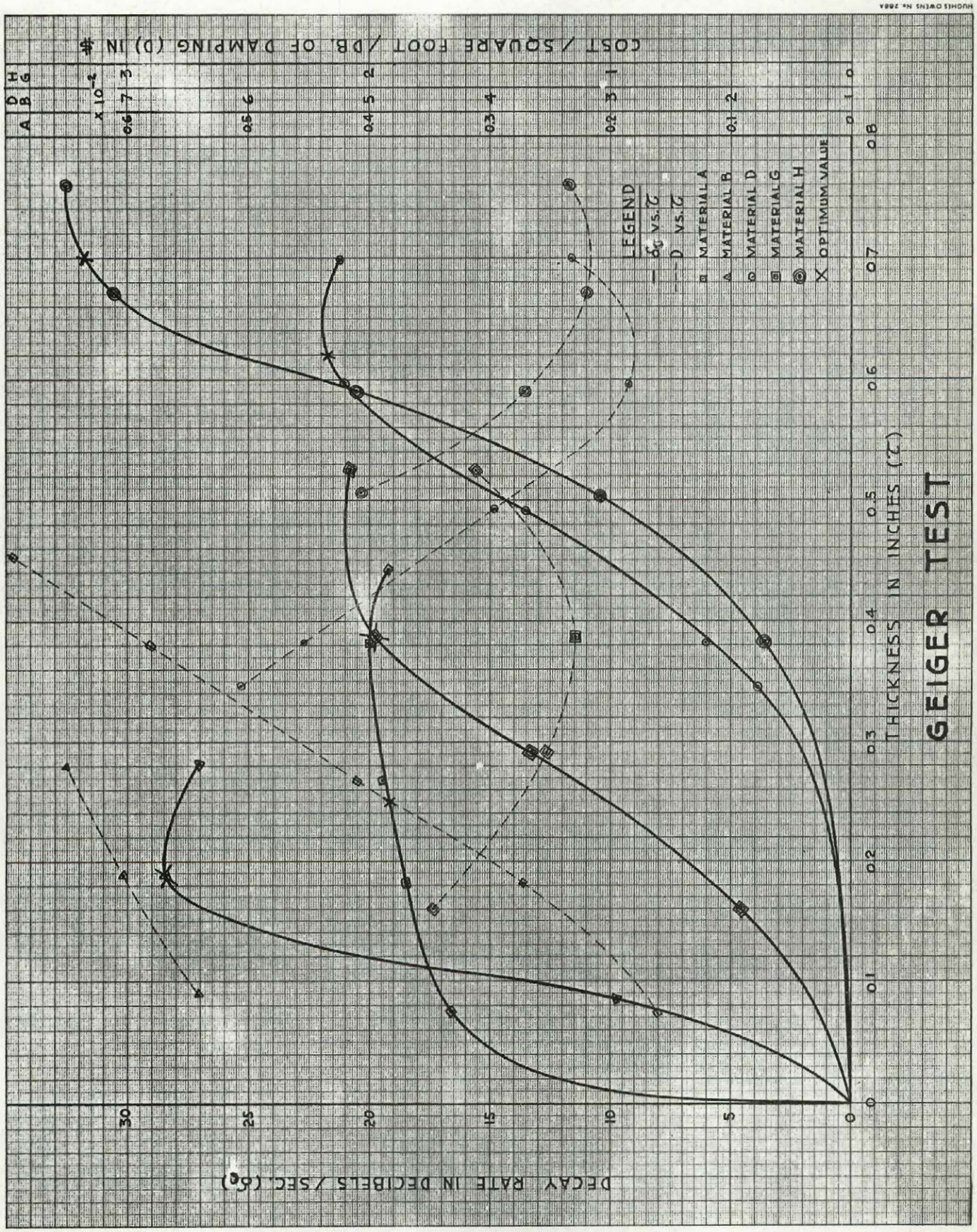
GEIGER TEST
THICKNESS IN INCHES (Z)
DECAY RATE IN DECIBELS / SEC. (δ_G)
COST / SQUARE FOOT / DB. OF DAMPING (D) IN #
LEGEND
δ_G vs. Z
D vs. Z
MATERIAL A
MATERIAL B
MATERIAL D
MATERIAL G
MATERIAL H
OPTIMUM VALUE
A B G D H
x 10⁻²

Figure (44)

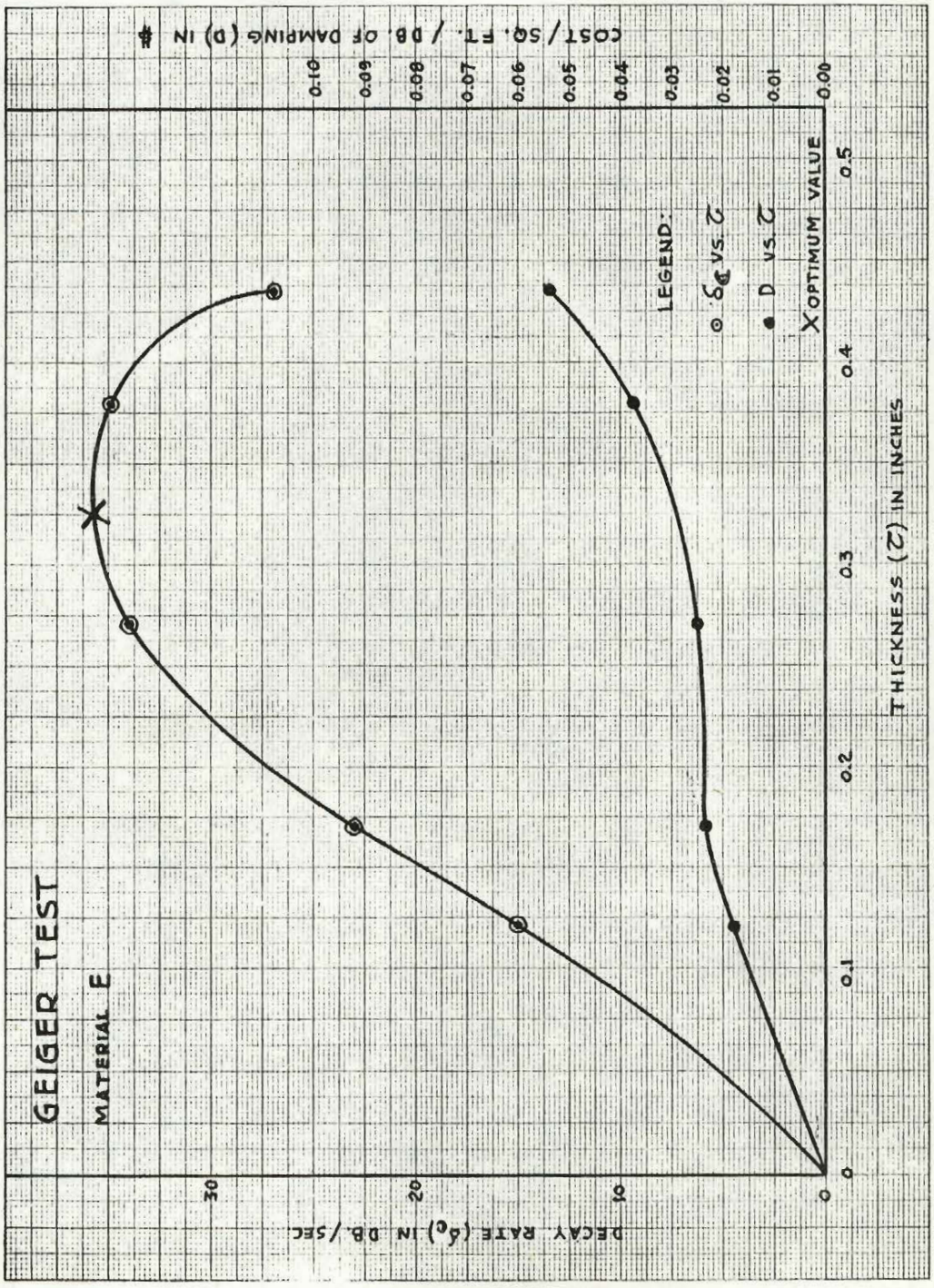
GEIGER TEST
MATERIAL E
DECAY RATE (δ_e) IN DB./SEC
COST/SQ. FT. / DB. OF DAMPING (D) IN $
THICKNESS (Z) IN INCHES
LEGEND:
δ_e vs. Z
D vs. Z
X OPTIMUM VALUE
0
10
20
30
0.00
0.01
0.02
0.03
0.04
0.05
0.06
0.07
0.08
0.09
0.10
0.1
0.2
0.3
0.4
0.5

Figure (45)

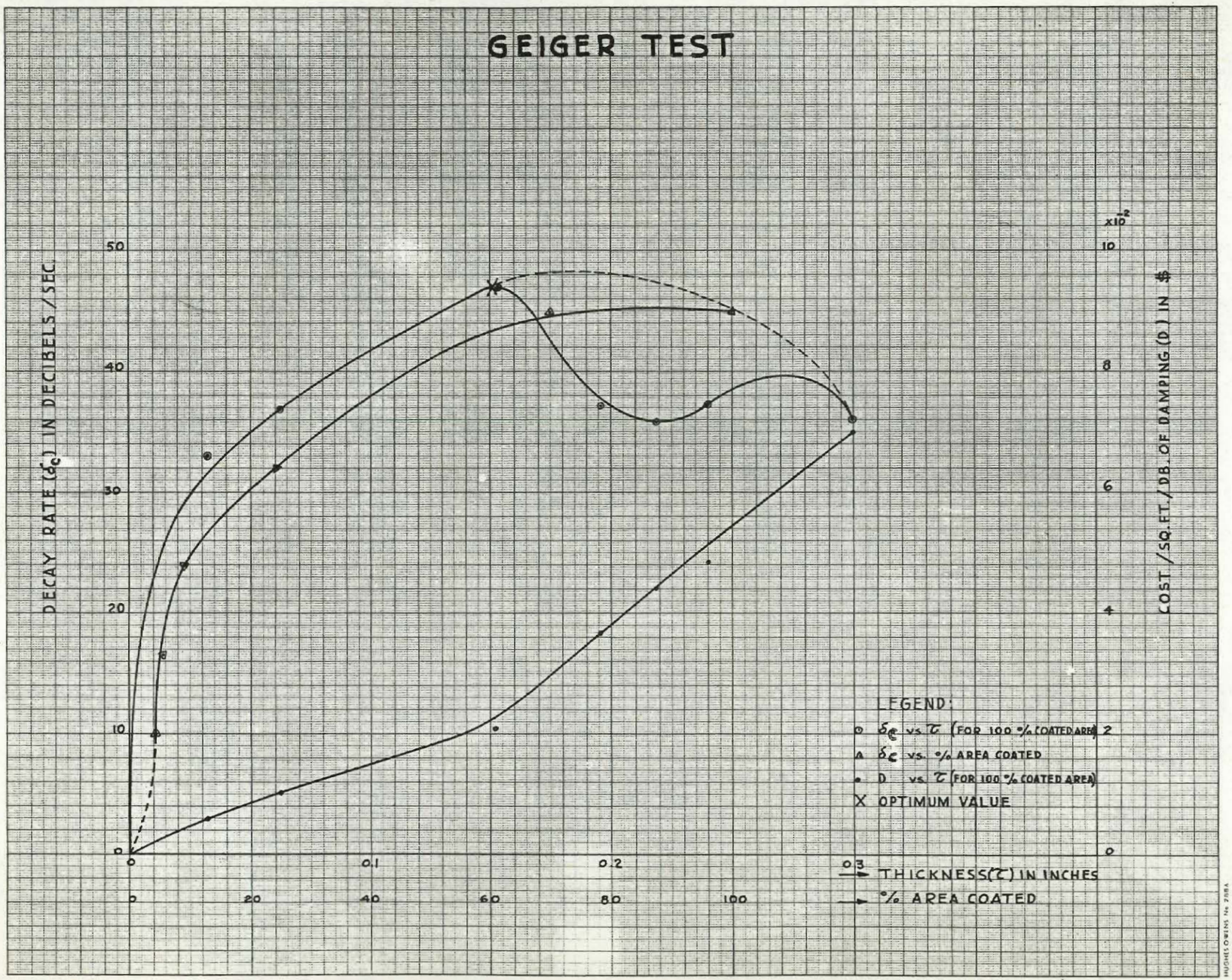

Material "F"
Figure (46)

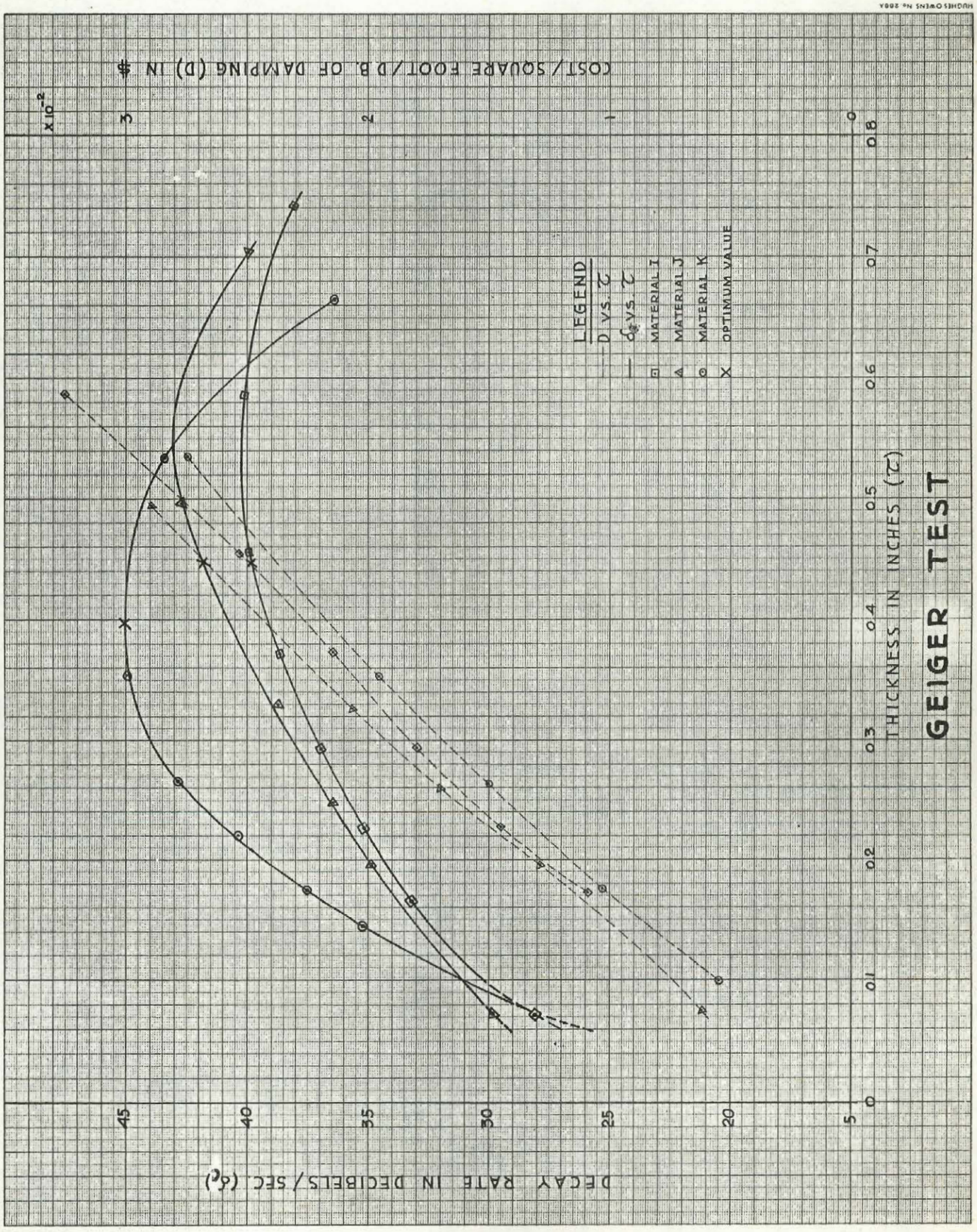
GEIGER TEST
DECAY RATE IN DECIBELS/SEC (δ_d)
COST/SQUARE FOOT/D.B. OF DAMPING (D) IN $
THICKNESS IN INCHES (τ)
LEGEND
D VS. τ
δ_d VS. τ
MATERIAL I
MATERIAL J
MATERIAL K
OPTIMUM VALUE
HUGHES OWENS No. 2884

Figure (47)

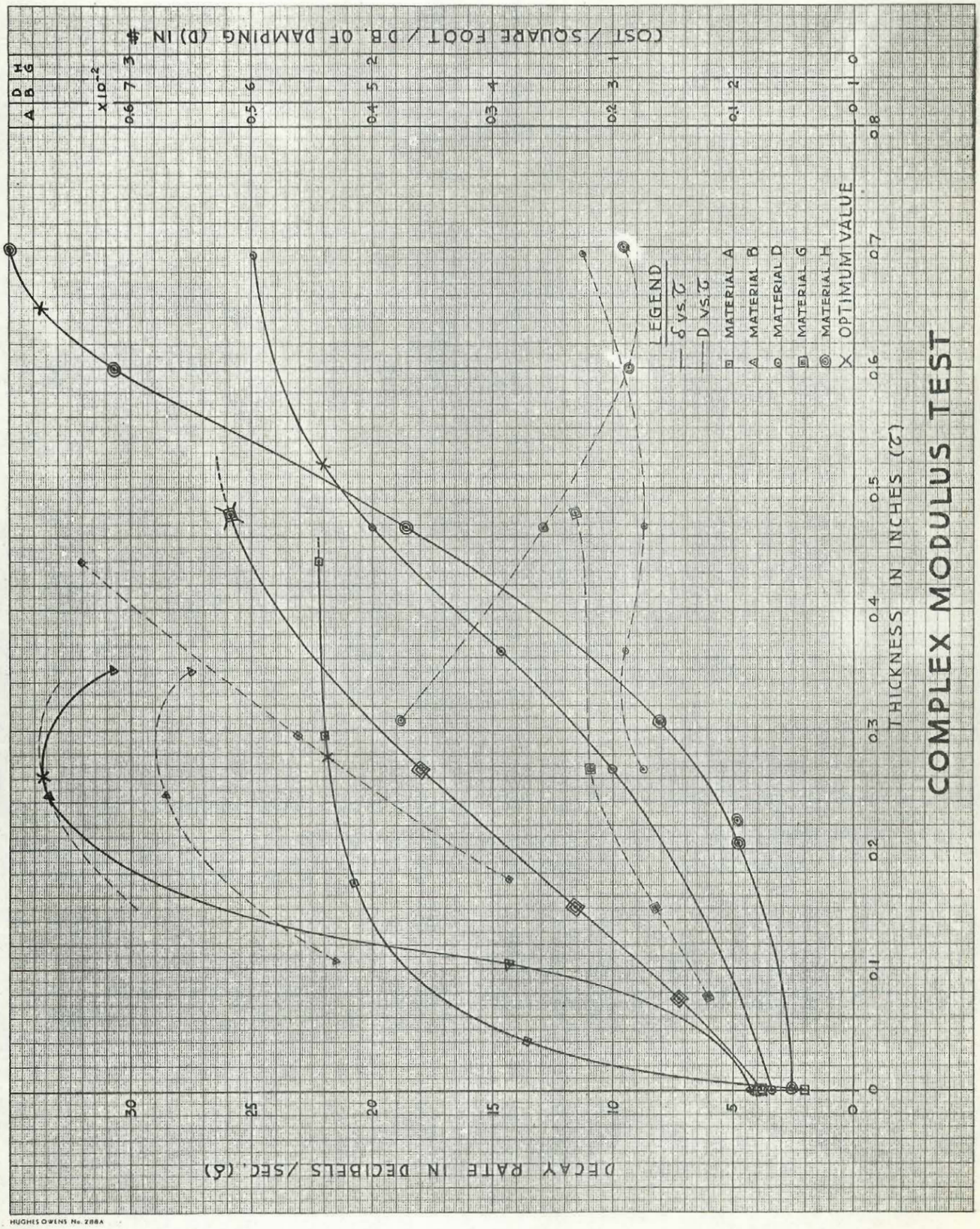
COMPLEX MODULUS TEST
DECAY RATE IN DECIBELS /SEC. (δ)
COST / SQUARE FOOT / D.B. OF DAMPING (D) IN $
THICKNESS IN INCHES (t)
LEGEND
δ vs. t
D vs. t
MATERIAL A
MATERIAL B
MATERIAL D
MATERIAL G
MATERIAL H
OPTIMUM VALUE
A B D G H
x10⁻²
HUGHES OWENS No. 288A

Figure (48)

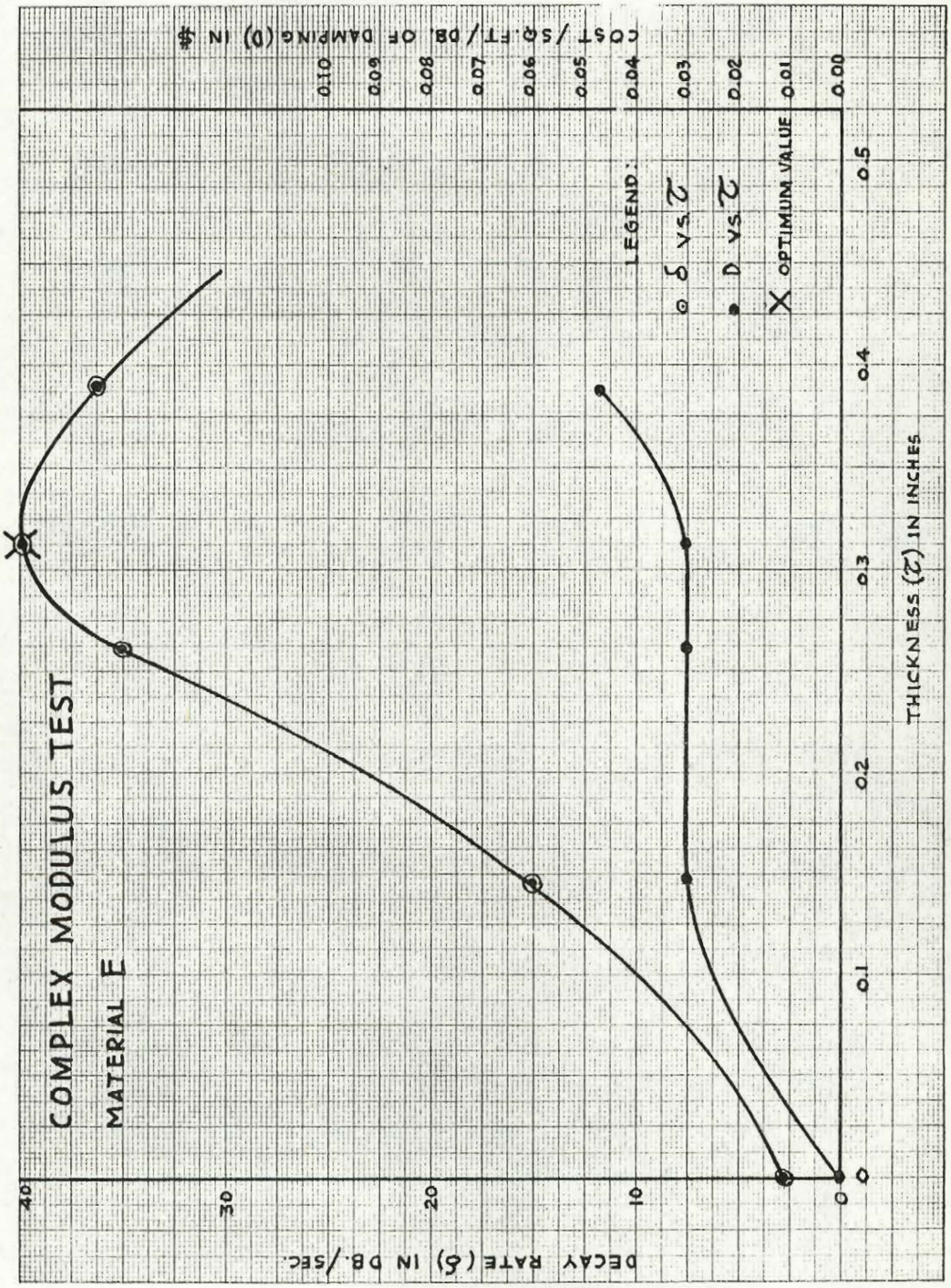
COMPLEX MODULUS TEST
MATERIAL E
DECAY RATE (δ) IN DB./SEC.
40
30
20
10
0
0
0.1
0.2
0.3
0.4
0.5
THICKNESS (T) IN INCHES
LEGEND:
δ VS T
D VS T
X OPTIMUM VALUE
0.00
0.01
0.02
0.03
0.04
0.05
0.06
0.07
0.08
0.09
0.10
DECAY RATE (δ) IN DB./SQ. FT./DB. OF DAMPING (D) IN #

Figure (49)

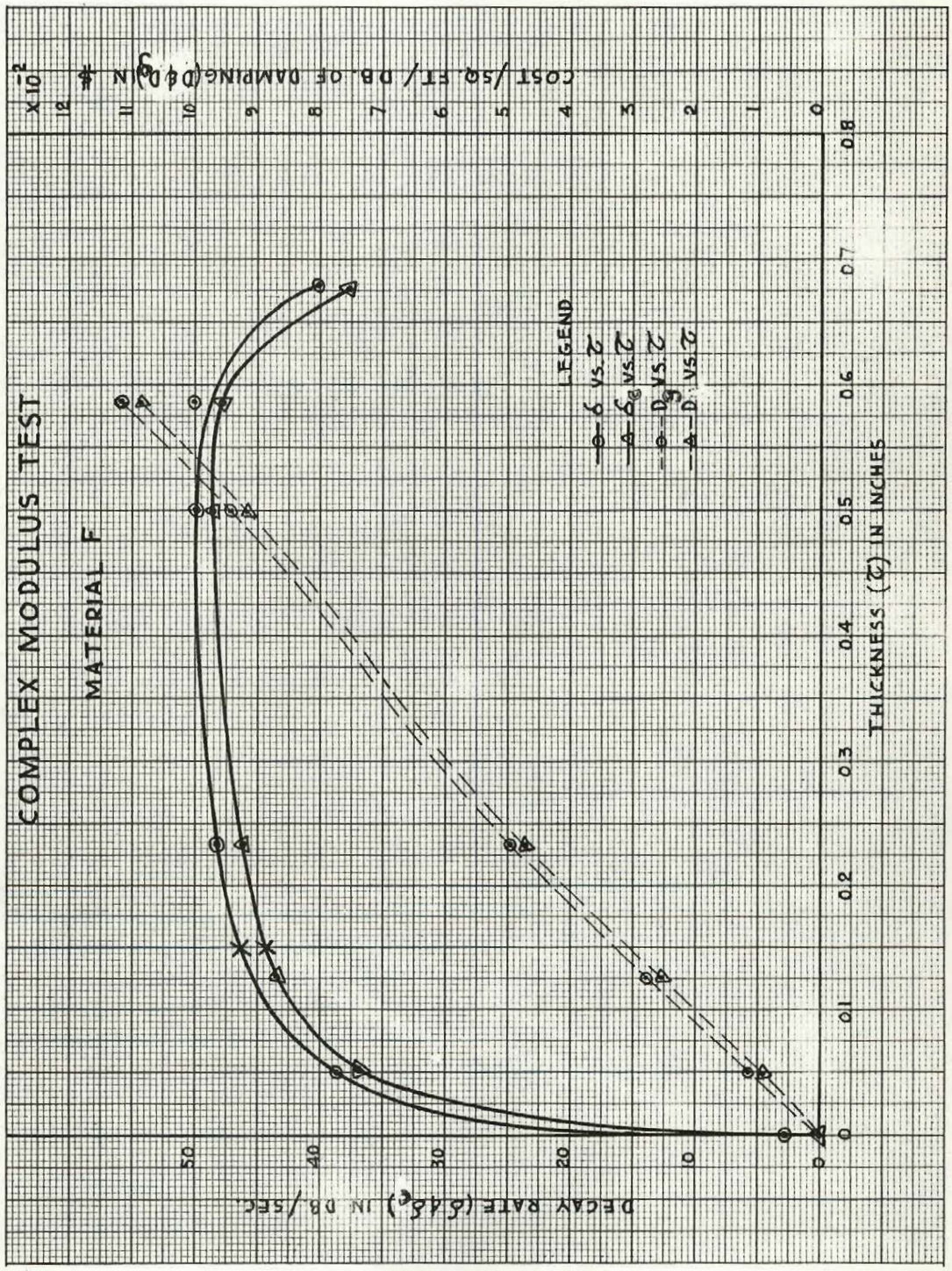
COMPLEX MODULUS TEST
MATERIAL F
LEGEND
$\mathcal{D}$ vs. $\mathcal{Z}$
$\mathcal{D}_a$ vs. $\mathcal{Z}$
$\mathcal{D}_g$ vs. $\mathcal{Z}$
$\mathcal{D}$ vs. $\mathcal{Z}$
DECAY RATE ($\delta_4 \delta_e$) IN DB/SEC.
COST/SQ. FT/ DB. OF DAMPING ($D_4 D_g$) IN $\$ \times 10^{-2}$
THICKNESS ($\mathcal{Z}$) IN INCHES
0
10
20
30
40
50
0
1
2
3
4
5
6
7
8
9
10
11
12
0.1
0.2
0.3
0.4
0.5
0.6
0.7
0.8

Figure (50)

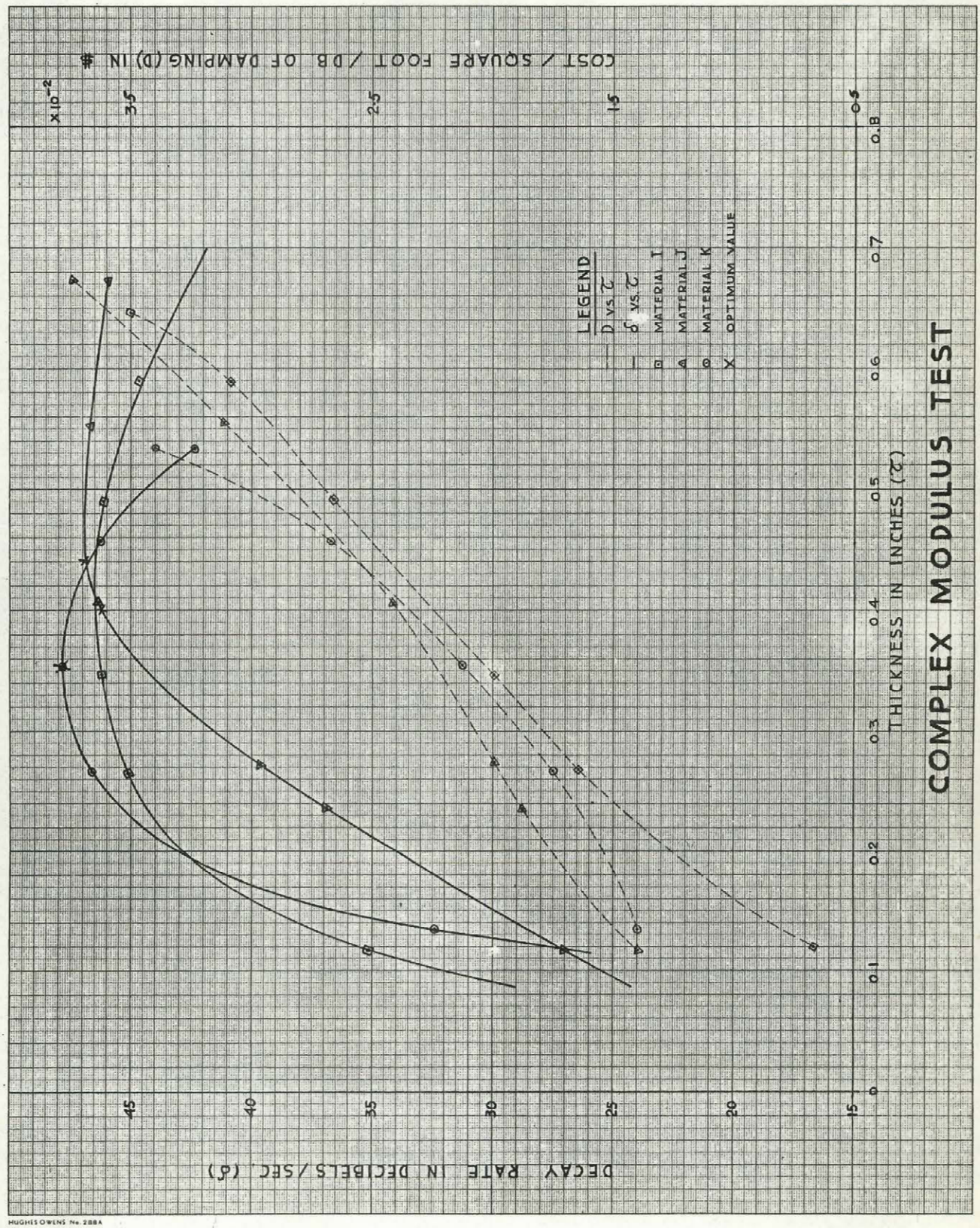
COMPLEX MODULUS TEST
DECAY RATE IN DECIBELS/SEC (δ)
COST / SQUARE FOOT / DB OF DAMPING (D) IN $
THICKNESS IN INCHES (τ)
LEGEND
D vs. τ
δ vs. τ
MATERIAL I
MATERIAL J
MATERIAL K
OPTIMUM VALUE
HUGHES OWENS No. 288A

Figure (51)

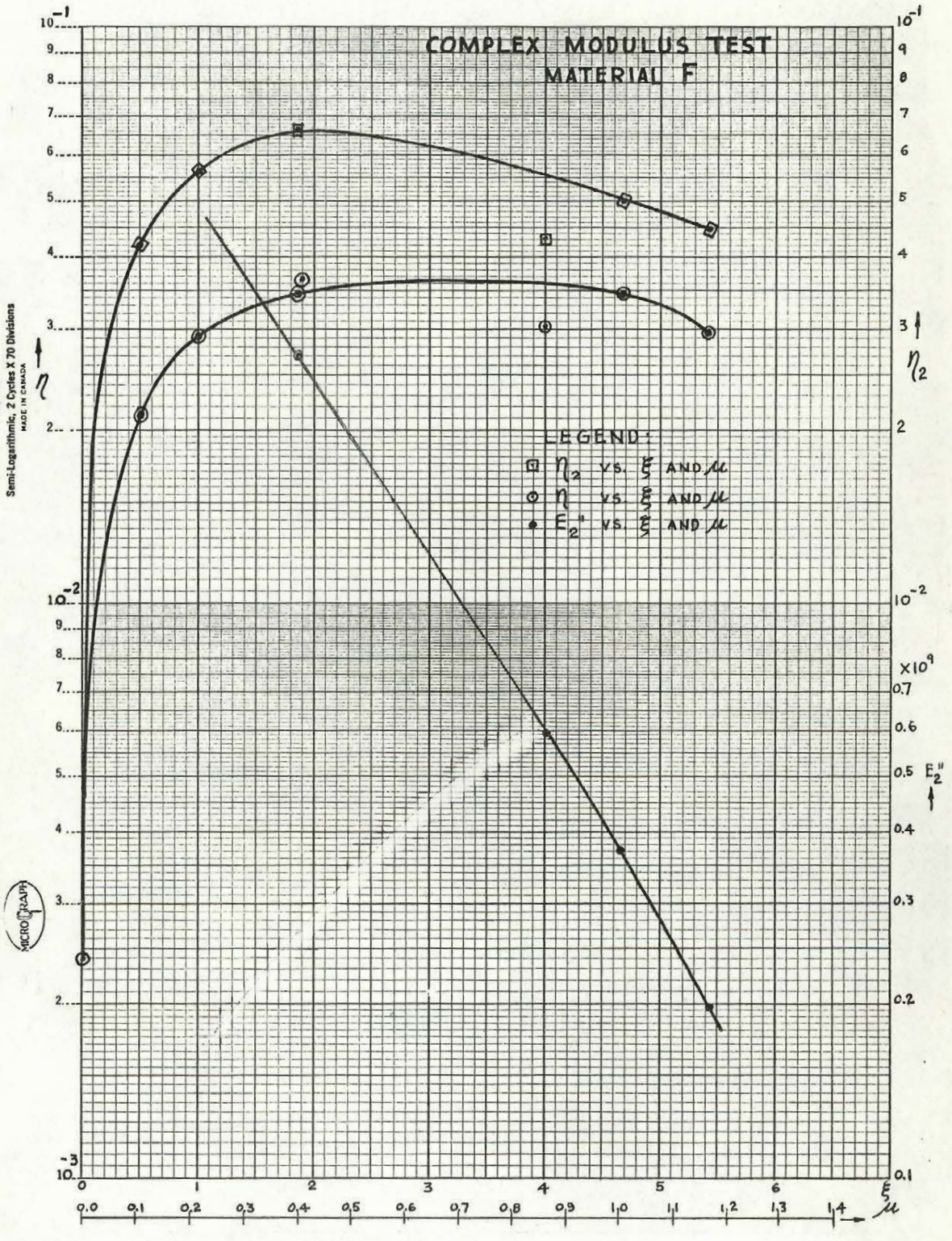
COMPLEX MODULUS TEST
MATERIAL F
LEGEND:
η_2 VS. ξ_μ AND μ
η VS. ξ_μ AND μ
E_2'' VS. ξ_μ AND μ
η
η_2
E_2''
$\times 10^9$
ξ_μ
G8-61
Semi-Logarithmic, 2 Cycles X 70 Divisions
MADE IN CANADA
KEUFFEL & ESSER CO.
MICROGRAPH

Figure (52)

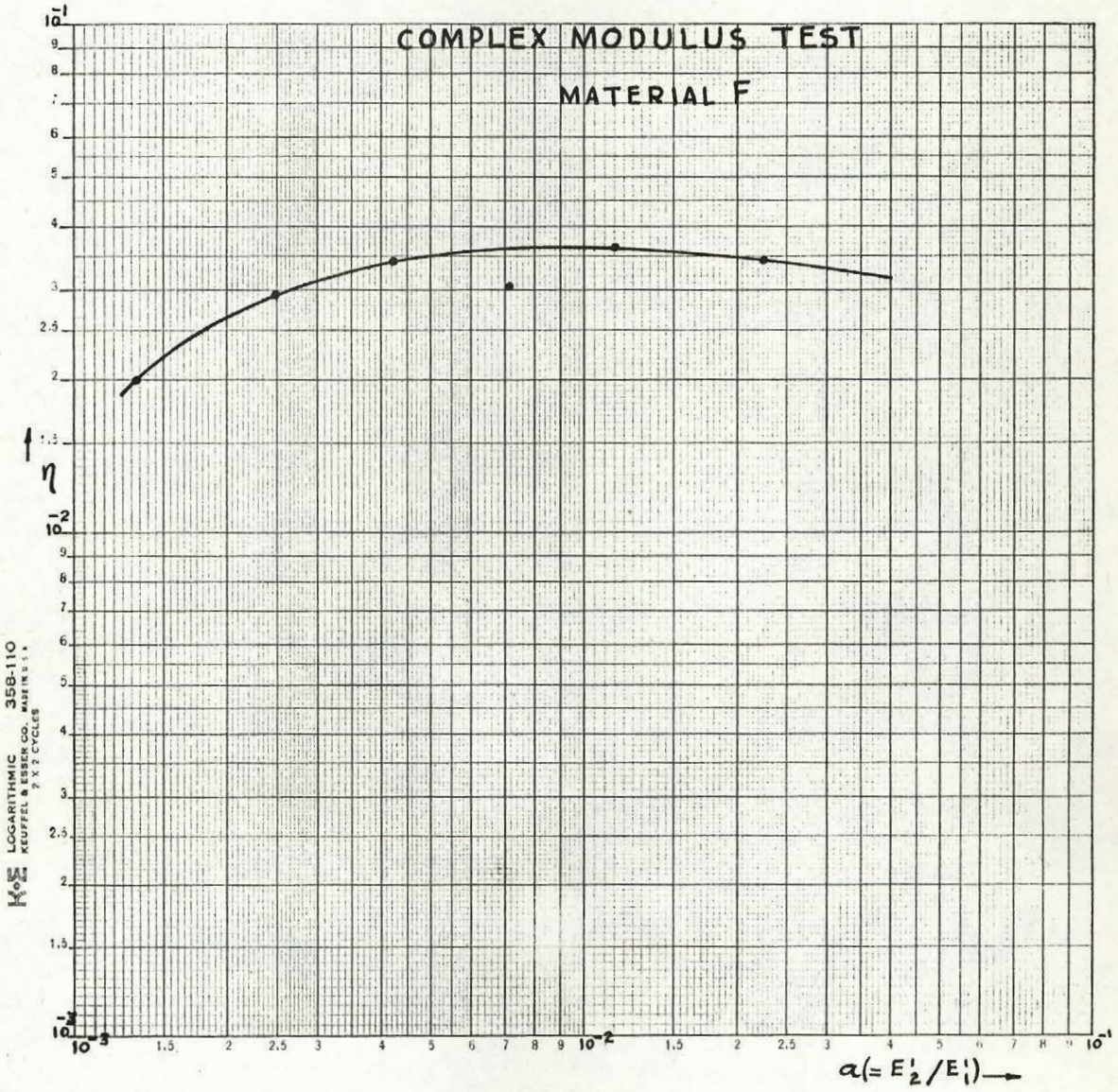
COMPLEX MODULUS TEST
MATERIAL F
η
a(= E'2/E'1)
LOGARITHMIC
KEUFFEL & ESSER CO.
358-110

Figure (53)

Most General Results

TABLE I - Test of Steel Samples

Sample	Type of Steel	Dimensions (Inches)	Mass (L_p) - lbs	Total length of bar - in.	Free length of bar - in.	Decay time (T_p) - sec.	Fundamental Resonant Freq. (f_{op}) - c.p.s.		Decay Rate (δ_p) db/sec.	Q-factor	Damping Material Used
							Calculated	Measured			
Plate 1	Hot-Rolled	20x20x1/4	28.150			18.30		192.00	3.28	1600	F,G
Plate 2	"	"	29.745			7.70		201.00	7.80	705	E.J
Plate 3	"	"	28.130			7.37		191.30	8.15	642	A,B,C, H,I.
Plate 4	"	"	28.277			13.20		193.60	4.55	1160	D,K
Bar 33 (Example)	Cold-Rolled	12x0.31x0.1255	0.129	12	9.29	30.00	45.63	45.50	2.00	622	A

Bar 33 is typical of the 54 total number of bars used for the Complex Modulus Test. The range of the decay rate (δ_p) for these bars was 1-4 db/sec, mainly due to different free lengths.

TABLE II

OPTIMUM FREQUENCY-RANGE

MATERIAL	RANGE IN C.P.S.
A	20 - 400
B	20 - 350
D	20 - 300
E	20 - 300
F	20 - 400
G	20 - 250
H	20 - 250
I	20 - 350
J	20 - 350
K	20 - 350

TABLE III

SOME PHYSICAL PROPERTIES

MATERIAL	APPROXIMATE DRYING TIME	ADHESION
A	2 days/0.07 inch layer	Fair
B	---	Good (for 1 layer only)*
D	12 days/0.15 inch layer	Poor
E	2 days/0.1 inch layer	Good
F	1-1/2 days/0.08 inch layer	Excellent
G	20 days/0.2 inch layer	Fair
H	20 days/0.2 inch layer	Fair
I	5 days/0.1 inch layer	Good
J	4 days/0.1 inch layer	Good
K	4 days/0.1 inch layer	Good

*The aluminum foil used with this material reduces the effective adhesion of secondary tape layers to the metal surface.

TABLE IV

OPTIMUM THICKNESS (GEIGER TEST)

MATERIAL	OPTIMUM THICKNESS (τ)-INCHES	DECAY RATE (δ_c) (at optimum (τ)) in db/sec,	Cost/sq.ft/ db of Damping (at optimum τ) - D(in $)
A	0.250	19.2	0.00384
B	0.1876	28.4	0.0704
D	0.620	21.8	0.0280
E	0.325	35.8	0.0290
F	0.1525	47.5	0.0204
G	0.386	19.8	0.0114
H	0.700	31.7	0.0108
I	0.450	39.8	0.0248
J	0.450	41.7	0.0268
K	0.40	45.0	0.0215

TABLE V

OPTIMUM THICKNESS (COMPLEX MODULUS TEST)

MATERIAL	OPTIMUM THICKNESS (τ) - INCHES	DECAY RATE (δ) AT OPTIMUM VALUE OF τ - db/sec.	COST/SQ.FT/DB OF DAMPING AT OPTIMUM VALUES OF τ and δ -D(in $)	DECAY RATE CORRECTED FOR DAMPING MATERIAL ONLY (δ_c)-db/sec.	COST/SQ.FT/DB OF DAMPING AT OPTIMUM VALUES OF τ AND δ_c - D(in $)
A	0.278	21.8	0.00438	19.8	0.00463
B	0.262	33.6	0.0772	31.4	0.0826
D	0.52	22	0.0276	20.8	0.0292
E	0.3125	40	0.030	37.7	0.0318
F	0.150	46.5	0.030	44.5	0.330
G	0.480	25.9	0.0116	24.4	0.0123
H	0.650	33.7	0.0090	31.9	0.00953
I	0.400	46.3	0.0225	42.4	0.0246
J	0.44	46.9	0.0255	43.0	0.0278
K	0.354	47.9	0.0213	44.0	0.0227

TABLE VI

PAD TESTS (MATERIAL C)

PAD	MATERIAL	THICKNESS (Inches)	DECAY RATE (δ_c) in db/sec. (GEIGER TEST) MATERIAL AVAILABLE *	
			PAD	LIQUID
C-1	Epoxy	0.125	37.08	- -
C-2	Epoxy	0.275	39.46	--
C-3	I	0.178	35.43	34.30
C-4	J	0.125	34.01	32.10
C-5	K	0.120	37.15	33
C-6	I	0.275	38.31	36.5
C-7	J	0.275	38.58	37.3
C-8	K	0.290	44.31	43.7

*These values were taken from Figure (47) and listed here for comparison.

TABLE VII

ORDER OF MERIT

The following is a table in which the tested damping materials are classified on the basis of three criteria.

DECAY RATE DB/SEC.				COST/SQ.FT/DB OF DAMPING (IN $)		REDUCTION IN RADIATED SOUND PRESSURE LEVEL	
ORDER OF GROUP*		ORDER OF MATERIAL		ORDER OF MATERIAL		GEIGER TEST	
GEIGER TEST	COMPLEX MODULUS TEST	GEIGER TEST	COMPLEX MODULUS TEST	GEIGER TEST	COMPLEX MODULUS TEST	L_g = 3.0** lbs.	τ = 0.15**
3	3	F	F	A	A	F	F
4	2	K	K	H	H	K	K
2	5	J	J	G	G	J	J
5	1	I	I	F	K	I	I
		E	E	K	I	A	B
		H	H	I	J	G	G
		B	B	J	D	B	A
		D	G	D	E	E	E
		G	D	E	F	H	H
		A	A	B	B	D	D

*See Section 3.2

**These values correspond to the optimum mass and layer thickness of material F.

TABLE VIII

MATERIAL A - GEIGER PLATE TESTS

Test No.	Test Plate No.	Thickness (Inches)	Temp. °F	EQUIVALENT CIRCUIT PARAMETERS						
				R_p Ohms	L_p Henrys	C_p mμf	R_g Ohms	L_g Henrys	C_g μμf	R Ohms
1	2	3	4	5	6	7	8	9	10	11
12	3	0.0736	83	52.70	28.13	24.63	116.78	2.558	1.803	169.48
16	3	0.182	85.8	52.70	28.13	24.63	137.96	4.46	1.163	190.66
21	3	0.250	84	52.70	28.13	24.63	150.39	5.99	0.812	203.09
24	3	0.268	84	52.70	28.13	24.63	160.06	7.62	0.712	212.76
28	3	0.382	82	52.70	28.13	24.63	175.42	9.87	0.625	228.11
34	3	0.442	80	52.70	28.13	24.63	174.25	11.32	0.496	226.95

L Henrys	C μμf	F_{op} c.p.s.	F_o c.p.s.	F_{og} c.p.s.	Q_p	Q_g	Q	δ_p	δ_g	δ	δ_c
12	13	14	15	16	17	18	19	20	21	22	23
30.68	24.30	191.3	184.4	74.13	641.3	10.2	209.7	8.14	198.4	24.00	16.53
32.59	24.12	191.3	179.6	69.90	641.3	14.19	192.78	8.14	134.43	25.42	18.40
34.125	23.90	191.3	176.3	72.17	641.3	18.06	186.03	8.14	109.01	25.86	19.15
35.75	23.80	191.3	172.6	68.33	641.3	20.43	182.13	8.14	91.28	25.86	19.45
38.00	23.69	191.3	167.8	64.07	641.3	22.64	175.53	8.14	77.23	26.08	20.06
39.45	23.46	191.3	165.5	67.19	641.3	27.41	180.66	8.14	66.89	25.00	19.19

REMARKS: Approximate drying time = 2 days for each 0.07" added layers.

5.2.2 Results of the Non-Uniform Coating-Thickness Tests

These tests were done using Plate No.1 and the coating thickness was varied in two ways:

(a) In the case of material F the thickness was kept uniform (at the optimum value), in a specified area and zero everywhere else on the plate surface. The layers were squares as shown in Photograph (11).

(b) In case of Material I the thickness was varied in a sinusoidal manner, except for the node lines which were left uncoated. (See Photograph (10)).

Figure (46) shows that the optimum range of the percent coating area for material F is 9 - 70%. For 9% coating area the available decay rate is 51% of that at 100% coating area.

The second non-uniform test was done on Plate 1 coated with 3.5 lbs of material I. The advantage of sinusoidal variation of the thickness in this test can be seen in the following table:-

	Uniform Thickness Test*	Sinusoidal Thickness Test
Material	I	I
Thickness	0.14 inches	0.5 inches max.**
Mass of layer	3.4 lbs	3.4 lbs
Decay Rate	35 db/sec.	50 db/sec.

* These values were taken from Figure (47)

**The thickness distribution was done as close to that of the Bending Moment as possible. (See expression for Z' - Appendix C.)

5.2.3 Breakdown of the Complex Modulus Method

As mentioned in Chapter 4, the vibrational stress in the steel bars, used in the Complex Modulus test, must not exceed a certain value. This value was mainly determined by:

(a) density and grade of the steel;

(b) physical dimensions of the bar.

These quantities determine the resonant modes and the dynamic modulus of elasticity (E_1'). If the stress exceeds the yield-point value, the strain will increase very rapidly while E_1' will decrease.

To study the effect of large vibrational stresses, Bar 34 was tested in both the elastic and plastic ranges. The bar dimensions were as follows:

Elastic conditions:

Length:	12.04 inches
Free Length:	9.10 inches
Width:	0.31 inches
Thickness:	0.1255 inches
Mass uncoated:	0.1315 lbs.

Other quantities were as follows:

Static modulus of elasticity	= 30×10^6 lbs/inch^2
Density	= 0.282 lb/in^3
Fundamental resonant freq. (f_{op})	= 46.6
Decay rate at f_{op}	= 2.72 db/sec,
Method used:	Reverberation-time
Clamping:	One end.

The input voltage to the exciter transducer was then increased in steps. At four times the original voltage, the bar was very noticeably bent at the clamping end, where the bending moment was a maximum, and the decay rate reached a value of 42.8 db/sec.

The test was repeated using another bar identical to Bar 34 and coated with a 0.105 inch layer of material J. At seven times the original safe voltage, the decay rate reached a value of 48 db/sec. However, the coating material was severely damaged and the experiment was hence discontinued.

5.2.4 Possible Improvements of the Testing Methods and Suggestions Regarding Their Application

1. The results given in Section 5.2.2 indicate that it is probably worthwhile to investigate further the use of partial and non-uniform coating in order to improve upon the damping efficiency, (i.e. decay rate per lb of a given damping material). This study could be carried out equally well using sample bars, where the bending moment distribution is maintained uniformly in the test sections. In such a distribution all the material in the coating layer will undergo the same bending moment, although not the same deflection*. One experimental

---

*The points of maximum deflection are determined by the resonant mode.

arrangement, where such a distribution can be obtained, is proposed in Chapter 8.

2. Section 5.2.3 presented the case where the coating material ceased to be viscoelastic and the Complex Modulus method was not adequate to determine the damping properties of the material beyond its yield point. Moreover, the coating material was damaged severely in one region (the clamping end), and there was no indication of how the material in the rest of the coating layer behaved.

In order to carry out this investigation it will be necessary to coat sample bars in certain regions* only, and record the decay rate as a function of the lateral vibration amplitudes. Families of curves can then be plotted relating the decay rates and the vibration amplitudes as functions of the thickness and location of the coating layer with respect to the points of maximum vibrations.

There are many practical applications where the above study could be useful. In certain structures (e.g. aircraft structures) it is not practical to coat all the points of maximum vibrations.

5.3 Discussion of the Results

5.3.1 The Resonance Curves

The shape of the resonance curves (Figures 9-26)

---

*These could be the regions of maximum bending moment and could be coated with the optimum thickness of the coating material.

as a function of the running parameter τ agreed well with the predictions of the equivalent circuit of Figure (4). The expressions for the resonant frequency of the coated plate (f_o) and the quality-factor (Q) can be written as follows:

$$f_o = \frac{1}{2\pi\sqrt{LC}} \qquad .....5.3.1$$

$$Q = \frac{2\pi f_o L}{R}$$

Where:

$$L = L_p + L_g \qquad .....5.3.2$$

$$R = R_p + R_g$$

$$C = \frac{C_p C_g}{C_p + C_g}$$

For the case of $\tau = 0$, $R_g = L_g = 0$ and the values of f_o and Q correspond to those of the steel plates alone, as shown in Table I. Though the dimensions of the steel plates were the same, their masses were not. Moreover, each plate had a different history from the others due to its unique carbon-to-steel ratio and past heat treatments*. These differences, plus experimental errors** and any others not

---

*It is a recognized fact that if any plate is split into two halves, the properties of each half may differ.

**These could be due to the measurement of the decay rate or to the location of the elastic supports.

known to the author, could account for the different values of f_o and Q for each plate.

For small values of τ, both R and L increase, while C decreases, depending on the nature of the coating material and its adhesion to the plate surface.*

The fact that the percent increase in R is much higher than that in L forces the quality-factor Q to decrease until the optimum value of τ is reached. Also the resulting value of f_o depends on the new parameters L and C and, in the case of non-bituminous materials, turns out to be slightly less than f_{op}.

As τ increases, R_g increases and the coating-layer mass L_g becomes comparable to L_p. Hence f_o and Q continue to decrease. The peaks of the resonance curves, however, become wider, and the measured values of Q and f_o become less accurate. Moreover, the ambient noise introduces additional errors.

The above process continues until the optimum value of τ is reached. At this point the proportional increase in L exceeds that of R and the ratio L/R begins to increase. Hence Q starts to increase (See Table VIII) while f_o might increase or continue to decrease, depending on the momentary values of L and C. In general, this depends on the damping

---

*Provided that the variations in the ambient temperature, humidity etc., are negligible.

material itself. From Figure (29) it can be seen that f_o continues to decrease (after the optimum value of τ is reached) in the case of bituminous materials. (See Section 3.2). On the other hand, from Figure (31) a contrary behaviour in the case of water-based materials can be observed. In Figure (30) an oscillatory behaviour for material F is apparent. (Synthetic group.). It will be shown later in Chapter 7, that f_o depends on the nature of the damping material and the geometry of the coating layer.

5.3.2 The Decay Rate (δ_c) vs. Thickness (τ).

The expression for δ_c was derived from the equivalent circuit (Figure (4)) and can be re-written as follows:

$$\delta_c = \delta \frac{R_g}{R_g + R_p} \qquad \text{.....5.3.3}$$

where $$\delta = -4.343 \frac{R}{L} = -4.343 \frac{R_p + R_g}{L_p + L_g}$$

hence:

$$\delta_c = -4.343 \frac{R_g}{L_p + L_g} = \frac{-4.343}{L_p} \frac{R_g}{1 + \frac{L_g}{L_p}}$$

$$= K_1 \frac{R_g}{1 + \frac{\rho A \tau}{L_p}} \qquad \text{.....5.3.4}$$

where: ρ = density of the damping material (lb/inch^3)

A = area of the coating layer in inch^2

K_1 = constant.

In the case of the uniform-thickness ρ, A and L_p are constant, for any given material and sheet sample, hence equation 5.3.4 can be written more conveniently as follows:

$$\delta_c = K_1 \frac{R_g}{1 + K_2\tau} \qquad \text{.....5.3.5}$$

where: K_1, K_2 are constants.

"δ_c" is the decay rate of the coated, but lossless, steel sample (plate or bar). In the case of the Geiger test, δ_c is usually referred to as the "Geiger Rating" of the damping material. Thus for $\tau = 0$, $R_g = 0$ and $\delta_c = 0$.

For small values of τ ($0 < \tau < 0.1$ inches, except for materials D and H) R_g increases rapidly. Hence the numerator in equation 5.3.5 increases more rapidly than the denominator, and therefore δ_c increases. This was the case for all the damping materials as shown in figures (44) - (47). Also the cost (curves D vs. τ) increases since δ_c is still below its optimum value.
(Note: In the case of the complex modulus test δ, rather than δ_c, was plotted against τ. This was due to the fact that δ_p was sufficiently small for all the test bars used. Hence a linear subtraction of 2 db/sec. from the values of δ given in Figures (47), (48), (49) and (51) gives δ_c to a 1% accuracy. This linear subtraction was suggested by Oberst[19] and was verified

---

[19] Oberst, op.cit. p.13

using equation 5.3.3. The cost values also increase by the ratio $\frac{2}{\delta-2}$ (or $\frac{2}{\delta}$ approximately). The values of δ_c and D at the optimum thickness were calculated and listed in Table V).

As the values of τ were increased further, δ_c increased but at a slower rate than before. This was due to the fact that the denominator in equation 5.3.5 was increasing rapidly. This process was the same for all the ten materials using either the Geiger or Complex Modulus tests. As the optimum thickness τ was reached, δ_c (or δ) was practically at its maximum value and decreased thereafter as expected. The behaviour of δ_c could alternatively be explained in terms of the behaviour of the quality factor (Q) mentioned previously.*

5.3.3 Optimum Values of the Thickness (τ) and Cost (D)

The optimum values of τ for the materials tested were marked on the δ_c vs. τ or δ vs. τ curves (see figures (44) - (51)). These values were obtained from the optimum values of the cost D on a break-even procedure as follows:

The value of τ which corresponded to the highest

---

*See equation 2.4.9.

value of δ_c was noted. The cost D* (in \$/sq.ft/db/sec. of damping) was plotted over a sufficient range on both sides of the chosen value τ. The shape of the resulting curve had (for most materials) a minimum. The correct value of $\tau_{optimum}$ was then read directly above this minimum. In the case of materials I, J and K this method did not apply as is evident from figures (47) and (51). The procedure then was to consider the first chosen value of τ (corresponding to the maximum decay rate) as the optimum.

The optimum values of τ, δ_c and D were listed in Tables IV and V for the Geiger and Complex Modulus tests respectively. The deviations of δ_c ranged from a minimum of 0.2 db/sec. (Material H) to a maximum of 4.6 db/sec. (Material G) between the two tests. The reason for the large deviation in material G was believed to be due to the drying (or curing) time. Being a bituminous material more drying time** was apparently necessary for the Geiger Plate Test, than for the Complex Modulus Test.

---

*The value of D for each material, coated at any particular thickness of τ', was calculated as follows:-

$$D = \frac{(\text{Mass } L_g \text{ in lbs}) \times (\text{cost/lb.})}{(\text{Area A in in.}^2)(\text{Decay Rate } \delta_c \text{ in db./sec,})}$$

L_g, A and δ_c were taken from the test corresponding to the particular value of τ'. The cost/lb. was taken from pages 58-67.

**The main difficulty with the aging of most bituminous materials was believed to be due to the naphtha solvent. To verify this a small sample was left in an aspirator and was found sufficiently dry after 12 hours.

While both materials G and H were given the same drying time (due to the apparent similarity) material H dried sufficiently to give accurate results.

5.3.4 The Decay Rate (δ) vs. Resonant Frequency (f_o)

The Complex Modulus test was adequate to find the decay rate of coated and uncoated bars as a function of the resonant modes. The resulting curves (shown in figures (34) - (43) indicate that the optimum frequency range for all the ten materials is 20-300 c.p.s. approximately. Table II gives the optimum range for each material separately.

The steel bars alone appeared to have low internal damping below 300 c.p.s. Above 300 c.p.s. the decay rate increased rapidly and dropped in the range 1000-2000 c.p.s.

The decay rate vs. frequency characteristic for coated bars appeared to be constant in the low-frequency range, where the increase in the decay rate was as high as 40 db/sec. in some cases. This constitutes the basic advantage of using mastic materials for vibration reduction.

5.3.5 Elastic Properties of Material F.

The basic elastic quantities η_2 and E_2'', were plotted for material F in Figure (52) as a function of the thickness ratio (ξ) and mass ratio μ. The optimum values of these quantities were as follows:

$$\eta_2 = 6 \times 10^{-2}$$

$$E_2'' = 4.3 \times 10^9 \text{ dynes/cm}^2 = 6.8 \times 10^4 \text{ lb/in}^2$$

which correspond to the following values of ξ, η and μ.

$$\eta = 3.1 \times 10^{-2}$$

$$\xi = 1.2$$

$$\mu = 0.26$$

The value of "a" (from Figure (53)) corresponding to the above value of η equals 4×10^{-2}. Hence:

$$E_2' = (E_1')(a)$$

$$= 28.2 \times 10^6 \times 4 \times 10^{-2}$$

$$= 1.13 \times 10^6 \text{ lbs/in.}^2$$

(The value of E_1' was calculated in Appendix B*).

The value of E_2' could be, alternatively, calculated as follows:

$$E_2' = E_2''/\eta$$

$$= \frac{6.8 \times 10^4}{6 \times 10^{-2}} = 1.13 \times 10^6 \text{ lbs/in}^2$$

The previous calculations show that material F has a high stiffness ratio (a) and small loss-factor (η_2). However, since E_2'' was found to be extremely high** this material is

---

*See Appendix B - Item 4, page B-4.

**As mentioned in Chapter 1 (reference 4), Namkina, Tartakovskii and Efrussi, obtained a value of 2.5×10^9 dynes/cm^2 for E_2'', using a bitumen-impregnated felt, as compared to 4.3×10^9 dynes/cm^2 for material F.

capable of reducing vibration amplitudes using very thin coatings, This is one reason for the selection of Material F for duct applications, as will be shown in Chapter 6.

5.3.6 Main Sources of Error

One of the main sources of error in the previous results was due to the adhesion problem. In general, mastic materials have an ingredient which ensures good adhesion to clean metal surfaces. However, as the thickness of the test material was increased, the adhesion between the layers τ_o, τ_1, τ_2 etc., was dependent on:

(a) nature of the material;

(b) drying time;

(c) surface condition of the layer.

One example of errors due to insufficient drying time was discussed in Section 5.3.3. An example, where it is believed that the conditions of the layer surface was a source of error, is shown in Figure (46), (δ_c vs. curve), for material F. As shown, this material was tested in seven layers τ_1 - τ_7. However, the sudden drop of δ_c at τ = 0.196 inches is believed to be due to the following:

(a) sudden change of temperature which might have affected the surface of layer τ_4.

(b) Poor adhesion between layers τ_4 and the greasy surface of τ_3. (This is a property of material F itself, and causes adhesion errors when the material is stratified.).

The dotted line shown in Figure (46) is the expected behaviour of the material if the layers $\tau_1 - \tau_7$ were each tested on a separate plate.

The adhesion between the layers τ_o (plate) and τ_1 was believed to be the reason for the deviations in δ_c for liquid and pad layers (shown in Table VI) at the same thickness.

Another important source of error was due to the determination of the accurate decay time T.* Since $\delta = 60/T$ (db/sec.) it can be seen that a 10% deviation in T results in a 9% deviation in δ .

5.3.7 Conclusions

1. The Geiger plate and Complex Modulus tests were found adequate in testing and classifying mastic materials using the decay rate criterion. Tables IV, V, and VII show that the results obtained using either test were in close agreement.
2. The Complex Modulus Method was found adequate in investigating the decay rate as a function of frequency. See Table II.
3. The Complex Modulus Method was found unsatisfactory in evaluating the correct decay rate at high vibration amplitudes. See Section 5.2.3.

---

*This was determined using the reverberation-time protractor mentioned in Section 3.2.

4. The Complex Modulus Method was found superior to the Geiger Plate test in giving additional information, regarding the elastic properties of mastic materials. (See Section 5.3.5). This information can be helpful for purposes of comparison with other materials, or for the improvement of the material itself.
5. Due to the size of the test plates, the Geiger Test was found extremely accurate in the evaluation of new application procedures. Using this test, it was concluded that 9% (of the total Geiger Plate area) was the optimum percent coating area for material F. Also, it was discovered that one coating layer, with a sinusoidal thickness-distribution, gave 15 db/sec. more decay rate than a uniform-thickness test gave, using equal mass of the material.

   Hence, the Geiger test is superior to the Complex Modulus test in its ability to give results which help to improve the application and damping efficiency of mastic materials. (See Section 5.2.2.).
6. The equivalent-circuit, derived in Chapter 2, proved to be a useful technique in explaining the damping behaviour of most materials for the various thickness and mass conditions of the coating layer.
7. The best mastic material tested in this project was material F which gave a decay rate of 47.5 db/sec. (at 0.1525 inches) using the Geiger Test and 44.5 db/sec. (at 0.15 inches) using the Complex Modulus Test. Moreover, material F was

found to have an extremely high dynamic modulus of elasticity (see Section 5.3.5), for small coating thicknesses. This made it the most suitable material for damping thin duct shells as will be seen in Chapter 6.

CHAPTER 6

VIBRATION-REDUCTION IN VENTILATION DUCTS

6.1 General

A ventilation duct is the transmission region of a ventilation system. This system usually consists of an input end (fan or blower), a transmission section (duct) and a receiving end.

The vibrations generated in such a system are either due to mechanical rotation at the input end or aerodynamic pressure fluctuations in the transmission section, or both. In either case, the vibration source is enclosed by a shell of some geometric shape which is also part of the system. This shell, therefore, undergoes two components of vibrations. The first is the component due to the natural resonant modes of the structure. The other is due to the pressure fluctuations of the incident air. These vibrations vary in amplitude, depending in general, on the speed of the fan blades, nature of the obstacles which the shell presents to the air flow and the properties of the turbulent boundary layer. The overall effect of these vibrations is the radiation of vibrational energy to the surroundings of the shell and the transmission of longitudinal air-pressure fluctuations.

The purpose of this chapter is to present the advantages of using mastic materials as a means of reducing vibration amplitudes in ventilation ducts.

6.2 Experimental Model

Figure (62) is a layout* of the experimental model having the following features of importance:

1. The speed of the fan was constant at 1200 r.p.m. It was coupled to a 4-pole, self-excited, 1800 r.p.m., synchronous motor. The advantages of constant fan-speed will be mentioned later.
2. The flexible canvas connection was used to isolate the duct from the structural vibrations of the source.
3. The duct was circular and had one rectangular-to-circular adaptor on each side. Curved, as well as flat, surfaces were available for coating.
4. The actual length of the duct was 15 times the diameter. Hence in order to simulate a longer duct, two obstacles were placed, as shown in the cross-section Y-Y . These obstacles were two flanges with the holes arranged so as to create some air turbulence. Also an egg-crate straightener was placed at the cross-section X-X in order

---

*This figure has been reduced to 30% of the original.

to create laminar air-flow. The exponential horn was used to attenuate the air-borne noise at the receiving end.

5. The duct was simply-supported on two flanges located at the connections to the adapters.

6.3 Experimental Procedures

(A) Coating Material:

In order to investigate the advantages of using mastics for duct applications, material F was chosen for the following reasons:

(1) Material F was superior since it had the highest decay rate at the optimum thickness.

(2) The optimum thickness for applying material F was the lowest of all ten materials (0.15 inches). The importance of applying thin coatings, centered at the points of maximum vibrations will be discussed later.

(3) Material F was found to give the maximum attenuation of the sound pressure level radiated by the Geiger plate. (See Figure (27) and (28).

(4) Material F had an extremely high dynamic modulus of elasticity.

B. Measuring Equipment:

In order to locate the points of maximum velocity and acceleration on the duct surface, the accelerometer was connected, as shown in Figure (55). The equipment was adjusted* to measure acceleration and velocity amplitudes.

*This was done following the instructions of the manufacturer.

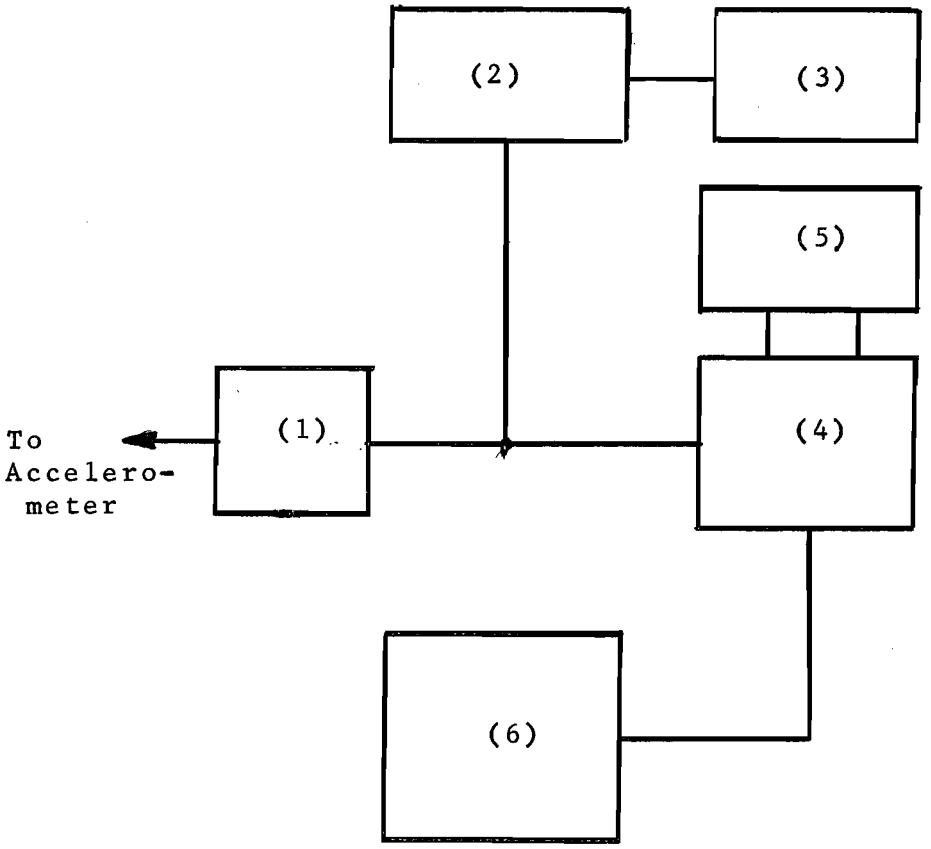

1. Vibration Pick-up Pre-amplifier
2. Frequency Analyzer
3. Cathode-Ray Oscilloscope
4. Microphone Amplifier
5. 1/3-Octave Filter Set
6. Level Recorder

Figure (55)
Diagram showing the Connections to the Accelerometer

The frequency analyzer and the microphone amplifier were calibrated such that one volt corresponded to 393.7 inch/sec.^{2} r.m.s. acceleration and 3.937 inch/sec. r.m.s. velocity * . Also, the acceleration and velocity amplitudes were recorded (using the level recorder) in db. (where the zero db. reference corresponded to 3937 inch/sec.^{2} and 39.37 inch/sec. respectively). The pressure fluctuations of the exhaust air were measured as sound pressure levels (using the condenser microphone), and recorded (on the level recorder) in db. (the zero db. reference for this measurement was 1 microbar).

C. Coating Procedure:

The vibration amplitudes were found to be large at various locations on the surface of the fan housing and the ventilation duct. However, some of these locations were difficult to coat with mastic materials, and hence a total of 13 points (anti-nodes) were finally selected for treatment. The procedure was in the following manner: At each of these points, a 3/4 inch screw was rigidly bolted to the wall of the shell. The external projecting length of the screw served as an attachment to the accelerometer and also as a means for measuring the thickness of the coating. The coating at the selected points was carried out in two stages so as to optimize the area and the thickness of the mastic layer. The area was optimized (or compromised) by first coating a small

---

* These calibrations were actually in the metric system of units and corresponded to 1,000 cm/sec.^{2} and 10 cm/sec. respectively.

circular patch (2.5 inches in radius) around the screw. The radius of the patch was then gradually increased until there was no further advantage as far as the reduction of velocity was concerned. The next step was to increase the thickness (τ) until, again, no remarkable advantage was obtainable with any further increase.

D. Measurement of the Air-borne Sound Pressure:

The condenser microphone was positioned at the throat of the exponential horn and was enclosed within a nylon shield to protect it from air streams. (See Photograph (18)). Due to this position, and since the horn was acoustically treated, the output of the microphone was a direct measure of the air-borne sound pressure.

The output of the microphone was fed into the input terminals of the frequency analyzer. Thus one set-up was suitable for measuring the air-borne sound pressure as a function of frequency.

6.4 Experimental Results

6.4.1 Vibration Measurements

A mentioned previously, there were a total of 13 points selected for coating. However, the results of the tests on three points only* are shown in Figures (56)-(58) and Table IX below.

---

*This was to avoid duplication of results.

TABLE IX

Results Of Vibration Measurements

Point	Coated Surface		Optimum radius (R) of coating Layer in inches	Optimum thickness (τ) of coating layer. In inches.	Dominant Freqs. (c.p.s.)	Velocity		Cost/sq.ft./db of damping (D) at optimum thickness τ - in$*	Acceleration	
	Thickness and Shape	Location				Reduction in db.	Reduction in %		Reduction in db.	Reduction in %
8	0.125 inches, flat.	fan-housing	3.50	3/32	240	10	68.3	0.0215	0.25	3
11	0.048 inches, cylindrical (14 inches in diameter)	Ventilation duct (Sect. 4 in Figure (62)).	4.43	1/16	180, 240	6.5	52.8	0.0353	1.00	11
13	0.048 inches, flat.	Adapter (Section 2 in Figure (62)	4.125	1/16	180, 240	13.5	78.9	0.0147	2.00	20.5

*This was calculated in the same manner as mentioned in Chapter 5.

6.4.2 Acoustic Measurements

The overall drop in the measured sound pressure level was 1.2 db. approximately (reference 0.0002 μbars). This drop was due to the vibration reduction at certain discrete frequencies, mainly 4 db. at 240 c.p.s. and 1.5 db. at 180 c.p.s. However, there were new frequencies in the sound spectrum. These were in the low (around 50 c.p.s.) and high (around 4000 c.p.s.) frequency ranges.

6.5 Discussion of the Results

The three quantities that describe vibrations are the acceleration, velocity and displacement. For harmonic vibration signals, these quantities can be related as follows: If the acceleration (A) equals a $\mathrm{Sin}(\omega t)$, where:

a = maximum acceleration amplitude.

ω = radian frequency.

Then the velocity (V) can be expressed as follows:

$$V = \int_o^t A\,dt = -\frac{a}{\omega}\,\mathrm{Cos}\,(\omega t)$$

and the displacement (S) as:

$$S = \int_o^t \int_o^t A\,dt\,dt = \frac{-a}{\omega^2}\,\mathrm{Sin}\,(\omega t)$$

However, for complex vibration-signals, the velocity and displacement can still be used, but they cannot be found mathematically from the measurement of acceleration.

The acceleration amplitude decreases as the mass of the vibrating panel is increased, provided that the driving force is kept constant*. The panel velocity, on the other hand, is proportional to the square root of the energy available for radiation as sound**. Since the driving force was not changed in this experiment, the acceleration-reduction criterion for testing mastic materials was not applicable. Hence, the reduction in velocity amplitudes was the valid criterion.

The velocity level, as shown in Figures (57) and (58), decreased as the values of R and τ were increased above zero. This decrease was expected to continue as R was increased***. The fact that the velocity did not decrease appreciable beyond R = 4.43 inches and τ = 1/16 inch is believed to be due to the following reasons:

(1) The deformation of the duct surface at points 11 and 13 was fully coated. Any further reduction in the velocity due to larger values of R would be due to a new deformation.

(2) Analogous to the case shown in Figure (46), τ reached an optimum value. Any further increase in τ would result in an increase in the velocity amplitude.

---

*This is obvious from Newton's Second Law.

**The velocity is analogous to the current in Figure (4).

***This was verified in the Geiger Plate Test for material F. See Figure (46).

(3) The mass of the coating layer introduced a slight variation in the geometry of the duct and caused the anti-nodes to shift to new locations. This shift was found to be in the order of one inch for all thirteen points, and slightly reduced the damping efficiency of the coating layer. This efficiency can hence be controlled by increasing R and keeping τ as low as possible.

Figures (56) - (58) show that the ratio of the optimum value of R to that of τ was quite high using material F.

The velocity amplitudes were different for the various selected locations on the duct surface. At each location there were amplitudes due to one or more of the following sources:-

(1) Pressure forces - These were mainly due to the air pulsations at 240 c.p.s.*

(2) Structure-borne vibrations - These were mainly due to the random excitation of the natural resonance frequency of the system and were found to be at 180 c.p.s.**

(3) Air turbulence - This covered a wide frequency range (40-5000 c.p.s.).

---

* The fan was driven by the synchronous motor at a constant speed of 1200 r.p.m. Since there were 12 blades on the fan rotor, the frequency of the air pulsations was, as verified experimentally, 240 c.p.s.

**The velocity amplitudes vs. frequency showed a strong component at 180 c.p.s. for all the selected anti-nodes on the duct surface. Since this was the only frequency maintained after coating, it was assumed to be the natural resonant frequency of the duct. This was verified by "shock exciting" the duct by a hammer blow and measuring the frequency of the decaying un-damped free-mode.

The above three sources are thus believed to be responsible for the dominant frequencies measured at points 8, 11 and 13, and shown in Table IX.

Point No.13 was considered to be at the most important location on the duct surface for the following reasons:

(1) It was near the output-end.

(2) It was excited by all the above-mentioned sources.

(3) While the air turbulence level was expected to be very high*, the effect of the preceding** coating layers was the remarkable reduction of this level. Hence, the test at point 13 served as an excellent test of mastic coatings under turbulent conditions. The result was that these coatings need only be placed at few vibration anti-nodes and they could still increase the bending stiffness of the shell to the extent that the amplitude at the output end could be highly attenuated.

6.6 Conclusions

1. Vibration measurements taken on ventilation ducts can be based on the velocity-amplitude criterion.

---

*This was due to the obstacles placed inside the duct.

**These are points 9, 10, 11 and 12 located on the duct surface between point 13 and the fan.

2. Mastic materials can, at a reasonable cost, reduce large vibration amplitudes (turbulent or harmonic) which fall within the optimum frequency range of these materials.
3. There was a 13.5 db. (or 78.9%) reduction in the velocity-level for a rectangular cross-section (Point No.13), and 6.5 db. (or 52.8%) for a circular section (Point No.11), of the ventilation duct model. The geometry of the coating layer, in each case, was circular having an optimum radius of 4.43 inches (63% of the circular-duct radius), and an optimum thickness of 1/16 inch.
4. There was an attenuation of 1.2 db. of the air sound pressure level due to the application of approximately 5 lbs. of a suitable mastic (material F) on certain vibration anti-nodes.

   The location of the condenser microphone prevented the attenuation measurements of the sound radiated from the duct surface.
5. It is believed that a more accurate test for the evaluation of mastic materials under turbulent vibration conditions can be carried out using the Geiger plate. The plate in this case can be driven by a complex voltage waveform and the supports modified to suit the test. In any case, the driving force will not generate sounds which interfere with the test.

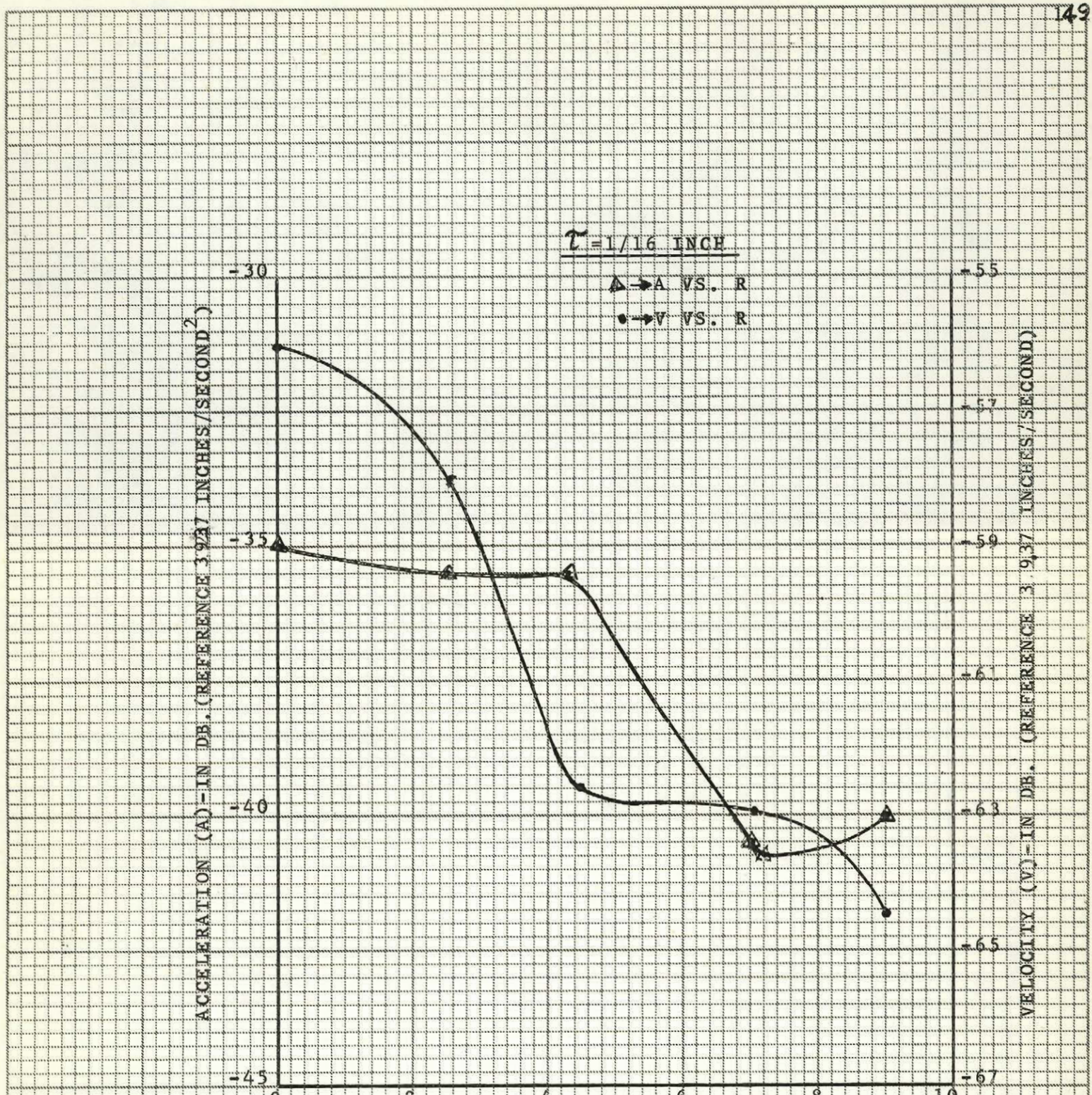

POINT NO. 11

FIGURE (56)

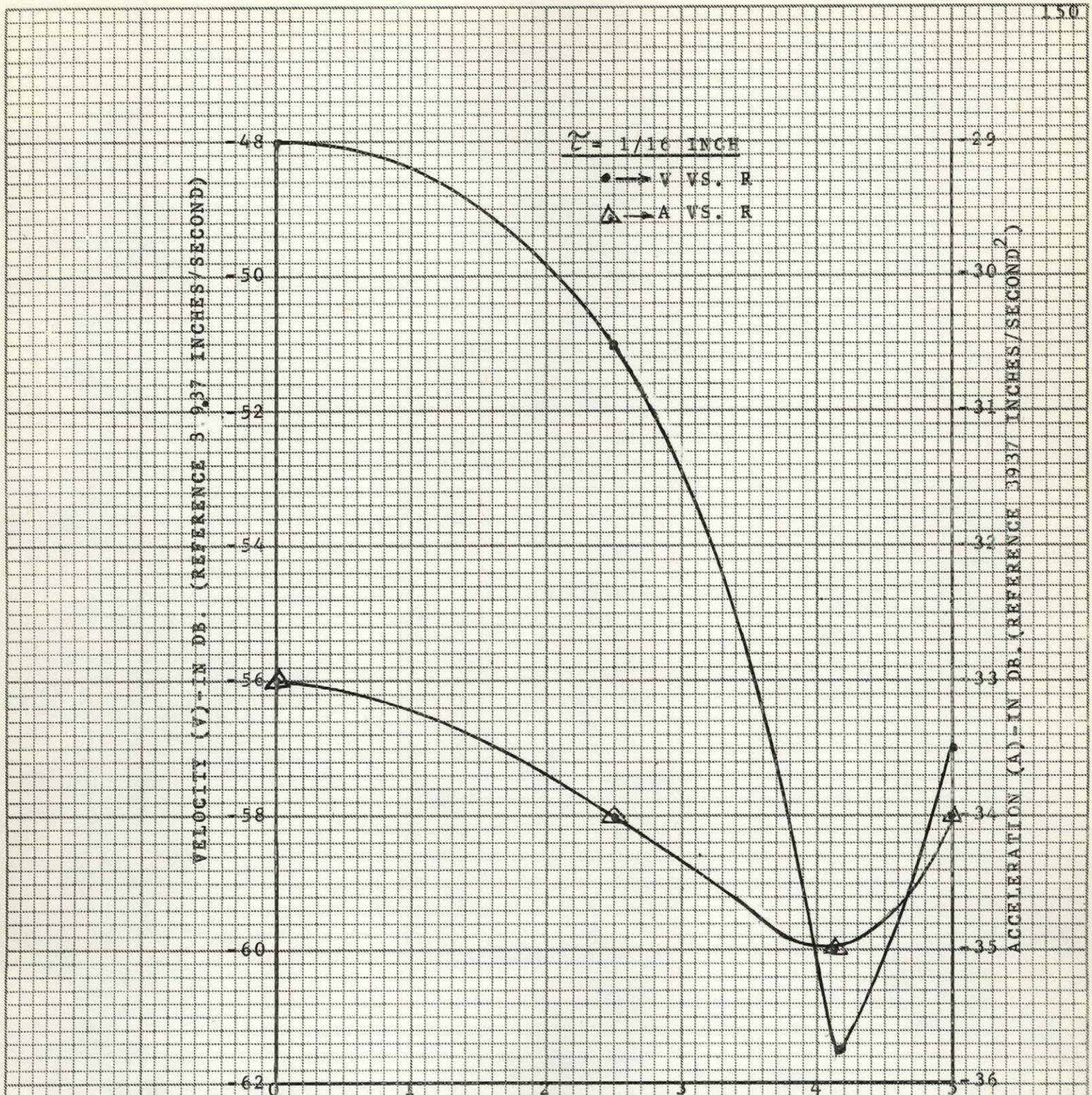

POINT NO. 13

FIGURE (57)

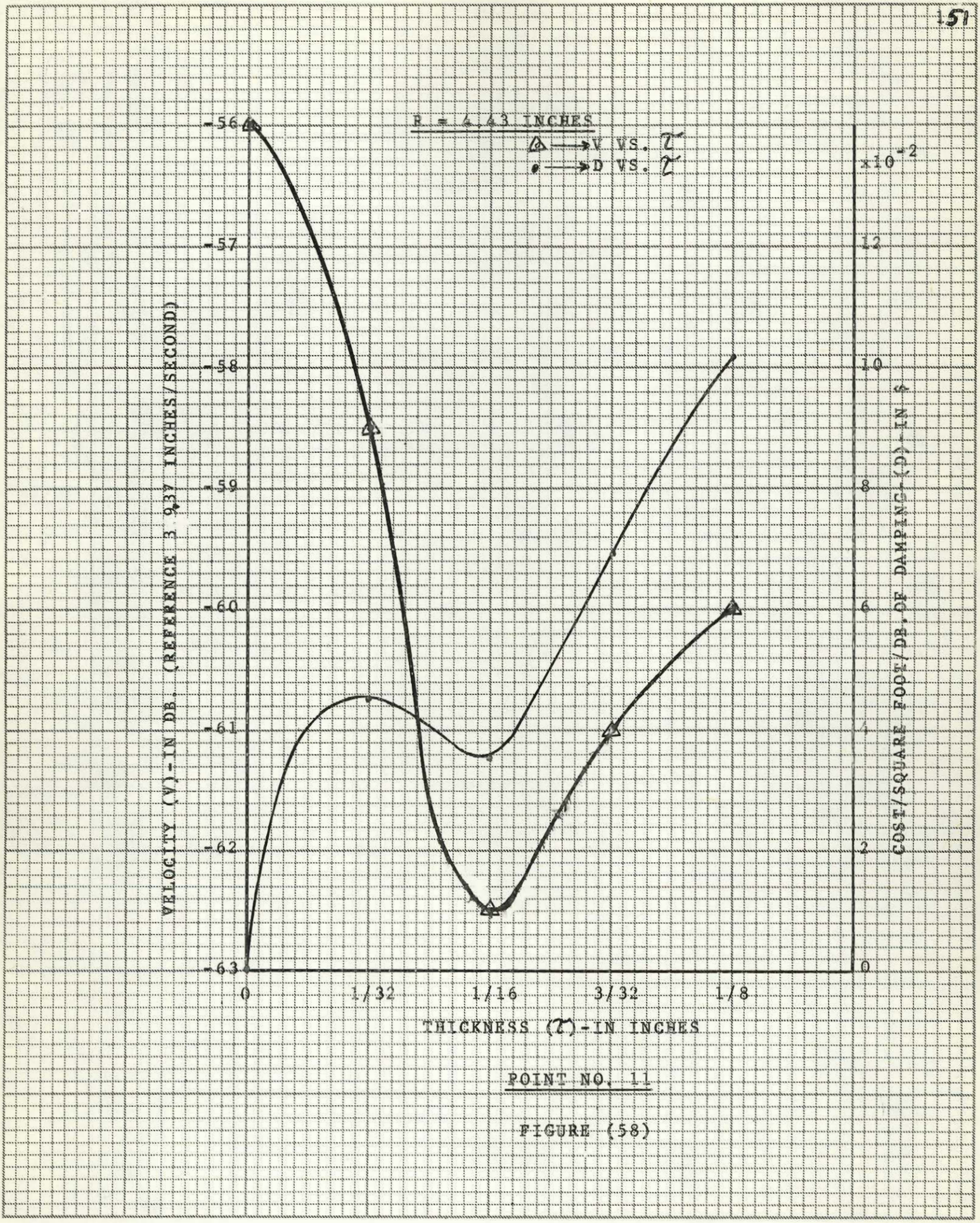

POINT NO. 11

FIGURE (58)

CHAPTER 7

UNIVERSAL CURVE FOR THE HYPOTHETICAL COATING LAYER

7.1 General

The equivalent circuit for coated steel plates, introduced in Chapter 2, can now be used to derive some useful quantities for practical applications. Since the parameters of the equivalent circuit were calculated for each test, some numerical results can also be obtained.

The theory presented in this chapter is based entirely on dimensional analysis techniques and was verified for three different types of damping materials. The results were restricted to a single temperature.

7.2 Dimensional Analysis

The physical quantities necessary for the analyses, together with their dimensions are listed below.

Physical Quantity	Symbol	Dimensions
Volume	V	L^3
Thickness	$\tilde{t}$	L
Mechanical Resistance	c	FTL^{-1}
Mechanical mass	m	FT^2L^{-1}
Mechanical Compliance $^{-1}$	K	FL^{-1}
Density	ρ	ML^{-3}
Elastic Constant	λ	$ML^{-2}T^{-2}$
Resonant Frequency of Coating Layer	ω_{og}	T^{-1}
Viscosity	μ*	$FL^{-2}T$

*This symbol was used in Chapter 5 to designate L_g/L_p.

Physical Quantity	Symbol	Dimensions
Decay rate of Coating Layer	δ_g	T^{-1}
Area	A	L^2

It should be noted that if one substitutes $MT^{-2}L$ for the force (F), all the above dimensions are reduced to the standard M, L, T (mass, length and time).

The elastic constant (λ) is defined as follows:

Force (F) = distance (L) x stiffness

= distance (L) x Area (A) x elastic constant (λ)

hence the elastic constant has the dimensions FL^{-3} or $ML^{-2}T^{-2}$ as shown above.

ANALYSIS FOR "δ_g"

The decay rate of the hypothetical coating layer can be assumed to be some function of V, τ, c, m, K. These five quantities can be used to form one dimensionless quantity π.

Hence

$$\pi = V^{\alpha} \tau^{\beta} c^{\gamma} m^{\delta} K^{\epsilon}$$

$$[0] = F^{\gamma+\delta+\epsilon} L^{3\alpha+\beta-\gamma-\delta-\epsilon} T^{\gamma+2\delta}$$

Thus

$$3\alpha+\beta-\gamma-\delta-\epsilon = 0$$
$$\gamma+\delta+\epsilon = 0$$
$$\gamma+2\delta = 0$$

We now have three equations and five unknowns.

However, according to the Buckingham π-Theorem[20] we can assign arbitrary values for any two of the five unknowns. If this is carefully done, we can form two different dimensionless groups of π. Hence:

$$\gamma = -2\delta$$

$$\epsilon = \delta$$

$$3\alpha + \beta - \gamma + \frac{\gamma}{2} + \frac{\gamma}{2} = 0, \text{ or } \alpha = -\beta/3$$

Thus:

$$\pi = V^{\alpha} \tau^{-3\alpha} c^{\gamma} m^{-\frac{\gamma}{2}} K^{-\frac{\gamma}{2}}$$

$$\pi = \left(\frac{V}{\tau^3}\right)^{\alpha} \left(\frac{c^2}{mK}\right)^{\frac{\gamma}{2}}$$

$$= f_1\left(\frac{V}{\tau^3}\right) \times f_2\left(\frac{c^2}{mK}\right)$$

where f_1 and f_2 are any two functions.

Hence:

$$\pi_1 = \frac{V}{\tau^3}$$

$$\pi_2 = \frac{c^2}{mK}$$

Where π_1 and π_2 are dimensionless groups of π and can be related as follows:

$$\pi_1 = f(\pi_2) \qquad f = \text{any function},$$

or

---

[20] F.Kreith, Principles of Heat Transfer, (International Textbook Co., 1960) pp.245-248.

$$\boxed{\frac{mK}{c^2} = f\left(\frac{V}{\tau^3}\right)} \qquad \text{.....7.2.1}$$

but δ_g has the dimensions of T^{-1} which are the dimensions of c/m. Similarly, ω_{og} has the dimensions of K/C.

Hence: $\frac{\omega_{og}}{\delta_g}$ is a function of

$\left(\frac{mK}{c^2}\right)$ or $\left(\frac{V}{\tau^3}\right)$. Therefore:

$$\delta_g = \omega_{og}\, \phi\left(\frac{V}{\tau^3}\right) \quad \text{or}$$

$$\delta_g = \omega_{og}\, \phi\left(\frac{A}{\tau^2}\right) \qquad \text{.....7.2.2}$$

where ϕ = any function.

ANALYSIS FOR "ω_{og}"

The resonant frequency of the hypothetical coating layer, ω_{og}, is assumed to depend (in a manner as yet to be determined) on the quantities ρ, V, τ and λ. The dimensional analysis should give two dimensionless groups (π_1 and π_2) for the same reasons mentioned in the analysis for δ_g. Let:

$$\pi' = \rho^{\alpha'} V^{\beta'} \tau^{\gamma'} \lambda^{\delta'} \omega_{og}^{\epsilon'}$$

$$[0] = m^{\alpha'+\delta'} L^{-3\alpha'+3\beta'+\gamma'-2\delta'} T^{-2\delta'-\epsilon'}$$

hence:
$$\alpha' + \delta' = 0$$
$$-3\alpha' + 3\beta' + \gamma' - 2\delta' = 0$$
$$-2\delta' - \epsilon' = 0$$

Therefore:

$$\epsilon' = -2\delta' = -2\alpha'$$

and

$$-3\alpha' + 3\beta' + \gamma' + 2\alpha' = 0$$

or

$$\gamma' + \beta' - \alpha' = 0$$

To form π_1 we can set $\gamma' = 0$.

Hence:

$$\pi_1' = \frac{\rho}{\lambda} \frac{\sqrt[3]{V}}{\omega_{og}^2}$$

To form π_2 we can set $\epsilon' = 0$. Hence:

$$\pi_2' = \frac{V}{\tau^3}$$

For reasons mentioned previously, we can write:

$$\pi_1' = G(\pi_2')$$

where G = any function, or

$$\frac{\rho}{\lambda} \frac{\sqrt[3]{V}}{\omega_{og}^2} = G\left(\frac{V}{\tau^3}\right)$$

if we solve for ω_{og}^2 and simplify, we can write the final result:

$$\boxed{\omega_{og}^2 = \left[\frac{\lambda}{\rho}\right]\left[\frac{G\left(\frac{V}{\tau^3}\right)}{\sqrt[3]{V}}\right]} \qquad \text{.....7.2.3}$$

ANALYSIS FOR "c"

The mechanical resistance "c", analogous to the "R_g" parameter of the equivalent circuit (see chapter 2) is assumed to depend on the quantities V, τ and μ. Using

dimensional analysis techniques, we can write the following dimensional equation:

$$\bar{\xi} = V^{\bar{\alpha}} \tilde{\tau}^{\bar{\beta}} \mu^{\bar{\gamma}}$$

or

$$(FTL^{-1})^{\bar{\delta}} = (L^3)^{\bar{\alpha}} \; (L)^{\bar{\beta}} \; (FTL^{-2})^{\bar{\gamma}}$$

hence:

$$\bar{\gamma} = \bar{\delta}$$

$$-\bar{\delta} = 3\bar{\alpha} + \bar{\beta} - 2\bar{\delta}$$

or

$$\bar{\beta} = \bar{\delta} - 3\bar{\alpha}$$

Thus:

$$\left(\frac{c}{\mu}\right)^{\bar{\delta}} = \bar{\phi}\left(\frac{V^{\bar{\alpha}}}{\tilde{\tau}^{3\bar{\alpha}-\bar{\delta}}}\right)$$

$$= \bar{\phi}\left(\frac{A^{\bar{\alpha}}}{\tilde{\tau}^{2\bar{\alpha}-\bar{\delta}}}\right)$$

where $\bar{\phi}$ = any function.

The expression for "c" can be written as follows:

$$\boxed{c = \mu\left[\bar{\phi}\left(\frac{A^{\bar{\alpha}}}{\tilde{\tau}^{2\bar{\alpha}-\bar{\delta}}}\right)\right]^{1/\bar{\delta}}} \qquad \text{.....7.2.4}$$

The value of "c" as a function of "$\tilde{\tau}$" was determined experimentally for material "F" (See Geiger Test results for Material "F", chapter 5). A plot of this relationship (see Fig. 54 on page 158) gives the following empirical equation:

$$c = 0.0166\,\tilde{\tau}^{0.125} \qquad \text{For constant area (A)}$$

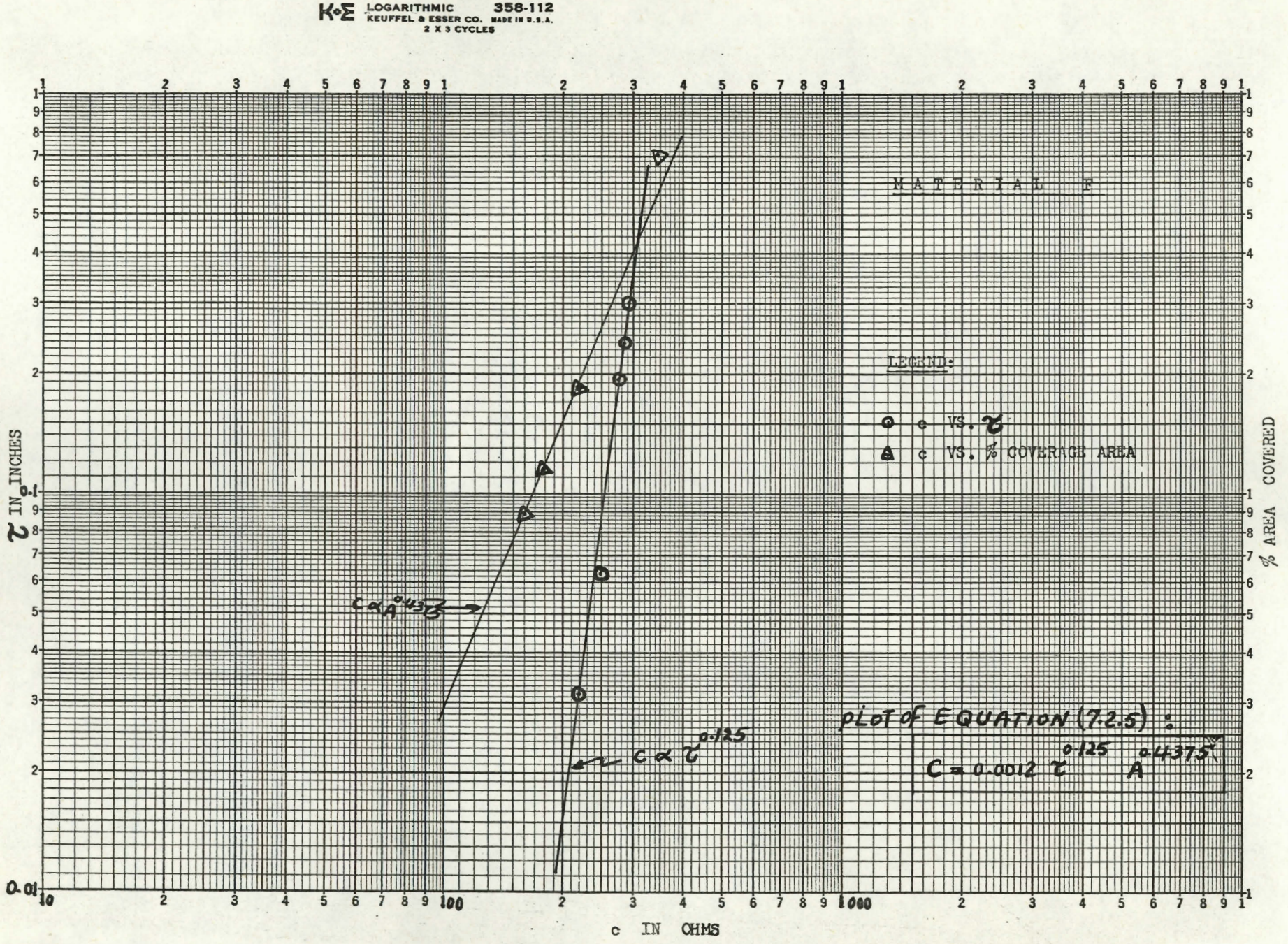
K&E LOGARITHMIC 358-112
KEUFFEL & ESSER CO. MADE IN U.S.A.
2 X 3 CYCLES
MATERIAL F
LEGEND:
c VS. τ
c VS. % COVERAGE AREA
c ∝ A^0.4375
c ∝ τ^0.125
PLOT OF EQUATION (7.2.5) :
C = 0.0012 τ^0.125 A^0.4375
τ IN INCHES
% AREA COVERED
c IN OHMS
0.01
0.1
1
10
100
1000

Figure (54)

The viscosity "μ" is a basic physical property, and is fixed for any given damping material, Hence:

$\bar{\delta} = 1$, $\bar{\phi}$ = a constant, and $c = B\mu \left(\frac{A^{\bar{\alpha}}}{\tau^{2\bar{\alpha} - \bar{\delta}}} \right)$

where B is a constant.

The value of $\bar{\alpha}$ and the product (Bμ) can then be evaluated and the final expression for "c" becomes:

$$c = 0.0012\, \tau^{0.125}\, A^{0.4375} \qquad \text{.....7.2.5}$$

Equation 7.2.5 was then checked with experimental results for the variations in c as a function of A (τ = constant).

Two sets of values for c and A were selected from these results and substituted in equation 7.2.5. as follows:

$c_1 = 215.10$ at $A_1 = 73.2$ in^2.

$c_2 = 159.19$ at $A_2 = 35.8$ in^2.

$$\frac{c_1}{c_2} = \frac{215.10}{159.19} = 1.35$$

$$\frac{0.0012\, \tau^{0.125}\, (73.2)^{0.4375}}{0.0012\, \tau^{0.125} (35.8)^{0.4375}} = 1.364$$

error ≐ 1%

Thus equation 7.2.5 is quite suitable for practical applications of material "F".

7.3 The Universal Curve

The expressions for δ_g and ω_{og}, derived in Section 7.2., can be combined as follows:

$$\delta_g = (\omega_{og})\,\phi\left(\frac{A}{\tau^2}\right) \qquad .....7.2.2$$

$$\omega_{og}^2 = \left[\frac{\lambda}{\rho}\right]\left[\frac{G\left(\frac{V}{\tau^3}\right)}{\sqrt[3]{V}}\right] \qquad .....7.2.3$$

Equation 7.2.3. can be expressed as :

$$\omega_{og} = f_1 f_2 \qquad .....7.3.1$$

where f_1 = a function depending on the properties of the damping material in question; f_2 = a function of the coating layer geometry.

Thus:

$$\delta_g = f_1 f_2 \phi \qquad .....7.3.2$$

But since f_1 has a particular value for any particular material, let

$$f_1 = \sqrt{\frac{\lambda}{\rho}} = K_g^{-1}$$

where K_g = constant, g = any damping material. Hence:

$$\delta_g = K_g^{-1} f_2 \phi$$

Equation 7.2.3 gives the value of f_2 in the following form:

$$f_2 = \sqrt{\frac{G\left(\frac{V}{\tau^3}\right)}{\sqrt[3]{V}}}$$

hence:

$$\delta_g = \sqrt{\frac{\lambda}{\rho}}\left[\frac{1}{\sqrt[6]{V}}\,\phi\left(\frac{A}{\tau^2}\right)\sqrt{G\left(\frac{V}{\tau^3}\right)}\right]$$

$$= \sqrt{\frac{\lambda}{\rho}}\left[\frac{1}{\sqrt[6]{A}\sqrt[6]{\tau}}\,\phi\left(\frac{A}{\tau^2}\right)\sqrt{G\left(\frac{V}{\tau^3}\right)}\right]$$

but

$$\frac{V}{\tau^3} = \frac{A}{\tau^2}$$

hence:

$$\delta_g = \left[\sqrt{\frac{\lambda}{\rho}}\right]\left[\frac{1}{\sqrt[6]{A}}\left(\frac{\sqrt[12]{A}}{\sqrt[12]{A}}\right)\frac{1}{\sqrt[12]{\tau^2}}\,H_1\left(\sqrt{\frac{A}{\tau^2}}\right)\right]$$

where:

$$H_1\left(\sqrt{\frac{A}{\tau^2}}\right) = \left[\phi\left(\frac{A}{\tau^2}\right)\right]\left[\sqrt{G\left(\frac{V}{\tau^3}\right)}\right]$$

Simplifying this expression further, we get:

$$\boxed{\delta_g = \left[\sqrt{\frac{\lambda}{\rho}}\right]\left[\frac{1}{\sqrt[4]{A}}\,H_2\left(\frac{A}{\tau^2}\right)\right]} \qquad \text{.....7.3.3}$$

where:

$$H_2\left(\frac{A}{\tau^2}\right) = \left(\sqrt[12]{\frac{A}{\tau^2}}\right)\,H_1\left(\sqrt{\frac{A}{\tau^2}}\right)$$

Equation 7.3.3 can be re-written in its final form to determine the universal curve:

$$\delta_g \sqrt[4]{A}\left[\sqrt{\frac{\rho}{\lambda}}\right] = H_2\left(\frac{A}{\tau^2}\right)$$

substituting $K_g = \sqrt{\frac{\rho}{\lambda}}$, we get:

$$\boxed{K_g \sqrt[4]{A}\,\delta_g = \bar{H}_2\left(\frac{\tau^2}{A}\right)} \qquad \text{.....7.3.4}$$

Where $\bar{H}_2 = H_2^{-1}$

A plot of ($K_g \sqrt[4]{A}\ \delta_g$) vs. $\left(\frac{\tau^2}{A}\right)$ is shown in the Fig. on p.163. In order to draw the curve, K_g was arbitrarily taken as unity for material F. Once the curve was plotted (using measured values of A, τ and δ_g), it was verified for a second material (I) using the following graphical procedure:

The values of A and τ^2 can be taken from one test of material "I". Using the curve (drawn for "F") we can determine the product $K_I \sqrt[4]{A}\ \delta_g$. Knowing the measured value of δ_g for material "I" and for the particular values of τ and A used in the test, K_I can be calculated. Using this value of K_I, the curve for the material I can be plotted using equation 7.3.4.

The procedure was repeated for a third damping material "K". The curves corresponding to the three materials essentially coincided. The deviations were small and were mainly due to the calculated value of K from experimental data.

The applications of this curve are restricted to room temperature (75°F).

For any desired values of δ, ω_o and A related to a vibrating panel, the value of K_g must be given. The equivalent circuit (see chapter 2) must then be used to determine δ_g

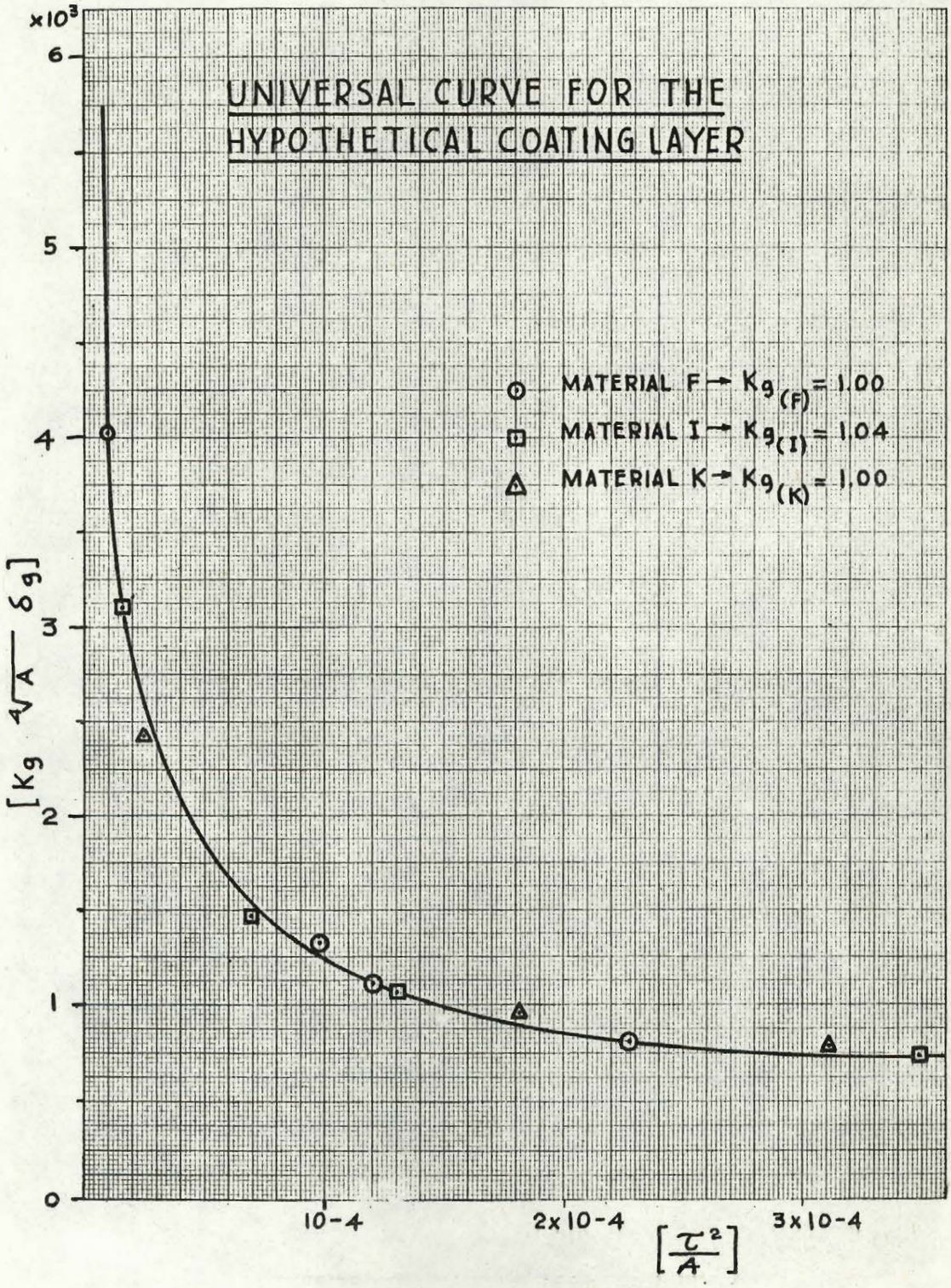
UNIVERSAL CURVE FOR THE
HYPOTHETICAL COATING LAYER
MATERIAL F → Kg(F) = 1.00
MATERIAL I → Kg(I) = 1.04
MATERIAL K → Kg(K) = 1.00
x10³
6
5
4
3
2
1
0
[Kg ∜A δg]
10-4
2x10-4
3x10-4
[τ²/A]

Figure (59)

For this the metal panel must be tested separately. The product ($K_g \sqrt[4]{A}\ \delta_g$) is then located on the ordinate of the graph and the corresponding value of (τ^2/A) obtained. For any value of the area A, the correct value of (τ), necessary to give (δ_g) db/sec. damping on an area (A) and material (g), is calculated.

7.4 The Specific Decay Rate

Aside from the previous analysis, we can form a dimensionless group from the quantities δ_g, ρ, V, and λ. Thus

$$\pi = V^{\alpha}\ \rho^{\beta}\ \lambda^{\gamma}\ \delta_g^{\epsilon}$$

or

$$[0] = (L^3)^{\alpha}\ (ML^{-3})^{\beta}\ (ML^{-2}T^{-2})^{\gamma}\ (T^{-1})^{\epsilon}$$

$$\beta + \gamma = 0$$

$$-2\gamma - \epsilon = 0$$

$$3\alpha - 3\beta - 2\gamma = 0$$

hence:

$$\gamma = -\epsilon/2$$

$$\beta = \epsilon/2$$

$$\alpha = \epsilon/6$$

Therefore:

$$\pi = \left(\delta_g \sqrt{\frac{\rho}{\lambda}}\ \sqrt[6]{V} \right)^{\epsilon}$$

but

$$\sqrt{\frac{\rho}{\lambda}} = K_g$$

hence:

$$\pi = \left(K_g\ \delta_g \sqrt[6]{V} \right)^{\epsilon}$$

Π is a dimensionless quantity and can be designated δ_s. Hence:

$$\delta_s = \left(K_g \, \delta_g \sqrt[6]{V} \right)^{\epsilon}$$

δ_g can be obtained from the equivalent-circuit for any coating layer thickness following the steps listed in Chapter 2. "K_g" is a physical property of the coating material whose volume is V. Hence δ_s is independent of the geometrical shape of the coating layer and hence can be called the Specific Decay Rate (dimensionless).

CHAPTER 8

SUGGESTIONS FOR FUTURE RESEARCH

8.1 General

The universal damping curve, presented in the previous chapter, can be made more useful after some quantities, related to the damping material constant (K_g) are evaluated. This requires a new experiment with the aim of separating each one of these quantities and determining its effect on K_g.

In order to carry out this investigation, it is necessary to be able to vary the thickness (τ) and the coating area (A) since these are two of the quantities mentioned above. The dependence of K_g on τ can be obtained using the Geiger plate or Complex Modulus Standard Tests. However, the measurements on A must be carried out under uniform bending moment conditions in the vibrating plate or bar. This, therefore, requires a modification of the standard tests or the design of a new one.

The tabulation of the quantities that are believed to determine K_g and the proposal for a new bar test are the contributions of this chapter.

8.2 Proposal for a New Bar Test

The Fig. on p. 167 is a schematic diagram of the proposed test. It consists of four systems as follows:

1. The exciting system: The electronic equipment is essentially the same as that used for the standard tests. The only improvement is the insertion of a constant-current source,

LEGEND

AB : BAR No. 1

CD : BAR Nº 2

1 : AUDIO OSCILLATOR

2 : POWER AMPLIFIER

3 : CATHODE RAY OSCILLOSCOPE

4 : FREQUENCY COUNTER

5 : CURRENT STABILIZER

6 : ELECTROMAGNETIC VIBRATOR

7 : ELECTROMAGNETIC PICK-UPS

8 : MICROPHONE AMPLIFIER

9 : COMPARATOR

10 : FRICTIONLESS PIN-CLAMPS

11 : ISOLATION CHAMBER AND SUPPORT FOR PIN-CLAMPS.

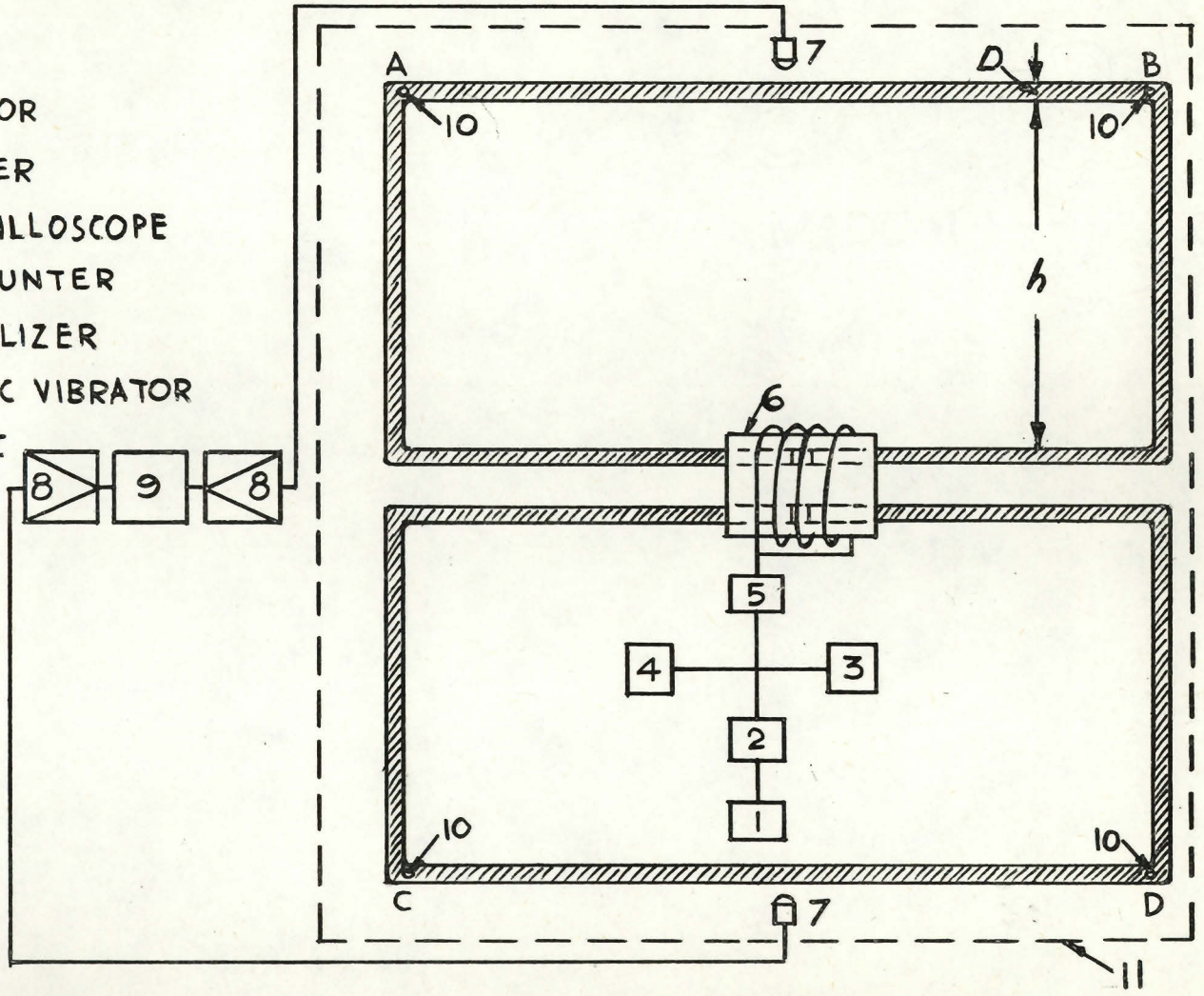

SCHEMATIC DIAGRAM OF THE PROPOSED EXPERIMENT

Figure (60)

the output current now being independent of the coil impedance. This system is suitable for exciting the fundamental as well as the higher order modes of the test bar.

2. The moment transmitting systems is arranged as shown in the figure. The pin-clamps are assumed to have unity transfer function (i.e. frictionless, etc), thus the bending moment is transmitted to the test section without loss.
3. The sample bars: These are identical and undergo uniform and equal bending moments when not coated.
4. The measuring system: This consists of two electromagnetic transducers each opposite the centre point of the bar. Their outputs can be processed as follows:

(a) Either amplified and compared on a comparator. (This could be a dual-beam oscilloscope, a two-channel recorder or a correlator);

(b) or rectified and the difference measured.

The advantage of this experiment is shown in the Fig. on p.169. In this figure the thickness of the test bars, AB and CD, is d inches. (In practice it could be 1/8 inch, say). If we assume a width of b inches and make b = 8d, then we can make the height h = 20d (say). The higher the value of h, the less is the effect of the axial forces in the test bars as shown below:

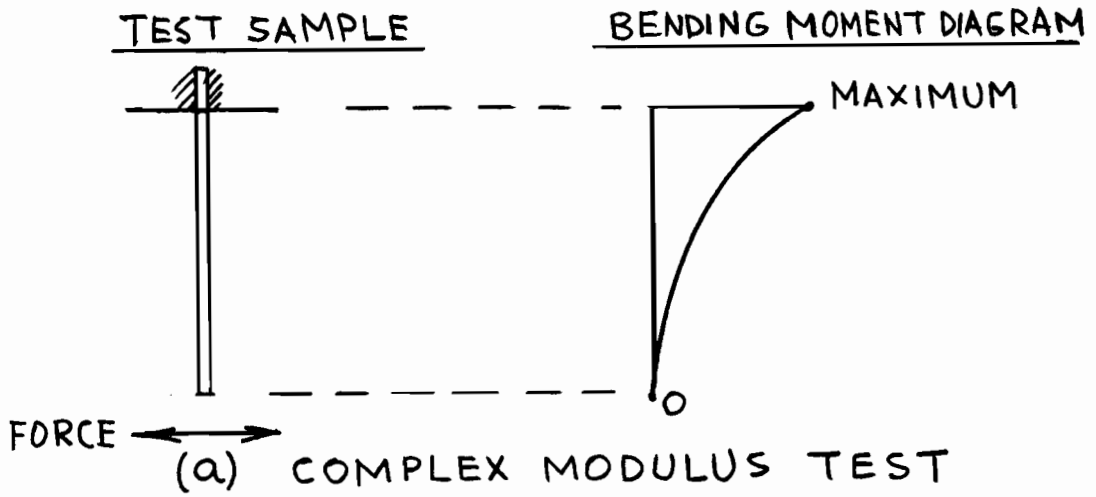

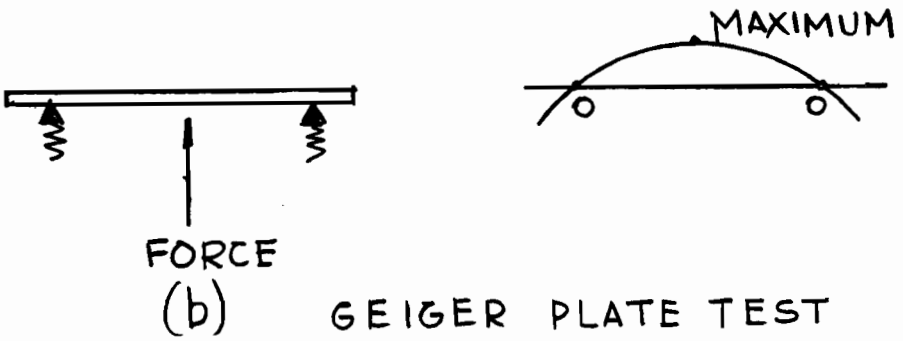

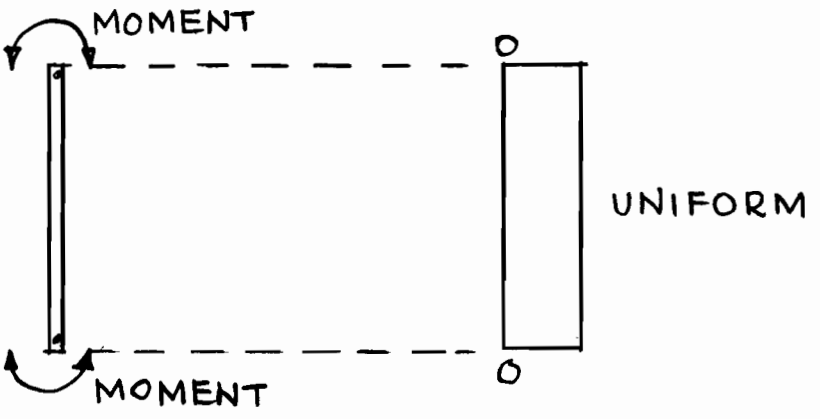

BENDING MOMENT DISTRIBUTION IN THE PROPOSED TEST COMPARED WITH THAT OF THE STANDARD TESTS

Figure (61)

Moment in each bar = M = P x 20d

where P + force exerted by the vibrator on each test bar.

The bending stress due to this moment = f_{bs}

$$= \frac{6M}{bd^2}$$

$$= \frac{6 \times P \times 20d}{(8d)(d^2)}$$

$$= \frac{15P}{d^2}$$

The axial stress due to the force P equals:

f_{as} = force/unit cross-sectional area of the bar

$$= \frac{P}{8dxd} = \frac{P}{8d^2}$$

The effect of f_{as} can be shown as a fraction of f_{bs} as follows:

$$\frac{f_{as}}{f_{bs}} = \frac{\frac{P}{8d^2}}{\frac{15P}{d^2}} = \frac{1}{120}$$

Hence $f_a < 1\%$ of f_b

However, any losses in the pin-clamps will cause a slight increase in the axial moments. As long as f_{as} is kept 1-2% or less of f_{bs}, it can be neglected in the final results.

The effect of f_{as} can be controlled by a proper design of the length h. The mechanical details of this experiment can be perfected or modified in the future. The author is merely suggesting one way of obtaining a uniform bending moment in the test bar. Thus a mastic layer, coated on such a bar, is subjected to the same bending moment everywhere. The measured decay rate should be higher, using this test, than that obtained from the Complex Modulus test with the same test sample in both cases. This is due to the fact that the total volume of the coating layer contributes more to the bending stiffness of the bar in order to prevent the lateral motion.

8.3 Suggested Topics for Experimental Study

The experiment proposed in Section 8.2 can be used to obtain the damping properties of any mastic material for a given layer thickness (τ) and area (A). If the set-up is adapted to have some additional features (such as temperature, pressure and humidity control), it could then be used to determine the constant K_g for any mastic material. The quantities that combine, in some manner or another, to determine the value of K_g, at any instant of time, are believed to be the following:

(a) elastic coefficient λ (defined previously);

(b) density ρ (ρ and λ actually define K_g);

(c) coefficient of volumetric expansion;

(d) coefficient of surface radiation;

(e) coefficient of thermal capacity;

(f) coefficient of thermal conductivity;

(g) temperature (θ).

From the above we note that as soon as the temperature (θ) is taken into account, a group of dependent variables must also be taken into account. K_g could then be plotted as a function of θ and the effect of the other quantities (items (c) to (f) above), shown by a family of curves on the same plot. The value of K_g is then used for the purpose of the universal curve, mentioned previously.

It is suggested that mastic materials should not be grouped on the basis of their apparent chemical composition, as was done in Chapter 3, but on the basis of the different types of viscoelastic flow. In general, most fluids fall under the Newtonian, pseudo-plastic, dilatant or Bingham[21,22], types of flow shown below. However, most viscoelastics are either thixotropic or rheopectic non-Newtonian types of flow, which is one reason why they do not maintain their damping properties at high vibrational frequencies, when they tend to liquify. Moreover, viscoelastic materials are, in general, time-dependent.

---

[21] F.R.Eirich, Rheology, (Academic Press, N.Y., 1956) Vol.1.

[22] W.L.Wilkinson, Non-Newtonian Fluids,(Pergamon Press, London,1960)

The time-dependence may be a temperature effect (which alters the viscosity) and no more. The history of these viscoelastics can be shown on a shear-rate vs. shear-stress diagram as a family of curves for various time conditions.

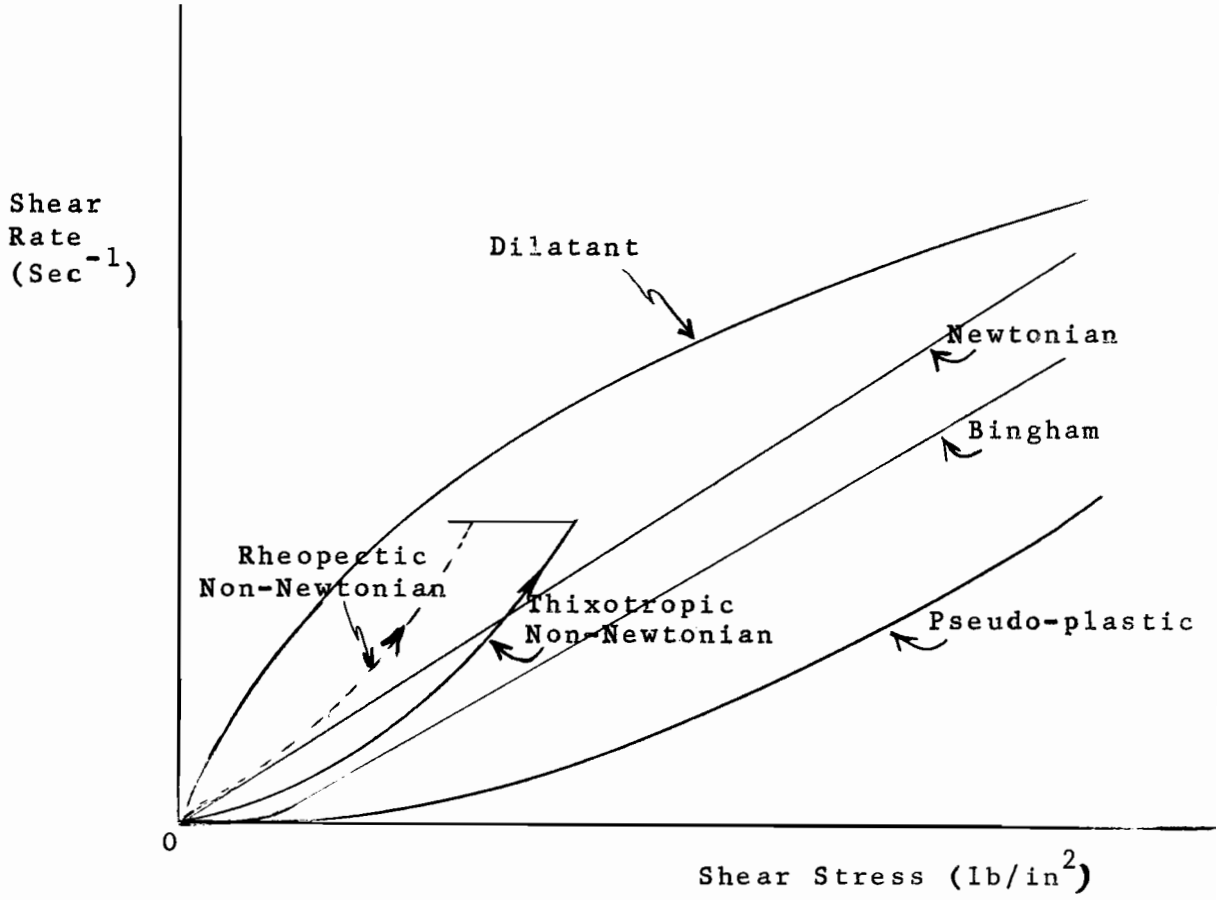

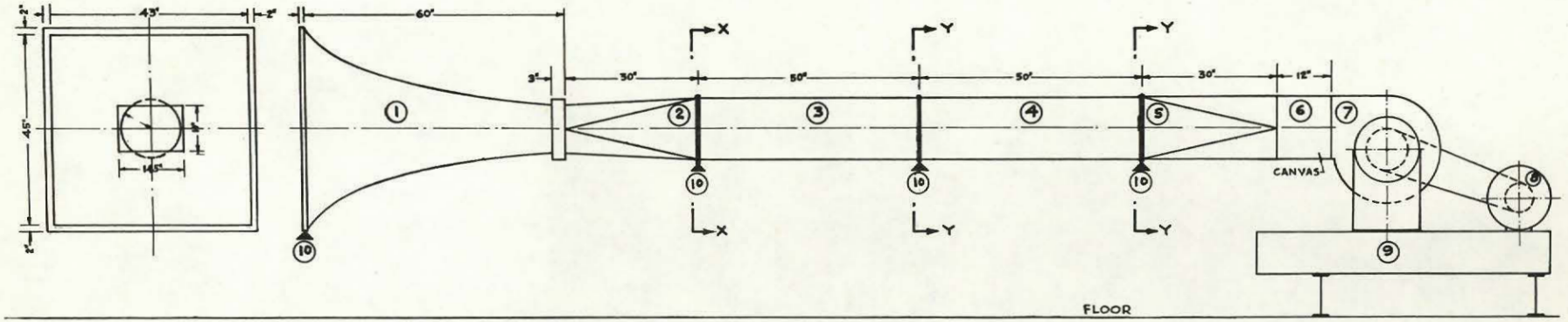

1 : EXPONENTIAL HORN
2 : CIRCULAR TO RECTANGULAR ADAPTER
3: " DUCT (44"ϕ)
4: " " "
5 : " TO RECTANGULAR ADAPTER
6: CANVAS CONNECTION
7: SIROCCO FAN, SIZE 135
8: 5 H.P. 1800 RPM, 220V. 3 PHASE SYNCHRONOUS MOTOR
9: I-BEAM SUPPORT.
10: ANGLE IRON - SIMPLE SUPPORT.

SECTION: X-X

SECTION: Y-Y

VENTILATION - DUCT MODEL LAYOUT
Scale: 1" = 1 Ft.

Figure (62)

APPENDIX A

LABORATORY REPORT (No.14)

GEIGER PLATE TEST

PHYSICAL READINGS:

1. Test Plate No. 1
2. Date: 21st July 1961
3. Coating material F.
4. Temperature: 78°F.
5. Dryness time: from 3 a.m. on 21st July untl 2 p.m. on 22nd July. (Net hours 35).
6. Layer thickness: 0.154 inch - average of 29 readings.
7. Total solids: not given. .
8. Shrinkage on drying: 25-28%.
9. Viscosity - not given
10. Colour - green
11. Thermal Conductivity (K-factor) - 0.175 BTU/hr/ft^2/°F/ft
12. Density 1.5 wet, Dry: not given.
13. Mass 28.15 lbs (bare plate); 31.156 lbs(coated plate)

INPUT READINGS:

14. Exciter voltage -- Peak, 40 v. r.m.s.
15. Magnetizing current -- Peak (not taken)
16. Resonant Frequency: 190.9 c.p.s.
17. Ambient SPL: 46 db.
18. Distance of supports from plate corners: 5-11/16 inch.
19. Distance of exciter from plate centre: 1/32 inch approx.

OUTPUT READINGS:

20. Q-factor of uncoated plate :1598.10

21. Decay rate of uncoated plate :3.28 db/sec.

22. Distance of condenser microphone from plate :5 inches.

23. Pass Band :150-300 c.p.s.

24. Harmonic output: none.

25. Maximum sound pressure level :63.1 db.

AMPLIFIER SETTINGS:

26. Input switch :condenser microphone

27. Meter range :80 db SL, 0.1 volts

28. Meter switch :r.m.s. standard damping

29. Meter reading: 3.1 db.

30. Range multiplier: x 1, 0 db

31. Weighting network: 20-35,000 curve C.

RECORDER SETTINGS:

32. Recording: No. 14

33. Potentiometer: 50 db

34. Lower limit frequency: 20 c.p.s.

35. Paper speed: 10 mm/sec.

36. Writing speed: 50 mm/sec.

37. Decay time: 1.2 sec.

38. Q-factor of coated plate: 104.19

39. Decay rate of coated plate: 50 db/sec.

40. Geiger rating of coating material: 47.03 db.sec.

41. Duration of test: 30 minutes.

COMMENTS: Thickness τ is approaching an optimum value.

APPENDIX B

LABORATORY REPORT (No.30)

COMPLEX MODULUS TEST

1. Bar No.: 45
2. Date: 16th August, 1961.
3. Coating material: F
4. Temperature: 78°F
5. Drying time: from 4 p.m. on 13th August until 12 p.m. on 16th August, 1961 (net hours 80).

BAR UNCOATED

6. Total bar length: 11.9 inches.
7. Width: 0.31 in.
8. Thickness: 0.1255 in.
9. Mass: 0.13 lbs.
10. Mass/unit length/unit width: 0.0352 lbs.
11. Density: 0.282 lbs/in^3
12. Static modulus of elasticity: 30×10^6 lbs/in^2
13. Clamping: top end
14. Free length: 9.56 in.
15. Q-factor: 418
16. Fundamental frequency: 41.8 c.p.s.
17. Higher modes: Measured - 268.8, 755.1, 1478, 2436, 3623 c.p.s.
    Calculated - 273.5, 753, 1478, 2430, 3640 c.p.s.
18. Decay time: 22 sec.
19. Recording No.: 30-1
20. Loss Factor: 2.39×10^{-3}
21. Decay rate: 2.727 db/sec.

COATED BAR

22. Total mass:0.218 lbs.

23. Total thickness:0.6278 inch

24. Thickness of coating:0.5023 in

25. Mass of coating:0.088 lbs

26. Mass/unit length/unit width:0.065 lbs.

27. Method used: Reverberation-time.

28. Decay time:1.2 sec.

29. Recording No.:30-2

30. Fundamental frequency:59.4 c.p.s.

31. Higher modes:236.4, 564, 1355, 1990 c.p.s.

32. Decay rate:50 db/sec.

33. Q-factor:32.4

INPUT READINGS:

34. Oscillator output:4.7 volts

35. Output impedance:60 ohms.

36. Exciter position:horizontal.

37. Distance of exciter from bar:0.125 in.

OUTPUT READINGS:

38. Pick-up position:horizontal

39. Distance of pick-up from bar:0.125 in.

40. Amplifier meter setting:r.m.s.

41. Meter range:0-10 volts.

42. Range multiplier x 0.03 or -30 db.

43. Recorder Potentiometer:50 db.

44. Lower limit frequency :20 c.p.s.

45. Writing speed :50 mm/sec.

46. Paper speed :0.10 mm/sec.

47. Dynamic modulus of elasticity: Real - 0.217×10^6
Imaginary - 0.168×10^4

48. Loss factor of damping material :0.04319

49. Phase angle between stress and strain : negligible.

50. Decay rate of material :48.52 db/sec.

CALCULATIONS

1. Loss-factor - η:

$$\eta = 2.2/(T\ f_n)$$

η = loss factor of coated bar

T = decay-time in sec..

f_n = nth resonant frequency of coated bar.

$$= 0.03086$$

2. Decay-rate of coated bar - δ:

$$\delta = 27.29\ \eta\ f_n = 60/T$$

$$= 50.0 \text{ db/sec.}$$

3. Resonant frequencies of uncoated bar - f_n'

$$f_1' = (0.1615\ H_1/L^2)\sqrt{\frac{E}{\rho}} \text{ c.p.s.}$$

Where:

H_1, L, E, ρ are thickness (inch)

free length (inch),

Static modulus of elasticity (lbs/ft^2)

and density (lbs/ft^3)

of steel bar respectively.

$$f_1' = 43.04 \text{ c.p.s.}$$

4. Dynamic modulus of elasticity of steel bar - E_1':

$$E_1' = 473.7\ (\frac{f_1'}{\beta_n^2})^2(\frac{L^2}{H_1})^2\rho \quad \text{dynes/cm}^2$$

$$= 7.48 \times 10^{-3}(\frac{f_1'}{\beta_n^2})^2(\frac{L^2}{H_1})^2\rho \quad \text{lbs/in}^2$$

$$= 28.2 \times 10^6 \text{ lbs/in}^2$$

Where: β_n = constant fixed for each mode and method of clamping.

5. Thickness Ratio - ξ

$\xi = H_2/H_1$ $\quad$ H_1 = thickness of coating layer in inches.

$= 4.0$

6. Ratio of Bending Stiffness - F^2

$$F^2 = \frac{B}{B_1} = \frac{1+2a\xi(2+3\xi+2\xi^2) + a^2\xi^4}{1+a\xi} \quad *$$

$$F = \sqrt{\frac{B}{B_1}} = \frac{\sqrt{\frac{B}{m}}\ \sqrt{1+\frac{m_2}{m_1}}}{\sqrt{\frac{B_1}{m_1}}}$$

$\mu = m_2/m_1$

$\sqrt{\frac{B_1}{m_1}} = 2\pi L^2 f_n/\beta_n^2$ ... For uncoated bar.

$\sqrt{\frac{B}{m}} = 2\pi L^2 f_n/\beta_n^2$ ... For coated bar.

where: Bending stiffness in lbs/in^2

[Quantities with no index relate to the coated bar, those indexed with (1) relate to uncoated bar, and those indexed with (2) relate to coating layer alone.]

m = (mass/unit length/unit width) in lbs.

$a = E_2'/E_1'$

$= 0.007716$

*Note: this equation is plotted in figures B-1 and B-2.

7. Loss Factors Ratio - G

$$G = \frac{\eta}{\eta_2} = \left[\frac{a\xi}{1+a\xi}\right]\left[\frac{3+6\xi+4\xi^2+2a\xi^3+a^2\xi^4}{1+2a\xi(2+3\xi+2\xi^2)+a^2\xi^4}\right]$$

$= 0.7146$

Note: This equation is plotted in Figure B-3.

8. Ealstic Constants of Coating Material:

$\eta_2 = \eta/G = 0.04319$

$E_2' = E_1' a$

$= 0.2175 \times 10^6$ lbs/in^2

$E_2'' = E_2' \eta_2 = 0.94 \times 10^4$ lbs/in^2

9. ψ - Phase-angle between stress and strain:

$\psi = \tan^{-1}(\eta_2)$

$\doteq 2.5^\circ$

10. Logarithmic Decrement - α:

$\alpha = \pi\eta_2 = 0.1357$

11. Quality factor - Q:

$Q = 1/\eta = 32.4$

12. Period of Damped Vibrations: t:-

$t = 1/(f_n\sqrt{1-\varphi^2})$ where: $\varphi = \alpha/2\pi$

$\doteq 0.024$ Sec.

Duration of test - 30 min. Taken by M.H.

COMMENTS: Optimum thickness passed.

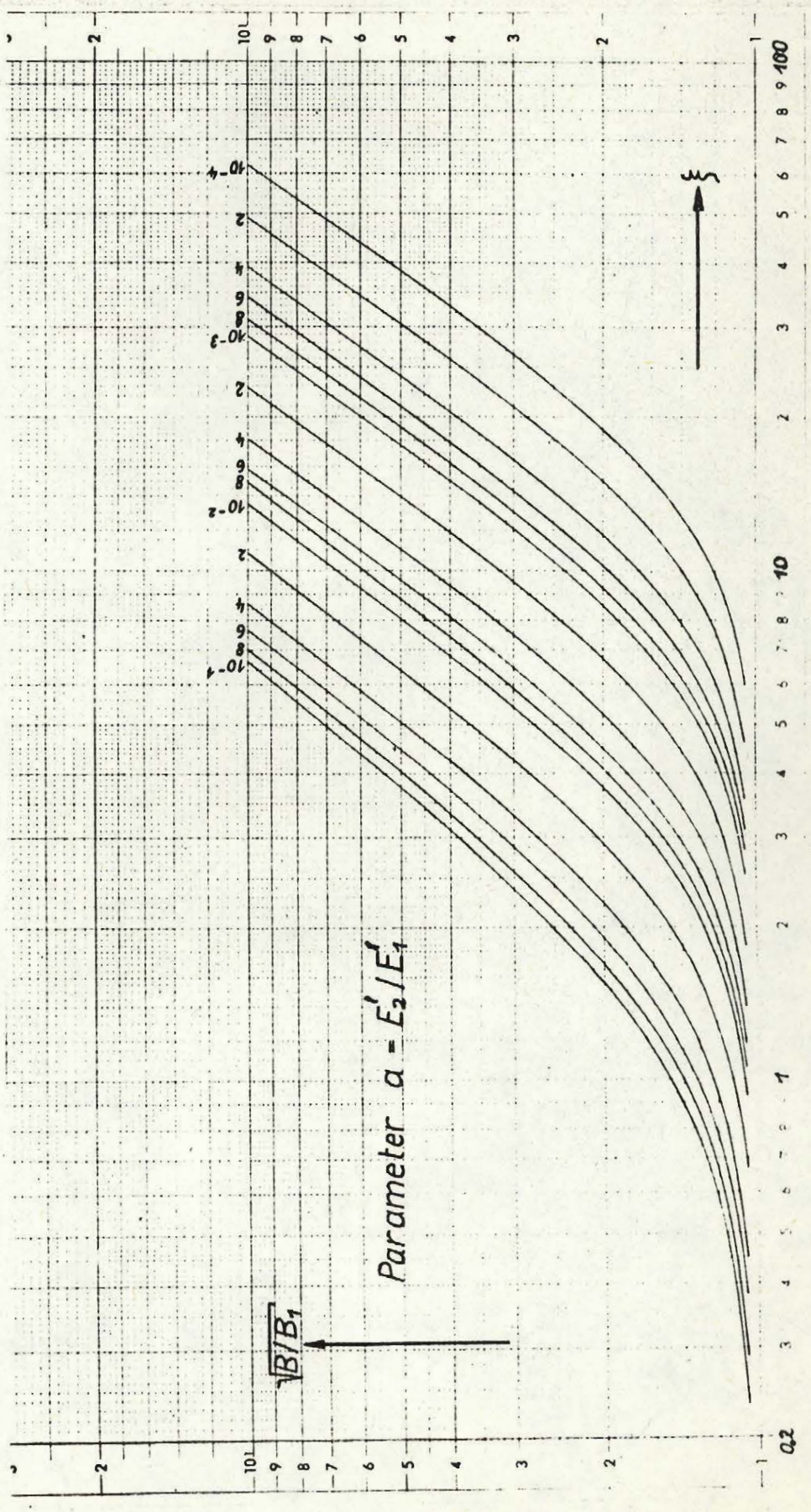

Figure B-1

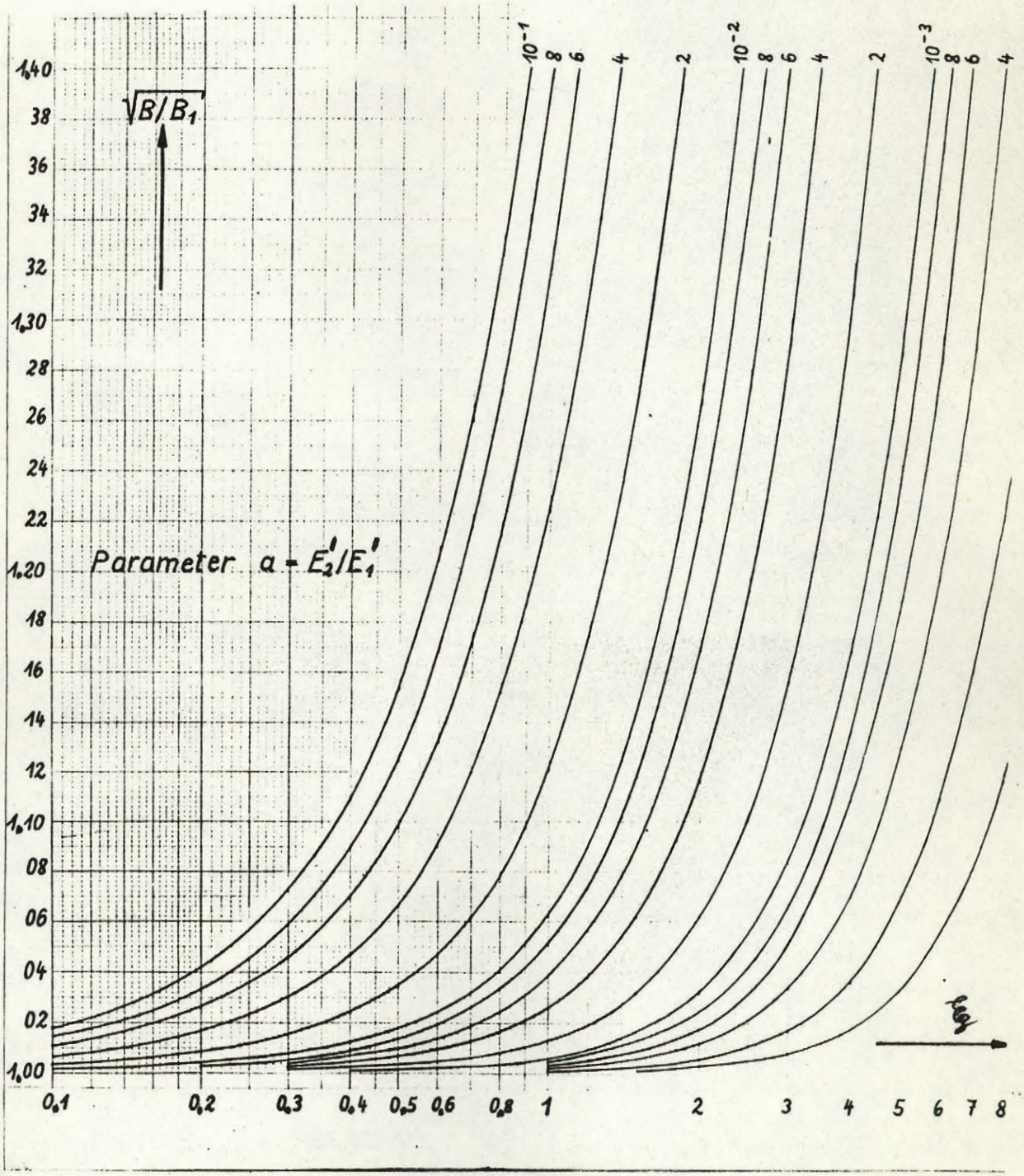
√B/B1
Parameter a = E2'/E1'
1,40
38
36
34
32
1,30
28
26
24
22
1,20
18
16
14
12
1,10
08
06
04
02
1,00
10-1
8
6
4
2
10-2
8
6
4
2
10-3
8
6
4
0,1
0,2
0,3
0,4
0,5
0,6
0,8
1
2
3
4
5
6
7
8

Figure B-2

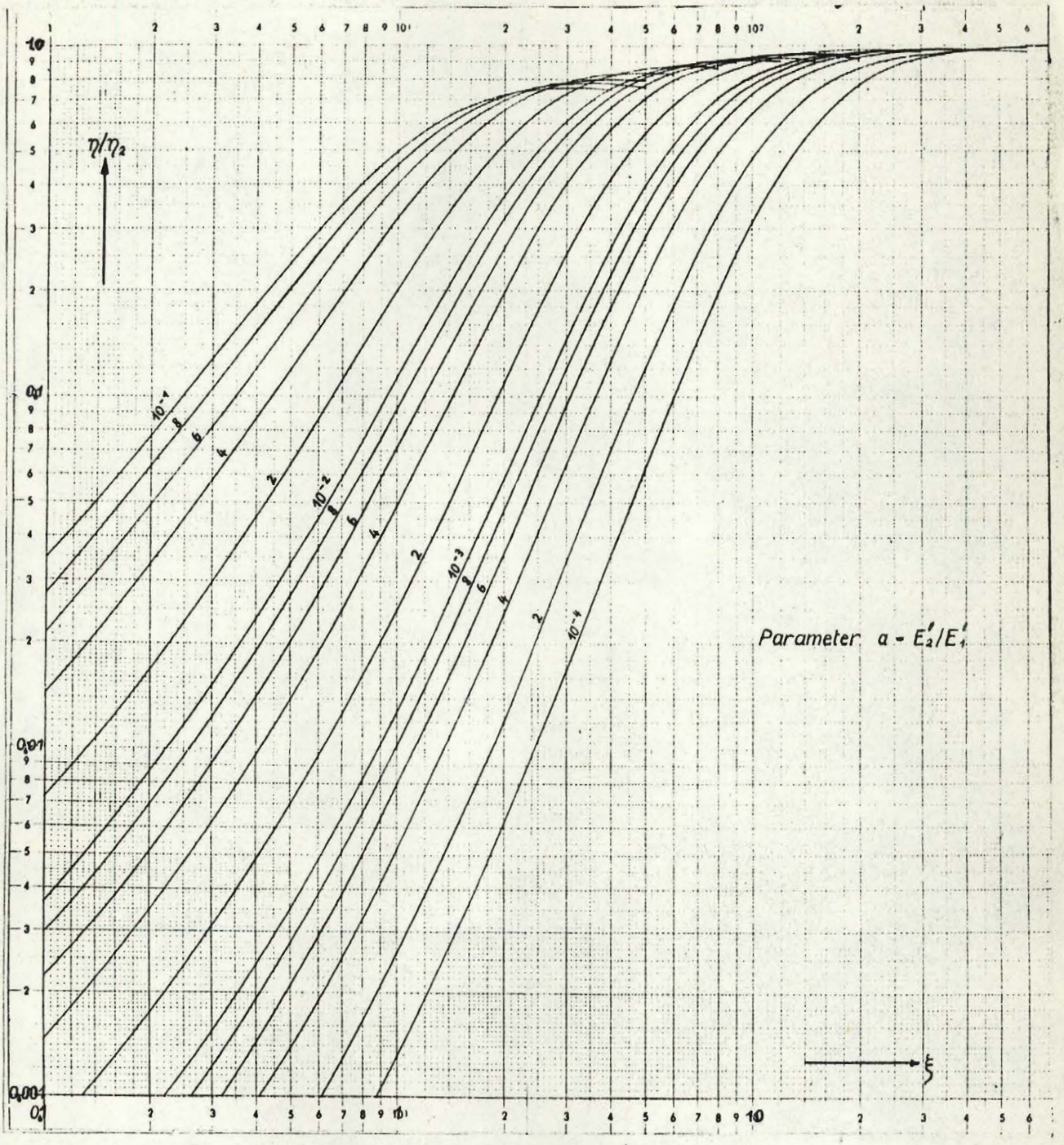

Figure B-3

APPENDIX C

ON THE FUNDAMENTAL MODE OF THE GEIGER PLATE

Theoretically a square plate supported at the points K,L,M and N of the figure below, bends in the manner shown. The nodes are straight lines, A-A' and B-B'.

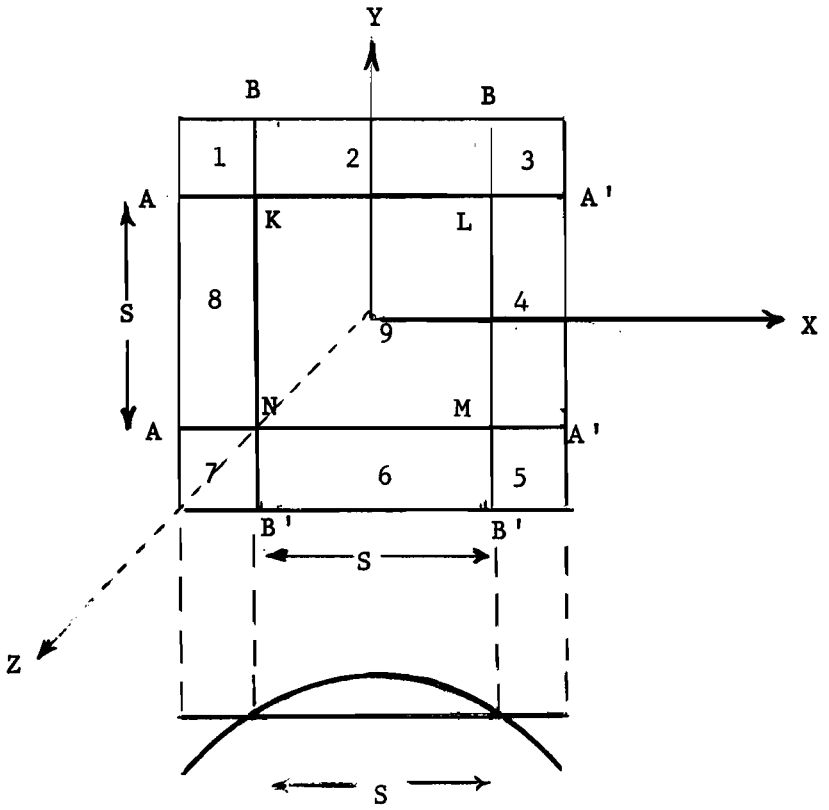

Bending Moment Diagram

The distance S is half a wavelength at the resonant frequency and is more than 10 inches (half the length of the plate). This is due to the fact that Poisson's ratio[1] and stresses

[1] R.V.Southwell, Theory of Elasticity, (OXFORD UNIVERSITY PRESS, 2nd Ed. 1949) p.115.

due to edge effects are appreciable. Also from plate theory it can be shown that the sides of the squares, 1, 3, 5, 7, are less than a quarter-wavelength each.

Since the overall bending of square 9 is a superposition of two cosine waves, we can evaluate the displacement Z'(in the vertical direction Z) as a function of X and Y for the fundamental mode. Thus:

$$Z' = A \cos KX \cos KY$$

where K = constant

A = maximum displacement at the centre of the plate

Z = 0 at the nodal lines.

Experimentally, these lines were found to have a width of approximately 1/2 inch. If we take the measured values for Plate 1 we can write:

$Z' = 0$ at $X = Y = 5.28$ inches
For $X = 0$, $\cos KX = \cos KY = 1$ and $Z' = A$
$S = 10.56$ inches

For $X = Y = 5.28$, $\cos KX = \cos KY = 0$

or $KX = KY = \pi/2$

Thus $K = 0.298$, and

$$Z' = A (\cos 0.298 X)(\cos 0.298 Y)$$

This equation was verified experimentally using the B and K type 4308 accelerometer and was used for a non-uniform thickness test*.

---

*See Section 5.2.2 and Photograph (10).